Distribution Statement

Distribution A: Public Release.

The views presented here are those of the author and are not to be construed as official or reflecting the views of the Uniformed Services University of the Health Sciences, the Department of Defense or the U.S. Government.

PHASE SEPARATION OF FUS: A POTENTIAL THERAPEUTIC TARGET IN CANCER AND NEURODEGENERATION

By

Izzy Owen

Dissertation submitted to the Faculty of the
Molecular and Cell Biology Graduate Program
Uniformed Services University of the Health Sciences
In partial fulfillment of the requirements for the degree of
Doctor of Philosophy 2021

UNIFORMED SERVICES UNIVERSITY OF THE HEALTH SCIENCES
SCHOOL OF MEDICINE GRADUATE PROGRAMS
Graduate Education Office (A 1045), 4301 Jones Bridge Road, Bethesda, MD 20814

FINAL EXAMINATION/PRIVATE DEFENSE FOR THE DEGREE OF DOCTOR OF PHILOSOPHY IN THE MOLECULAR AND CELL BIOLOGY GRADUATE PROGRAM

Name of Student: Izzy Owen

Date of Examination: August 31, 2021
Time: 10:00 AM

DECISION OF EXAMINATION COMMITTEE MEMBERS:

	PASS	FAIL
DOUGHTY.MARTIN.L.1287263747 Digitally signed by DOUGHTY.MARTIN.L.1287263747 Date: 2021.09.01 12:58:47 -04'00'	__X__	____
Dr. Martin Doughty DEPARTMENT OF ANATOMY, PHYSIOLOGY & GENETICS Committee Chair		
[redacted]	__X__	____
Dr. Frank Shewmaker DEPARTMENT OF BIOCHEMISTRY Dissertation Advisor		
Rachel Cox Digitally signed by Rachel Cox Date: 2021.08.31 17:17:26 -04'00'	__X__	____
Dr. Rachel Cox DEPARTMENT OF BIOCHEMISTRY Committee Member		
IORDANSKIY.SERGEY.1536484872 Digitally signed by IORDANSKIY.SERGEY.1536484872 Date: 2021.09.01 12:16:23 -04'00'	__X__	____
Dr. Sergey Iordanskiy DEPARTMENT OF PHARMACOLOGY Committee Member		
LIECHTI.GEORGE.WARREN.1461677009 Digitally signed by LIECHTI.GEORGE.WARREN.1461677009 Date: 2021.09.01 09:30:11 -04'00'	__X__	____
Dr. George Liechti DEPARTMENT OF MICROBIOLOGY Committee Member		

UNIFORMED SERVICES UNIVERSITY OF THE HEALTH SCIENCES
SCHOOL OF MEDICINE GRADUATE PROGRAMS
Graduate Education Office (A 1045), 4301 Jones Bridge Road, Bethesda, MD 20814

APPROVAL OF THE DOCTORAL DISSERTATION IN THE MOLECULAR AND CELL BIOLOGY GRADUATE PROGRAM

Title of Dissertation: "Phase Separation of FUS: A Potential Therapeutic Target in Cancer and Neurodegeneration"

Name of Candidate: Izzy Owen
Doctor of Philosophy Degree

DISSERTATION AND ABSTRACT APPROVED:

DOUGHTY.MARTIN.L.1287263747 Digitally signed by DOUGHTY.MARTIN.L.1287263747 Date: 2021.09.09 11:52:55 -04'00'

DATE: September 10, 2021

_____ ___X_____
Dr. Martin Doughty
DEPARTMENT OF ANATOMY, PHYSIOLOGY & GENETICS
Committee Chair

_[redacted] ____X____
Dr. Frank Shewmaker
DEPARTMENT OF BIOCHEMISTRY
Dissertation Advisor

Rachel Cox Digitally signed by Rachel Cox Date: 2021.09.01 07:37:39 -04'00'

_____ ___X_____
Dr. Rachel Cox
DEPARTMENT OF BIOCHEMISTRY
Committee Member

IORDANSKIY.SERGEY.1536484872 Digitally signed by IORDANSKIY.SERGEY.1536484872 Date: 2021.09.01 12:30:28 -04'00'

_____ ___X_____
Dr. Sergey Iordanskiy
DEPARTMENT OF PHARMACOLOGY
Committee Member

LIECHTI.GEORGE.WARREN.1461677009 Digitally signed by LIECHTI.GEORGE.WARREN.1461677009 Date: 2021.09.01 09:11:01 -04'00'

_____ ____X____
Dr. George Liechti
DEPARTMENT OF MICROBIOLOGY
Committee Member

ACKNOWLEDGEMENTS

A special thank you to my advisor, Frank Shewmaker. The wealth of knowledge I have gained from you is unmatched. I am a confident, strong, and meticulous researcher because of you and your mentorship. Your guidance has been invaluable and is something I will cherish for the rest of my career.

Thank you to my committee, Dr. Martin Doughty, Dr. Rachel Cox, Dr. Sergey Iordanskiy, and Dr. George Leichti for your encouragement and consistent guidance.

Thank you to my lab members Shannon, Gabe, Debra, Hala and Matt for making each day at work something to look forward to. I am excited for the day we finish the hit "FUS-FUS Baby."

A huge thank you to my USU friends that became family, Brad, Sully, Nate, Elizabeth, and Gina. Together, we have all come so far. Thanks for all of the study sessions, game nights, volleyball matches, nights out, and endless laughs.

A loving thank you to Coll Dininny, the man who has been there everyday through all of the trials and tribulations that come with the rigor of this degree. I couldn't ask for a better support system. I love you and am thankful for all that you have done and sacrificed for me over these last four years.

Lastly and most importantly, I would not have made it this far without the support of my family. To my siblings, Svea, Erin, Chris, Emmy and Vince, and parents, Lois and Drew Owen: thank you. Your love and consistent support has kept me going and kept a smile on my face. You all have had an integral role in raising me and getting me to this stage of my life and for that I couldn't be more grateful.

DEDICATION

I dedicate this work to my mother, Lois Owen.

"All that I am, or hope to be, I owe to my mother" -Abraham Lincoln

You have given me the world and would give me the stars and the moon if you could. Your support has been unconditional and unwavering. Life has been unfair and unruly towards you, but somehow you still find a way to shine and be the best Mom and Nana our family could ever ask for. My strength, perseverance, and dedication are all a direct reflection of you. I am proud to be your daughter and thankful for this life you have blessed me with. This ones for you, Mom.

COPYRIGHT STATEMENT

The author hereby certifies that the use of any copyrighted material in the dissertation entitled:

"PHASE SEPARATION OF FUS: A POTENTIAL THERAPEUTIC TARGET IN CANCER AND NEURODEGENERATION "

is appropriately acknowledged and, beyond brief excerpts, is with the permission of the copyright owner.

Izzy Owen
MOLECULAR AND CELL BIOLOGY PROGRAM
Uniformed Services University
August 31, 2021

DISCLAIMER

The views presented here are those of the author and are not to be construed as official or reflecting the views of the Uniformed Services University of the Health Sciences, the Department of Defense or the U.S. Government.

ABSTRACT

Phase separation of FUS: A Potential Therapeutic Target in both Cancer and Neurodegeneration

Izzy Owen, Doctor of Philosophy, 2021

Thesis directed by: Frank P. Shewmaker, Ph.D., Associate Professor, Department of Biochemistry

Fused in Sarcoma (FUS) is a ubiquitously expressed, predominantly nuclear protein that functions in RNA and DNA metabolism. FUS contains an N-terminal prion-like domain (PrLD) that has the ability to drive liquid- and solid-phase transitions through self-association. The liquid phase of FUS is thought to be a functional state, whereas the solid phase has been linked to cellular toxicity. The PrLD of FUS has causative implications in both myxoid liposarcoma (MLS) and amyotrophic lateral sclerosis (ALS). In MLS, we hypothesize FUS-driven phase separation of FUS-CHOP is the underlying mechanism of oncogenic transcriptional activation, while in ALS, disruption of solid phase aggregation, leaving FUS in a functional liquid-phase, could reduce cellular toxicity. Using both disease models we show phase separation as a potential therapeutic target by characterizing FUS-CHOP phase separation in cells and providing evidence that phosphorylation can disrupt toxic FUS aggregation.

In MLS, the PrLD of FUS is fused to a transcription factor, CHOP, resulting in oncogenic transcriptional reprogramming. Ubiquitous overexpression of CHOP alone does not cause MLS, providing a necessary role of the PrLD in driving oncogenesis. We characterize PrLD-dependent phase separation of FUS-CHOP in cells and *in vitro.* In

cancer cell lines, we show endogenous FUS-CHOP localization to known biomolecular condensates at super-enhancer sites. These data suggest FUS-driven phase separation of FUS-CHOP is a targetable mechanism underlying oncogenesis.

To better understand regulation of FUS phase transition, we used an established ALS-FUS model to study post-translational modification of the PrLD. Our previous work showed phosphorylation or phosphomimetic substitution at 12 (PIKK consensus sites) of the 32 putative phosphorylation sites in the PrLD disrupts both liquid- and solid-phase transition of FUS. Here, we characterized the phosphorylation of non-PIKK consensus sites in the PrLD both in cells and *in vitro*. We showed ALS-FUS is phosphorylated in cells and can phase separate in the cytoplasm. Further, we used a yeast model and purified protein to show 4 phosphomimetic substitutions throughout the PrLD can disrupt toxic aggregate formation. These data show FUS-driven phase separation occurs in both MLS and ALS and could be modulated by phosphorylation of the PrLD.

TABLE OF CONTENTS

LIST OF TABLES

LIST OF FIGURES

CHAPTER 1: The Role of Fused in Sarcoma's Prion-like Domain in Disease

Fused in Sarcoma (FUS) has a detrimental role in both cancer (*e.g.* myxoid liposarcoma (MLS)) and neurodegeneration (*e.g.* amyotrophic lateral sclerosis (ALS)). In both diseases, the prion-like domain of FUS drives pathogenic self-association resulting in a liquid and/or solid-phase transition. Understanding the mechanisms of FUS phase transition, specifically the interactions of FUS prion-like domains, in both diseases is necessary for the development of novel therapeutics for patients and their families. Here, we evaluate a potential mechanism of FUS-CHOP-induced oncogenesis by understanding the propensity of FUS to drive oncogenic liquid-liquid phase separation in cells. Additionally, we use an established ALS-FUS model to determine how post-translational modifications can modulate FUS liquid and solid-phase transition as a potential therapeutic in disease.

LIQUID-LIQUID PHASE SEPARATION

This work is centralized around the phenomena of liquid-liquid phase separation (LLPS), which is a condensation of specific macromolecules into liquid phases that are distinct from the bulk nucleoplasm or cytoplasm (Hyman et al., 2014). Condensate formation is largely driven by weak interactions between proteins with intrinsically disordered regions (IDRs), repeated motifs, and nucleic acids (Owen and Shewmaker, 2019). Because most IDRs are not structurally limited, they can make numerous favorable interactions that result in demixing, leaving a condensed phase and a dilute phase (Hyman et al., 2014). The condensed phase, often compared to an oil droplet in water, occurs at a specific time and place in the cell allowing for a function to occur (Courchaine et al., 2016).

The interactions between IDRs occur via noncovalent, weak binding forces and are often non-static, dynamic and less specific than those interactions driving globular protein conformations (Shin and Brangwynne, 2017). The network of interactions formed by the multivalent macromolecules reduces their solubility and allows for an entropy-driven demixing from the bulk solution (Banani et al., 2017; Majumdar et al., 2019). The interactions that drive LLPS are electrostatic, pi-pi, cation-pi, hydrophobic, and hydrogen bonding (Martin and Mittag, 2018; Murthy et al., 2019) (Figure 1).

Condensates formed via LLPS, often referred to as biomolecular condensates or membraneless organelles, are functional organelles, including stress granules(Molliex et al., 2015), processing bodies (Brangwynne et al., 2009), promyelocytic leukaemia (PML) bodies (Lallemand-Breitenbach and de The, 2018), Cajal bodies (Neugebauer, 2017), transcriptional start sites (Laflamme and Mekhail, 2020), super enhancers(Sabari et al., 2018), nuclear paraspeckles (McCluggage and Fox, 2021), and the nucleolus (Berry et al., 2015). Biomolecular condensate formation allows for temporal organization of the densely packed cellular environment resulting in an array of functions, including translational pausing, RNA processing, DNA repair and replication, and gene expression (Laflamme and Mekhail, 2020; Peng et al., 2020).

Biomolecular condensates also have a role in disease, specifically neurodegeneration and cancer (Boija et al., 2021; Jiang et al., 2020; Nedelsky and Taylor, 2019). Several RNA-binding proteins associated with neurodegenerative diseases have the ability to phase separate in cells (Franzmann and Alberti, 2019). It is hypothesized that RNA-binding proteins can undergo aberrant liquid-phase separation, which subsequently leads to solid-aggregation of proteins in diseased neurons (Franzmann and

Alberti, 2019).In cancer, several processes are dysregulated, which result in malignancy. Some of these oncogenic processes involve condensate-associated proteins. Proteins linked to condensate formation have also been shown to have dysregulated roles in transcription (Boija et al., 2018; Kamagata et al., 2020), epigenetic regulation (Larson et al., 2017; Li et al., 2020), cell signaling (Huang et al., 2019; Nair et al., 2019), immune signaling (Du and Chen, 2018), ribosome biosynthesis (Feric et al., 2016), protein degradation (Bouchard et al., 2018), DNA repair (Kilic et al., 2019; Singatulina et al., 2019), RNA splicing (Guo et al., 2019), DNA replication (Parker et al., 2019), autophagy (Fujioka et al., 2020; Mulcahy Levy and Thorburn, 2020), and proteasomal degradation (Manasanch and Orlowski, 2017; Yasuda et al., 2020) in different types of cancer. Understanding the diverse interactions that drive condensate formation is a potential therapeutic target in both types of diseases (Wheeler, 2020).

Modulation of LLPS via post-translational modifications

Many proteins that undergo LLPS are highly susceptible to enzymatic post-translational modifications due to the open conformation of the IDRs (Bah and Forman-Kay, 2016; Owen and Shewmaker, 2019). Post-translational modifications (PTMs)-such as phosphorylation, methylation, acylation, glycosylation, alkylation, and ubiquitination as well as oxidation, deimidation, and deamidation-of phase-separating proteins function as molecular on/off switches for LLPS (Owen and Shewmaker, 2019). PTMs alter charge, hydrophobicity, size and structure of IDRs. Because of the nature of the interactions underlying phase separation, PTMs can either strengthen or weaken the

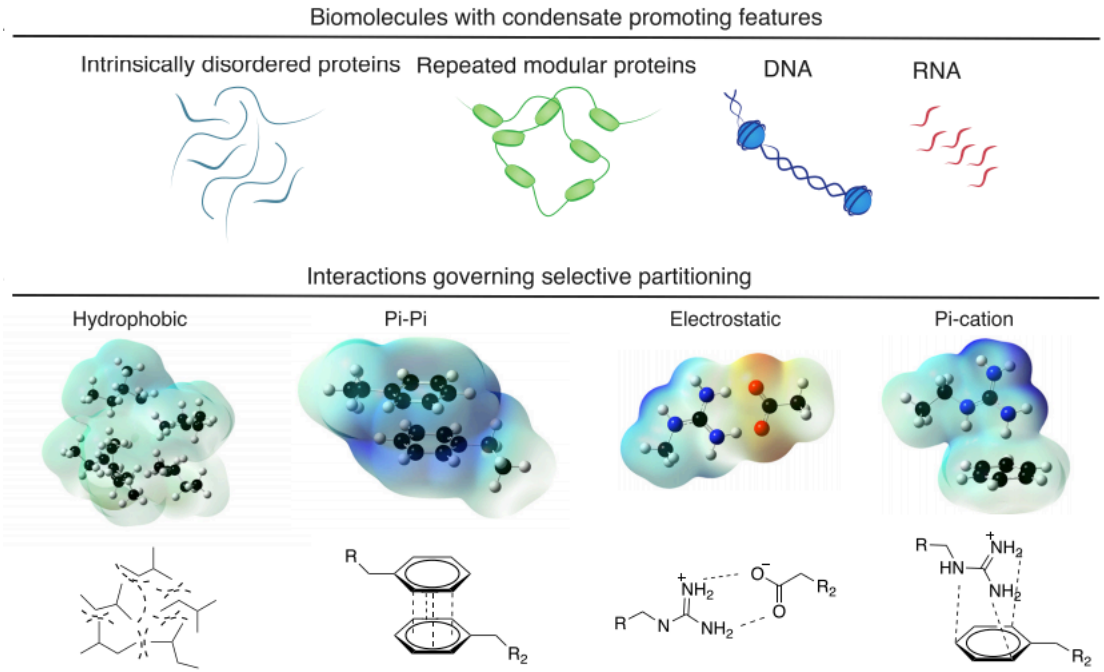

Fig 1. Common features that drive condensate formation.

LLPS is governed by macromolecules that contain IDRs, repeat motifs, and by nucleic acids. Above are common interactions that drive condensate formation. Figure adapted from Boija *et al* (Boija et al., 2018).

forces driving condensate formation (Aguzzi and Altmeyer, 2016). Here, we assess the FUS's ability to drive LLPS, as well as how PTMs can modulate its phase transitions.

FUSED IN SARCOMA

Fused in Sarcoma (FUS) or translocated in liposarcoma (TLS) was first identified in the early 1990s as an oncogenic fusion protein (Crozat et al., 1993). Over the past 30 years, FUS has been characterized in numerous cellular processes and diseases, including MLS, ALS, and frontotemporal dementia (Chen et al., 2019a; Yu et al., 2019).

FUS is composed of 526 amino acids forming 6 different domains. FUS contains an N-terminal prion-like domain (PrLD), a glycine-rich region, three Arginine-Glycine-Glycine rich regions (RGG), an RNA-recognition motif (RRM), a zinc-finger domain (ZnF), and a PY-nuclear localization sequence (NLS) (Figure 2) (Monahan et al., 2017). The central focus of this work is the role of the FUS PrLD, its ability to drive FUS phase transition, and its implications in disease. The PrLD received its name because of its sequence homology to yeast prion-domains, which induce self-propagation of solid aggregates (discussed below).

The N-terminus of FUS (aa ~1-214) is an IDR; it lacks hydrophobic and charged residues, is not confined to a secondary structure and is highly susceptible to PTMs (Rhoads et al., 2018b). FUS is widely studied for its ability to functionally phase separate *in vitro* and in cells (Burke et al., 2015; Gal et al., 2011; Levone et al., 2021; Monahan et al., 2017; Murthy et al., 2019).

Physiologically, FUS is predominantly nuclear and has several known functions. Characterized functions include RNA metabolism, DNA damage repair, cellular stress

response, and transcription (Chen et al., 2019a; Mastrocola et al., 2013; Sama et al., 2013; Tan et al., 2012). FUS is involved in RNA splicing factor recruitment, spliceosome assembly, and nucleo-cyoplasmic shuttling of mRNA transcripts (Meissner et al., 2003; Yang et al., 1998; Zinszner et al., 1997). FUS is also important in the DNA damage response (DDR), as knockdown of FUS results in a reduced induction of DNA repair (Wang et al., 2013). When DNA is damaged, FUS is phosphorylated and rapidly recruited to double stranded DNA cleavage sites and Holliday junctions where its function is necessary for downstream signaling (Gardiner et al., 2008; Wang et al., 2013).

During a cellular stress (caused by oxidative or osmotic stress), FUS has prosurvival functions and is recruited to cytoplasmic ribonucleoprotein (RNP) granules (Sama et al., 2013). Lastly, FUS is involved in transcriptional activation and repression of a subset of genes involved in cell-cycle regulation, neurodegeneration, DNA repair and genomic stability (Tan et al., 2012). FUS can physically bind DNA using its ZnF, but recruitment of FUS to sites of DNA binding depends on the PrLD (Yang et al., 2014). When FUS is knocked down, there is an increase in transcriptional pausing at transcriptional start sites (TSS), increase in RNA polymerase 2 (Pol 2) recruitment, and premature termination of transcripts, providing evidence that FUS plays an important role in regulating Pol 2 at TSS (Schwartz et al., 2012).

FUS function is essential in several cellular aspects, making its role in disease detrimental to normal function. In myxoid liposarcoma (MLS), *FUS* is involved in a chromosomal translocation, which results in the formation of a fusion protein (Knight et al., 1995). The N-terminus of FUS becomes fused to the transcription factor

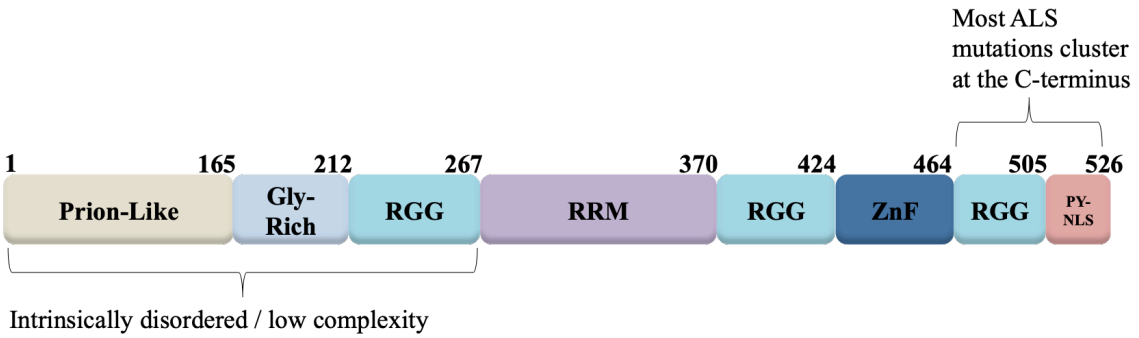

Fig 2. Schematic of Fused in Sarcoma

FUS is comprised of numerous domains. The N-terminus of FUS contains an intrinsically disordered region, which is included in the myxoid liposarcoma fusion proteins FUS-CHOP. The C-terminus of FUS has a PY-nuclear localization sequence and is commonly mutated in amyotrophic lateral sclerosis.

CCAAT/Enhancer binding protein (C/EBP) homologous protein (CHOP). The expression of FUS-CHOP causes aberrant transcriptional reprogramming resulting in tumorigenesis, but the exact mechanism of FUS-CHOP-induced oncogenesis has not been elucidated. In amyotrophic lateral sclerosis (ALS), FUS is often mutated at the C-terminus, disrupting the NLS, resulting in mislocalization to the cytoplasm (Vance et al., 2013). FUS cytoplasmic inclusions have been identified along neuroanatomical tracts of the central nervous system, in both upper and lower motor neurons, of ALS patients (Armstrong, 2017). Both gain-of-function and loss-of-function mechanisms have been attributed to mutant FUS expression in ALS (Ishigaki and Sobue, 2018; Sharma et al., 2016). Currently, there is no treatment to disrupt FUS pathological aggregate formation and no cure for ALS. In both diseases, the PrLD drives FUS self-association and phase transition aiding in pathogenesis.

FUS IN DISEASE

Myxoid Liposarcoma (MLS)

MLS is a subtype of liposarcoma that is characterized by the cytogenetic hallmark of t(12;16)(q13;p11)(Knight et al., 1995). This chromosomal translocation results in a new gene product *FUS-DDIT3* and the fusion protein FUS-CHOP (Figure 3A). Expression of FUS-CHOP results in adipoblast rich tumors predominantly located in the lower extremities of patients (Creytens, 2019). The mechanism of FUS-CHOP-induced oncogenesis has yet to be elucidated.

There are 11 different *FUS-DDIT3* transcripts identified from patient samples all of which include varying lengths of the N-terminus of FUS (all fusions include the PrLD) fused to full-length CHOP (Figure 3B) (Oikawa et al., 2012; Powers et al., 2010). CHOP

is a tightly regulated transcription factor, only expressed during adipocyte differentiation and under a cellular stress response (Ohoka et al., 2007; Yang et al., 2017). CHOP is under the control of the FUS promoter in FUS-CHOP fusions, but ubiquitous over expression of CHOP alone in a mouse model is not enough to induce oncogenesis (Perez-Losada et al., 2000). The N-terminus of FUS provides unidentified oncogenic capacity to CHOP (Perez-Losada et al., 2000). FUS and CHOP are both diffuse nuclear proteins, but interestingly, FUS-CHOP is localized to distinct nuclear puncta (Thelin-Jarnum et al., 2002). The punctate pattern of expression is dependent on the N-terminus of FUS, as truncation results in diffuse nuclear localization (Goransson et al., 2002). Previous literature shows self-association and condensation of transcription factors and fusion proteins with IDRs can induce transcriptional reprogramming (Boehning et al., 2018; Boija et al., 2018; Boija et al., 2021; Cho et al., 2018; Crump et al., 2021; Gurumurthy et al., 2019; Lu et al., 2019; Lu et al., 2020; Sabari et al., 2018; Taniue and Akimitsu, 2021; Wei et al., 2020; Zuo et al., 2021). A recent *in vitro* study showed a potential role of FUS phase separation in driving oncogenesis, but these data have not been characterized in cells (Zuo et al., 2021).

FUS is a member of the FET family of proteins, which includes FUS, Ewing's sarcoma protein (EWS), and TATA-binding protein-associated factor 15 (TAF15). Like FUS, EWS and TAF15 both have been identified as fusion oncogenes in various types of cancer (Kovar, 2011). EWS-FLI1 fusions cause Ewing's sarcoma, the second most common pediatric and adolescent bone malignancy (Balamuth and Womer, 2010). Recent work has shown the PrLD of EWS confers an oncogenic transcriptional advantage that FLI1 does not have alone in

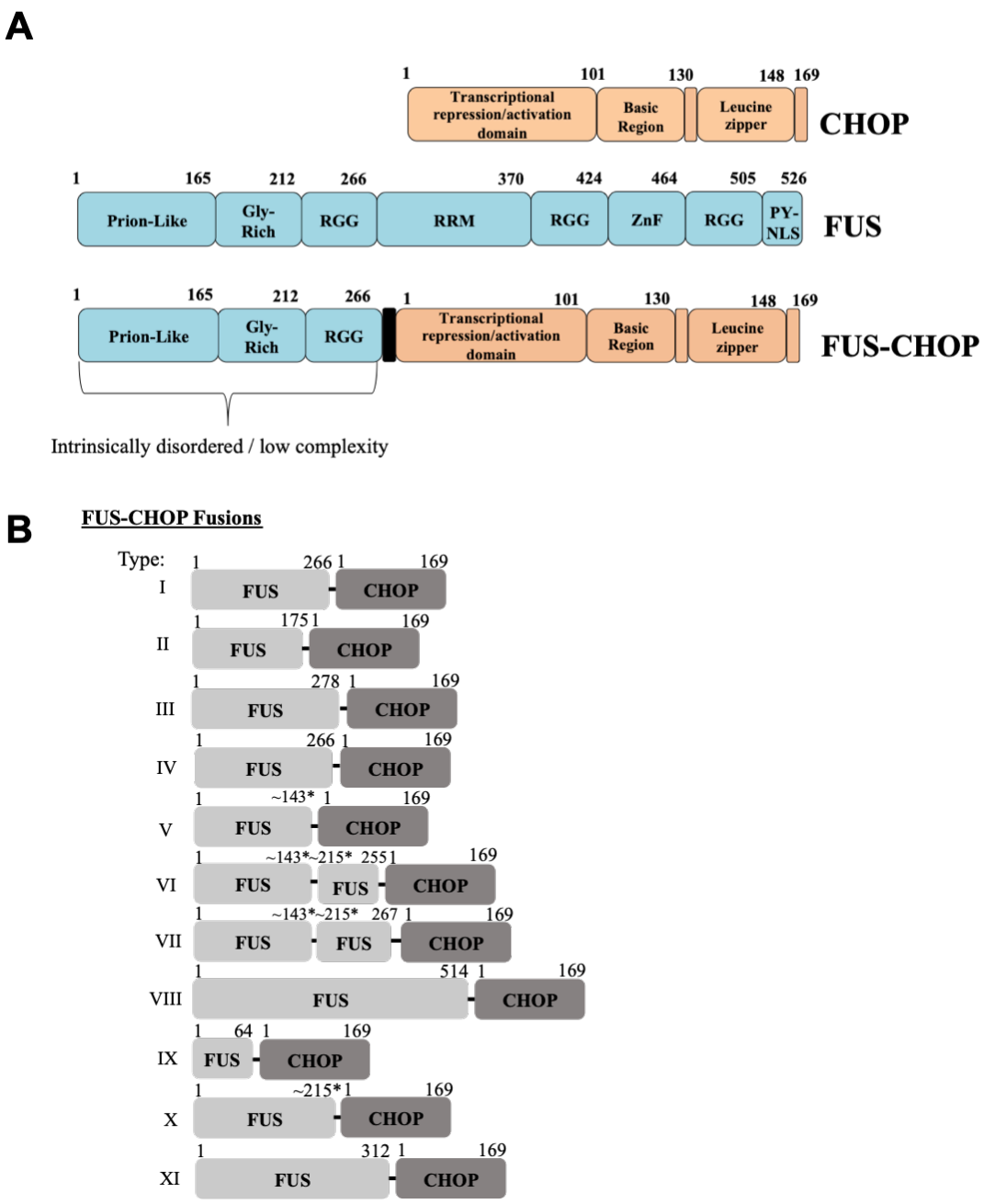

Fig 3. Schematic of the FUS-CHOP Fusion Proteins.

(A) FUS-CHOP type I contains the first 266 amino acids of FUS fused to full length CHOP. (B) There are 11 different types of FUS-CHOP fusions that have been identified in patients, all of which include varying lengths of FUS (all include the prion-like domain) fused to full length CHOP (Perez-Mancera and Sanchez-Garcia, 2005).

cells (Boulay et al., 2017). Mutations in the PrLD of EWS that disrupt phase separation were also shown to reduce EWS-FLI1 oncogenic effects (Boulay et al., 2017). EWS-FLI1 localizes to small nuclear hubs in Ewing's sarcoma cell lines and phase separates in the nucleus upon ectopic expression (Chong et al., 2018). In an *in vitro* study, EWS-FLI1 could undergo LLPS and EWS-FLI1 condensates can recruit Pol 2 to promote transcriptional activation when localized to their recognized binding sites. This transcriptional activation was reduced when condensate formation is disrupted by high salt concentrations (Zuo et al., 2021). These data suggest the FET oncogenic fusion proteins could be providing aberrant phase separation capacity to transcription factors, which results in transcriptional reprogramming and tumorigenesis.

Amyotrophic Lateral Sclerosis

ALS is a progressive neurodegenerative disease caused by deterioration of both upper and lower motor neurons (Hardiman et al., 2017). ALS initially presents with loss of gross motor control that eventually worsens and results in respiratory failure and death within 2-5 years of disease onset (Amado and Davidson, 2021). There are few effective treatments available for ALS patients and no known cure for this disease (Orszulak et al., 2016).

The majority of ALS cases are sporadic, but ~10% are familial cases and can be attributed to a known gene mutation ~70% of the time (Chia et al., 2018). In most cases of familial ALS (fALS), the known gene mutation is inherited through an autosomal dominant manner, but some do occur through recessive and X-linked inheritance (Boylan, 2015). The most common genes associated with fALS cases are chromosome 9 open reading frame 72 (*C9Orf72),* superoxide dismutase 1 (*SOD1)*, TAR DNA-binding

protein 43 kDa *(TDP-43)* and *FUS* (Siddique and Ajroud-Driss, 2011). A characteristic of fALS, and the proteins listed above, is proteinaceous inclusions (or aggregates) in deteriorating neurons that consist of the mutated gene's protein product (Blokhuis et al., 2013).

FUS linked mutations and cytoplasmic inclusions in ALS patients were first discovered in 2009 (Figure 4) (Kwiatkowski et al., 2009; Vance et al., 2009). Since, numerous groups have worked to understand aggregation propensity, mechanism, and modulation of aggregate formation. There are over 50 autosomal dominant FUS mutants that have been identified in fALS (Mejzini et al., 2019). In the majority of cases, mutations in FUS are localized to the C-terminus, disrupting the NLS, resulting in cytoplasmic mislocalization; but, there are cases in which FUS is mutated in the N-terminal PrLD, resulting in a highly-aggregate prone form of FUS (Patel et al., 2015; Shang and Huang, 2016). Like full-length FUS, mutant FUS has the ability to undergo PrLD-driven LLPS *in vitro* (Patel et al., 2015). Because of this capability and the observed aggregates in patient neurons, it is hypothesized that persistence in a liquid-phase separated state seeds favorable interactions that induce a pathogenic solid-phase transition (Monahan et al., 2017; Patel et al. 2015). In other neurodegenerative diseases, such as Alzheimer's disease and Parkinson's disease, proteinaceous inclusions (consisting of amyloid-β, tau, α-synuclein, etc.) are often rich in amyloid aggregates, but in ALS, the protein aggregates have different characteristics and are considered amyloid-like (Araki et al., 2019; Flores et al., 2016; Kryndushkin et al., 2011; Oakley et al., 2020; Sangwan et al., 2017).

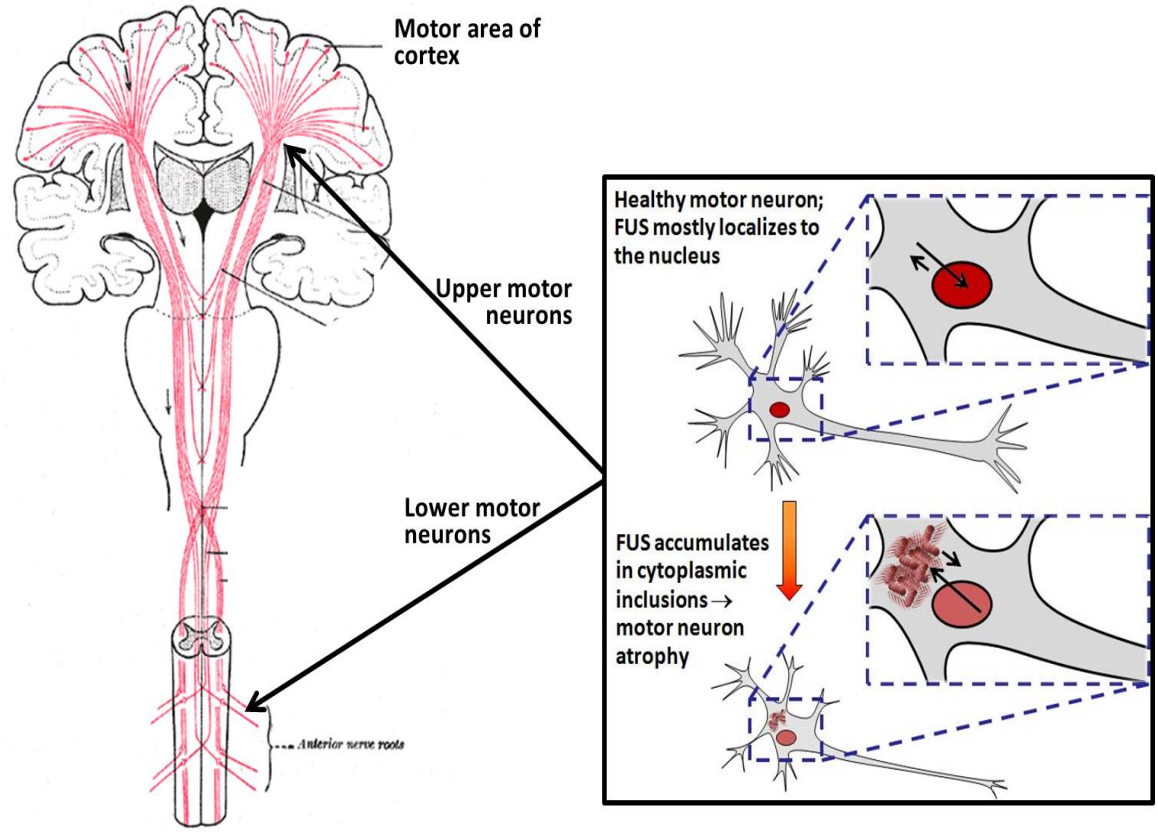

Fig 4. FUS accumulation in motor neurons in ALS

Mutant FUS accumulates in the cytoplasm in both upper and lower motor neurons in ALS. FUS mislocalization and aggregation is linked to neuronal deterioration.

There are multiple hypotheses surrounding FUS aggregates and cellular toxicity in ALS. Because FUS is sequestered into cytoplasmic inclusions and is not performing its general functions in the nucleus, loss of function toxicity has been identified as a mechanism of neuronal degeneration (Sun et al., 2015). Conversely, gain-of-function toxicity has also been evaluated with cytoplasmic FUS inclusions (Devoy et al., 2017; Sharma et al., 2016). ALS-FUS has altered, not disrupted, RNA binding capacity in the cytoplasm when compared to wild-type FUS or the other FET family proteins (Hoell et al., 2011). RNA binding is necessary for ALS-FUS pathogenesis, as mutant FUS with a non-functional RRM does not cause cellular toxicity (Daigle et al., 2013). The exact mechanism of FUS aggregate-driven cellular toxicity has not been fully elucidated, but protein aggregation in ALS is a known pathogenic hallmark.

Over the past decade, more work has highlighted protein aggregation as an important and potential therapeutic target (Malik and Wiedau, 2020; Mejzini et al., 2019). Scientists have developed antibody therapies (Maier et al., 2018; Pozzi et al., 2019), vaccines (Zhao et al., 2019), therapies targeting autophagy factors and the proteasome (Benatar et al., 2018; Maher, 2019; Mandrioli et al., 2019) and gene therapies (Bravo-Hernandez et al., 2020) to disrupt toxic aggregate formation. Our previous work with ALS-FUS utilized PTMs to disrupt the potential liquid-to-solid phase transition of FUS (Monahan et al., 2017; Rhoads et al., 2018a). Controlling the pathogenic solid aggregation in ALS could diminish FUS toxicity and therefore reduce motor neuron loss.

FUS PRION-LIKE DOMAIN

In both diseases described above, FUS is the driver of pathology. As previously, mentioned FUS contains an N-terminal PrLD, named because of its sequence homology

to yeast prion domains (Udan and Baloh, 2011). Yeast prions are proteinaceous infectious particles that can adopt distinct conformations that allow for self-propagation through recruitment of native protein (Prusiner, 1982; Wickner, 1994). Prions are historically known for their ability to form amyloid aggregates with in-register parallel cross-β structures, a conformation that is driven by the prion domain (Shewmaker et al., 2006). More recently, data has shown yeast prions and proteins with homologous PrLD can undergo a liquid-phase transition before a solid-phase transition is achieved (Gotor et al., 2020; Iglesias et al., 2019; Peskett et al., 2018).

The PrLD of FUS is enriched in uncharged polar amino acids, specifically serine, tyrosine, glycine, and glutamine (SYGQ). The PrLD alone is both sufficient and necessary for FUS liquid and solid-phase transitions (Kato et al., 2012). Nonspecific hydrogen bonding, pi-pi interactions, and hydrophobic interactions are the driving forces underlying PrLD-driven phase separation (Murthy et al., 2019). Disruption of these interactions results in dissolution of droplets or abrogation of droplet formation. Full-length FUS utilizes the PrLD interactions, but also depends on the dispersed RGG regions throughout the protein (Kato et al., 2012). Charged arginine residues can form cation-pi bonds with the aromatic side chains of tyrosine residues in the PrLD (Burke et al, 2015.; Kato et al., 2012; Patel et al., 2015). Cation-pi bonds are important for FUS phase separation as mutating tyrosine residues abrogates condensate formation (Kato et al., 2012; Lin et al., 2017).

FUS is studied for its liquid-phase separating capabilities, but is more well known for the toxic aggregates it can form in ALS. The aggregates of FUS are found along neuroanatomical pathways, suggesting a cell-to-cell transfer of mutant FUS in a prion-

like manner of transmission (R). FUS PrLD has a core region (amino acids 39-95) that constitutes the structure of the aggregates (Murray et al., 2017). This core drives FUS into cross-β fibrils, similar to those formed by yeast prion proteins (Kato et al., 2012; Murray et al., 2017). Cross-β architecture requires each monomer to be folded in β-sheet conformations, and to be aligned in-register with the following monomer (Shewmaker et al., 2006). This tight compaction is accomplished by specific interactions that occur between the monomers (Shewmaker et al., 2006). The core fibrils alone are reactive to thioflavin T, a dye used as a common diagnostic for amyloid aggregates, but in patient neurons, FUS fibrils are not detectable by these amyloid stains, making these fibrils unique and difficult to diagnose as amyloid (Murakami et al., 2015; Murray et al., 2017; Nomura et al., 2014).

The interactions driving FUS liquid- and solid-phase transition are sensitive, making them a target for therapeutic interventions. As previously mentioned, IDRs can be highly post-translationally modified. In the FUS PrLD alone, 34 residues can be post-translationally modified, with majority of these modifications (32 of 34) classified as putative phosphorylation sites (identified by mass spectroscopy or nuclear magnetic resonance) (Rhoads et al., 2018b). Phosphorylation of the PrLD occurs at serine or threonine residues and adds negative charges to the previously polar amino acid (Rhoads et al., 2018b). FUS can be phosphorylated by DNA-PK and ATR, two of the phosphoinositide 3-kinase-like kinases (PIKKs), following DNA damage (Gardiner et al., 2008; Rhoads et al., 2018a). The PIKKs have a known consensus site of S/T-Q; throughout the PrLD of FUS there are 12 PIKK and 20 non-PIKK consensus sites. We

previously confirmed two of the PIKK consensus sites (Ser26 and Ser30) are phosphorylated in the nucleus following DNA damage (Rhoads et al.).

Addition of phosphoryl groups to the PrLD adds negative charges throughout an inherently uncharged domain. Our previous work shows introducing 12 phosphomimetic substitutions (S/T > E) at the PIKK consensus sites or incubating the protein with DNA-PK *in vitro* disrupted both liquid and solid-phase transition of FUS (Monahan et al., 2017). Phosphorylation of FUS at the unconfirmed PIKK sites, the other 20 non-PIKK consensus sites, as well as under different types of cellular stress has not been evaluated.

FUS PrLD-driven liquid and solid phase transition

The liquid phase separated state of FUS is thought to be a functional transition, whereas the solid state is often linked to ALS pathology (Patel et al., 2015). FUS functionally phase separates at sites of DNA damage, in nuclear paraspeckles and in cytoplasmic stress granules (Kedersha and Anderson, 2007; Levone et al., 2021; Shelkovnikova et al., 2014). FUS is recruited to sites of DNA damage as part of the DNA damage response. When LLPS-deficient FUS is expressed in cells, phase separation and recruitment of repair proteins is reduced, suggesting a functional role for FUS phase separation in cells (Levone et al., 2021). Stress granules form temporarily to halt translation and reserve ATP during a cellular stress response (Kedersha and Anderson, 2007). FUS, as well as other RNA-binding proteins, and mRNA transcripts are recruited to stress granules where they demix, forming condensates, to reserve cellular energy (Pakravan et al., 2021). Liquid phase separation is generally observed as a favorable, functional condensation of macromolecules.

Persistence in the liquid phase separated state has been shown to lead to insoluble aggregate formation *in vitro* (Figure 5)(Murakami et al., 2015). Recombinant FUS will liquid-phase separate *in vitro* and over time evolve into irreversible aggregates (Murakami et al., 2015; Rhoads et al., 2018a; Rhoads et al., 2018b). Mutant FUS can phase separate *in vitro*, but when compared to control, ALS-associated mutations in FUS exacerbate the pathological phase transition (Patel et al., 2015). The *in vitro* data and the propensity of FUS to undergo a liquid phase transition in cells suggest this liquid-to-solid phase transition could be occurring in disease neurons.

Understanding the interactions necessary for liquid-phase transition and subsequent solid-phase transition are important for identification of therapeutic targets. Controlling the phase-transition landscape by targeting FUS PrLD could prove to be an efficacious therapy in controlling the debilitating effects FUS has in both myxoid liposarcoma and amyotrophic lateral sclerosis.

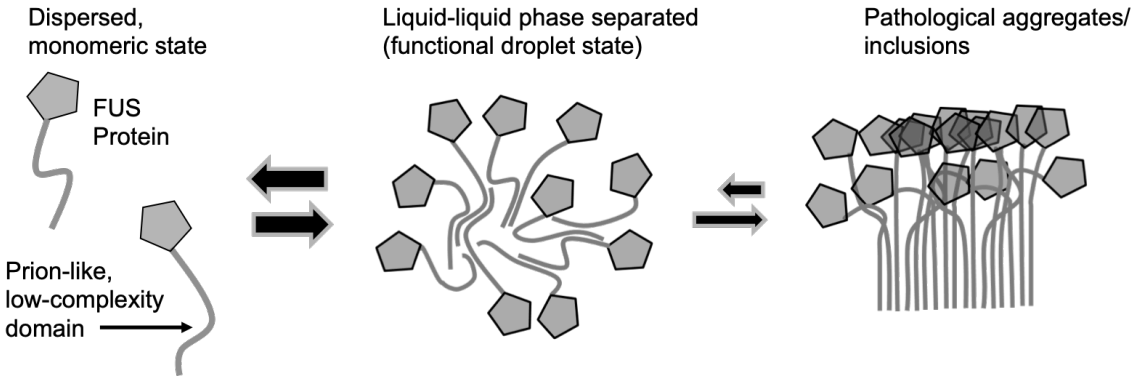

Fig 5. FUS liquid- to solid-phase transition

It is hypothesized that persistence of a high concentration of FUS in the liquid-phase separated state could seed favorable interactions that induce a solid-phase transition resulting in patholoigcal solid aggregation.

CHAPTER 2: The oncogenic transcription factor FUS-CHOP can undergo nuclear liquid-liquid phase separation

Izzy Owen[1], Debra Yee[1], Hala Wyne[1], Theodora Myrto Perdikari[2], Victoria Johnson[3], Jeremy Smyth[4], Robert Kortum[5], Nicolas L. Fawzi[3] and Frank Shewmaker[1]

1- Department of Biochemistry and Molecular Biology, Uniformed Services University, Bethesda, MD, USA

2- Center for Biomedical Engineering, Brown University, Providence, RI, USA

3- Department of Molecular Pharmacology, Physiology, and Biotechnology, Brown University, Providence, RI, USA

4- Department of Anatomy, Physiology and Genetics, Uniformed Services University, Bethesda, MD, USA

5- Department of Pharmacology and Molecular Therapeutics, Uniformed Services University, Bethesda, MD, USA

Published in *Journal of Cell Science,* August 2021.

ABSTRACT

Myxoid liposarcoma is caused by a chromosomal translocation resulting in a fusion protein comprised of the N-terminus of FUS (fused in sarcoma) and the full-length transcription factor CHOP (CCAAT/Enhancer Binding Protein Homologous Protein). FUS functions in RNA metabolism and CHOP is a stress-induced transcription factor. The FUS-CHOP fusion protein causes unique gene expression and oncogenic transformation. Though it is clear the FUS segment is required for oncogenic transformation, the mechanism of FUS-CHOP-induced transcriptional activation is unknown. Recently, some transcription factors and super enhancers were proposed to undergo liquid-liquid phase separation and form membraneless compartments that recruit transcription machinery to gene promoters. Since phase separation of FUS depends on its N-terminus, transcriptional activation by FUS-CHOP could result from the N-terminus driving nuclear phase transitions. Here, we characterized FUS-CHOP in cells and *in vitro*, and observed novel phase-separating properties relative to unmodified CHOP. Our data indicate FUS-CHOP forms phase-separated condensates at super enhancer transcriptional sites. We provide evidence that the FUS-CHOP phase transition is a novel oncogenic mechanism and potential therapeutic target for myxoid liposarcoma.

INTRODUCTION

Soft tissue sarcomas (STS) are diagnosed in roughly 12,000 patients in the United States each year with a mortality rate of approximately 40% (Siegel et al., 2015). Liposarcoma is the most common type of STS, accounting for around 20% of all adult STS diagnoses (Bock et al., 2020; Perez-Losada et al., 2000). Myxoid liposarcoma

(MLS) is the second most common liposarcoma and is distinguished by the cytogenetic hallmark of t(12;16)(q13;p11) (Bock et al., 2020; Suzuki et al., 2012). This chromosomal translocation creates a novel fusion protein composed of the N-terminus of FUS (fused in sarcoma) and full-length CHOP (CCAAT/Enhancer Binding Protein (C/EBP) Homologous Protein).

FUS is a ubiquitously expressed, predominantly nuclear DNA and RNA binding protein that functions in the DNA damage response, transcription, and RNA metabolism (Chen et al., 2019a; Tan et al., 2012; Zinszner et al., 1997). The N-terminal prion-like domain of FUS (~aa1-165) (PrLD) is required for FUS self-association, chromatin binding, and transcriptional activation (Yang et al., 2014). CHOP is a member of the C/EBP family of transcription factors that play a role in differentiation, proliferation, and energy metabolism in various cell types (Hu et al., 2018). Normally, CHOP expression is suppressed, but upregulated during differentiation and following cellular stress (Ohoka et al., 2007; Yang et al., 2017). In MLS, the fusion protein, FUS-CHOP, is expressed under the control of the FUS promoter, resulting in ubiquitous expression. Importantly, ubiquitous overexpression of CHOP alone in nude mice does not result in MLS, whereas expression of FUS-CHOP from the same promoter does, indicating that FUS provides novel oncogenic properties to the fusion protein (Perez-Losada et al., 2000).

Genome wide occupancy analysis of MLS cell lines found that 60% of FUS-CHOP protein mapped to putative enhancers, occupying 97% of super enhancers (SEs) defined by the presence of the H3K27ac chromatin modification (Chen et al., 2019b). SEs are clusters of transcriptional enhancers that recruit a high density of transcriptional regulators and machinery (Thandapani, 2019). In cancer, SEs can contain numerous

mediators, signaling factors, RNA polymerase II, and chromatin modifications (such as H3K27ac), which function together as regulators of oncogene expression (Bradner et al., 2017). In liposarcomas, SEs are involved in amplifying cancer pathways, cell migration, and angiogenesis (Chen et al., 2019b). A recent hypothesis is liquid-liquid phase separation (LLPS) of protein activators into condensates at SEs can control gene expression (Sabari et al., 2018; Schneider et al., 2021). Such condensation of macromolecules into distinct liquid-phase states ─ sometimes called membrane-less organelles (MLOs) or biomolecular condensates ─ is attributed to many cellular functions that require spatiotemporal regulation (Banani et al., 2017; Boija et al., 2021). The results of numerous studies suggest RNA polymerase II, transcription factors, coactivators, super-enhancer sequences, mediator proteins (MED1), and other transcriptional machinery containing IDRs functionally undergo LLPS at transcriptional start sites, regulating gene expression (Boehning et al., 2018; Boija et al., 2018; Boija et al., 2021; Cho et al., 2018; Crump et al., 2021; Gurumurthy et al., 2019; Lu et al., 2019; Lu et al., 2020; Sabari et al., 2018; Wei et al., 2020).

FUS and homologous proteins, EWS and TAF15, have been shown to undergo LLPS under several conditions (Chong et al., 2018; Maharana et al., 2018; Patel et al., 2015) and recruit the C-terminal domain of RNA polymerase II into *in vitro* condensates (Burke et al., 2015). During transcription, FUS and RNA polymerase II are suggested to co-localize into nuclear condensates (Thompson et al., 2018). In an MLS cell line, FUS-CHOP was found to co-localize at SEs with BRD4 – a protein that is proposed to control gene expression through the formation of phase-separated condensates at SEs (Sabari et al., 2018). FUS's N-terminal intrinsically disordered, low-complexity (LC) region (~aa 1-

212) facilitates LLPS in cells and *in vitro* (Burke et al., 2015; Monahan et al., 2017), and importantly, all MLS-causing FUS-CHOP translocations contain portions of this LC sequence (Oikawa et al., 2012; Powers et al., 2010). Similarly, the N-terminal regions of FUS, TAF15 and EWS are all translocated in various forms of sarcomas and leukemias, including Ewing's sarcoma, when fused to any of about a dozen transcription factors (Kovar, 2011). Previous work has shown FUS-CHOP localizes to nuclear punctate structures whereas FUS and CHOP are individually diffuse nuclear proteins (Thelin-Jarnum et al., 2002). These punctate structures were eliminated by truncation of FUS's LC region, thus restoring diffuse localization of FUS-CHOP when large segments of the LC region were removed (Goransson et al., 2002). The FUS-CHOP nuclear puncta have been shown to be distinct from other nuclear bodies, such as PML bodies, but interestingly, cajal bodies were shown to localize to the periphery of some of the puncta (Goransson et al., 2002; Thelin-Jarnum et al., 2002). The mechanism by which FUS-CHOP induces oncogenesis remains unknown; however, based on the above observations, we hypothesized that FUS-CHOP has novel phase-separating properties that may induce oncogenesis through condensate formation at transcription sites.

Here, we evaluate the propensity of FUS-CHOP to undergo LLPS *in vitro* and in cells. We assess localization of FUS-CHOP in MLS cancer cell lines and we demonstrate that ectopically expressed FUS-CHOP nuclear puncta have distinct liquid-like characteristics. We also observe FUS-CHOP puncta to colocalize with BRD4, which is a marker of phase-separated SEs (Sabari et al., 2018). Likewise, our results suggest FUS-CHOP can undergo a liquid-phase transition in the nucleus, which could provide the

mechanism for its emergent gain-of-function oncogenicity. This may be a general mechanism for transcriptional activation by fusion oncoproteins with IDRs.

RESULTS

Recombinant FUS-CHOP undergoes LLPS *in vitro*.

Both recombinant full-length FUS and its LC region have previously been shown to undergo LLPS *in vitro* (Burke et al., 2015; Patel et al., 2015). Likewise, droplets formed by FUS LC fused to Gal4 have liquid-like dynamics when assessed by fluorescence recovery after photo-bleaching (FRAP) (Zuo et al., 2021). To determine if recombinant oncogenic FUS-CHOP can undergo LLPS under similar conditions *in vitro*, we purified the most common type of FUS-CHOP translocation, type II (11 truncation variants of FUS-CHOP have been characterized from patient samples, with the most common being type II and type I, respectively (Figure 14)) (Bode-Lesniewska et al., 2007; Oikawa et al., 2012). FUS-CHOP type II contains the first 175 amino acids of FUS fused to full-length CHOP. CHOP's transcriptional activation and repression domain, basic region for DNA binding, and leucine zipper are included in all FUS-CHOP fusions (Figure 6A, 14). Using the N-terminal maltose binding protein (MBP) tag that we previously used for full-length FUS (Burke et al., 2015; Monahan et al., 2017; Owen et al., 2020), we purified FUS-CHOP type II and CHOP (as a control) from *Escherichia coli* (attempts to purify FUS-CHOP type I were not successful due to insolubility) (Figure 6A). Similar to our previous observations for wild-type full-length FUS (Burke et al., 2015; Monahan et al., 2017; Owen et al., 2020), upon cleavage of the MBP tag with TEV protease, we observed FUS-CHOP type II droplet formation (Figure 6B). Concomitant with phase separation, we observed increased turbidity over time for FUS-CHOP type II

(Figure 6C). CHOP alone showed no droplets or marked turbidity after cleavage of the MBP tag, demonstrating that elements within FUS's LC sequence drive phase separation. We also assessed FUS-CHOP type II phase separation via turbidity over time with varying salt concentrations (Figure 6D). The phase behavior of FUS-CHOP is more sensitive to the presence of salt in solution compared to previous observations of full-length FUS. At concentrations of salt above 150 mM, we observed an increase in turbidity, suggesting a decrease in solubility likely due to "salting out" of the regions that contribute to hydrophobic interactions, similar to that observed with FUS LC alone (Burke et al., 2015; Monahan et al., 2017). Overall, these data suggest that the LC domain of FUS provides FUS-CHOP a greater capacity to self-associate and undergo LLPS relative to the unfused CHOP protein.

Ectopically expressed FUS-CHOP-eGFP is undergoing LLPS in the nucleus.

Previous work showed ectopically expressed FUS-CHOP-GFP type II formed distinct nuclear puncta (Thelin-Jarnum et al., 2002). For localization controls, we first ectopically expressed both FUS-eGFP and CHOP-eGFP in NIH 3T3 cells and confirmed diffuse nuclear localization for both proteins (Figure 7A). We then ectopically expressed FUS-CHOP type I and type II eGFP-tagged fusion proteins (Figure 7B,C), and observed numerous round nuclear puncta of both the type I and type II constructs (Figure 7D). To ensure these structures were not the result of the eGFP tag, we also expressed untagged FUS-CHOP type I and type II (Figure 7C); the untagged proteins formed similar punctate structures (Figure 7D). Because this nuclear punctate localization pattern of FUS-CHOP is not diffuse like either wild-type FUS or CHOP (Figure 6A), we hypothesized the

puncta are phase-separated condensates driven by FUS's intrinsically disordered LC region.

Phase-separated condensates in cells are typically characterized by three hallmarks: spherical in shape, undergo fusion upon touching, and rapid internal dynamics and external exchange (Hyman et al., 2014). We used live-cell imaging to assess the puncta in 3-Dimensions. We observed spherical nuclear puncta of FUS-CHOP-eGFP type I and type II (Figure 8A). Imaging the cells over time revealed free movement around the nucleus consistent with Brownian motion. We observed frequent fusion events in which a single sphere formed when two spheres made contact (Figure 8A, 15). To quantify internal rearrangement and external exchange of FUS-CHOP puncta, we used fluorescence recovery after photobleaching (Figure 8B). Previous work indicates that intracellular liquid-state condensates have half-times of recovery from seconds to minutes (Banani et al., 2017). Here, we bleached both type I and II puncta and observed an average half-time of recovery of ~19 seconds and ~14 seconds, respectively (Figure 8C, D). CHOP-eGFP FRAP data were included as a diffuse control. Together these data show that ectopic FUS-CHOP forms nuclear condensates and has the major hallmarks of LLPS.

We also observed that the type I puncta moved more rapidly (they were less static) than the type II. We hypothesize that the RGG repeats present in the longer type I fusion (but not the type II; Figure 6A, 7B) could be driving additional protein-protein (Ryan et al., 2018; Wang et al., 2018) or protein-RNA interactions (as the LC does not interact with RNA (Burke et al., 2015)), leading to more mobility throughout the nucleus. However, we did not pursue this observation further.

Phase separation of FUS-CHOP-eGFP is dependent on the FUS prion-like domain.

FUS's LC domain is composed of a PrLD followed by a short glycine-rich region (Figure 6A) - both of which are IDRs with little complexity in their amino-acid composition. PrLDs are frequently linked to both LLPS and formation of pathological inclusions in neurodegenerative diseases (March et al., 2016). FUS's PrLD facilitates LLPS of wild-type FUS (Burke et al., 2015), but its truncation inhibits LLPS (Patel et al., 2015). In earlier work when the PrLD of FUS-CHOP fusions was serially truncated, there was a concomitant dissolution of nuclear puncta (Goransson et al., 2002). To determine the dependence of phase separation on the PrLD (~aa 1-165), we removed the first 25, 50, 75 and 125 amino acids in type I and type II fusion constructs of FUS-CHOP-eGFP and expressed them in NIH 3T3 cells (Figure 9A, B). We observed retention of punctate structures upon removal of up to 50 amino acids (type I is shown in Figure 9C; identical results for type II are in Figure 16B). Removing 75 or 125 amino acids resulted in a diffuse pattern of expression (Figure 9C, 16). Increasing the concentration of FUS-CHOP-eGFP DNA (full length or truncated) in cellular transfections did not yield observable changes in nuclear pattern of expression, indicating LLPS is determined by the length of FUS's PrLD, but not expression levels.

Several studies have indicated tyrosine motifs have an impact on phase separating proteins (Chong et al., 2018; Lin et al., 2017; Murthy et al., 2019). When 10 tyrosine-to-serine mutations are introduced in the EWS-FLI1 fusion protein, a significant reduction of self-association is observed in cells (Chong et al., 2018). Here, a similar trend is observed as removal of the first 75 amino acids of FUS also removes 11 tyrosine motifs and diminishes FUS-CHOP phase separation. The relationship between number of

tyrosine motifs present and phase separation capabilities is consistent with all of the truncations utilized in this study (Table 1, Figure 9). We further characterized how these truncations affected puncta formation by quantifying the amount of transfected cells with nuclear puncta (Figure 9D). We observed a decreasing trend of puncta formation with increasing truncation length. To characterize how the PrLD of FUS affects FUS-CHOP LLPS, we used FRAP to quantify recovery time of the truncated proteins within the puncta. We observed a quicker half-time of recovery as the PrLD was shortened, suggesting length can affect dynamic movement into or within the phase-separated condensate (Figure 9E). Type I condensates contain more of FUS's N-terminal sequence (266aa) and consistently recover slower than type II (175aa), including truncated proteins. The length and low-complexity features of FUS's PrLD appear to be the dominant factors in governing FUS-CHOP LLPS as opposed to any particular sequence element.

The above observation suggests that the interactions driving FUS-CHOP phase separation require most of the PrLD to be intact (See Figure 6A). These data could point to a special feature or structure in the region spanning residues 51 to 75 of the FUS PrLD; yet, our previous work suggests that the PrLD does not populate specific rigid structures even in the liquid form (Murthy et al., 2019). Therefore, we also created internal PrLD truncations to test if the location of the truncation is not important, but instead if the total length of the PrLD present determines phase separation. To this end, we created FUS-CHOP constructs with internal PrLD deletions. We deleted amino acids 50-75, 75-125, and 50-125 in both FUS-CHOP-eGFP type I and type II constructs (Figure 10A, 17A) and ectopically expressed them in NIH 3T3 cells to determine their effects on LLPS

(Figure 10B, C). As with the N-terminal truncations, these constructs were observed to form spherical nuclear punctate structures upon removal of 25 or 50 amino acids (Figure 10C). Removing 75 amino acids within the PrLD resulted predominantly in a pattern of diffuse expression in the nucleus. We quantified the percentage of transfected cells with nuclear puncta and observed the same trend as the N-terminal truncations (Figure 10D).

To determine if DNA binding is necessary for FUS-CHOP phase separation, we created a previously established DNA binding mutant lacking the basic region of CHOP (amino acids 101-122; ΔDBD) (Figure 10A) (Ubeda et al., 1996). When FUS-CHOP ΔDBD was expressed in cells, we observed no disruption in nuclear condensate formation (Figure 10C, 17C), suggesting that LLPS is not dependent on CHOP's DNA-binding ability. These data suggest that the PrLD is the main driver of FUS-CHOP-eGFP phase separation and its length and low-complexity composition determine in-cell phase separation.

FUS-CHOP is localized in small nuclear punctate structures in myxoid liposarcoma cell lines.

We next sought to characterize endogenous FUS-CHOP in patient-derived cells. We assessed endogenous expression and localization of FUS-CHOP in three different MLS cell lines. MLS-402 and MLS-1765 were both established and immortalized by transfection with SV40 large T-antigen, while DL-221 was spontaneously immortalized from patient tumor samples (Aman et al., 1992; de Graaff et al., 2016; Thelin-Jarnum et al., 1999). MLS-402 and DL-221 both contain type I fusions like we used in ectopic expression, while MLS-1765 has a type VIII fusion that encompass the first 514aa of FUS (Figure 11A, 14). All three cell lines showed FUS-CHOP localized to small nuclear

punctate structures in every cell, similar to those seen in a previous study evaluating oncogenic EWS-FLI1 fusions in cancer cell lines (Figure 11B)(Chong et al., 2018). Localization of FUS-CHOP in all cell lines was punctate and nuclear, but expression levels of type VIII were greater than type I fusions (Figure 11C). Fixed-cell imaging indicated smaller punctate structures in the cancer cell lines than observed for the ectopically expressed proteins in NIH 3T3 cells.

SE protein BRD4 localizes with FUS-CHOP.

In a previous study, FUS-CHOP was shown to occupy 9% of active promoter sites and 60% of putative enhancer sites in an MLS cell line (Chen et al., 2019b). Using ChIP-seq, the authors found that FUS-CHOP occupied 40% of the same enhancers as BRD4 (Chen et al., 2019b), which itself localizes to enhancer sites marked by acetylated histones (Loven et al., 2013). The authors concluded that FUS-CHOP and BRD4 cooperate at oncogenic SEs in MLS (Chen et al., 2019b). Importantly, BRD4 has an intrinsically disordered C-terminal domain that purportedly drives its phase separation into nuclear puncta at super enhancers in cell models (Sabari et al., 2018). If FUS-CHOP is undergoing LLPS at SEs in our MLS cell lines, then we would predict colocalization with BRD4 at nuclear puncta.

We probed our MLS cancer cell lines for BRD4 puncta and assessed its colocalization with FUS-CHOP (Figure 12A). The average Pearson's correlation coefficient between BRD4 and FUS-CHOP was 0.440, 0.438, and 0.478 in MLS-1765, MLS-402, and DL221 cell lines, respectively (Figure 12B). We also evaluated colocalization in our ectopic-expression model. We expressed both FUS-CHOP-eGFP type I and type II in NIH 3T3 cells and probed for BRD4 (Figure 12C). We saw small

BRD4 puncta throughout the nucleus in the control, but in the FUS-CHOP-GFP expressing cells, BRD4 localized to the large FUS-CHOP-eGFP puncta. The average Pearson's correlation coefficient between BRD4 and FUS-CHOP was 0.688 and 0.780 for type I and type II FUS-CHOP-eGFP, respectively. These data suggest FUS-CHOP and BRD4 occupy the same nuclear condensates at SEs and FUS-CHOP could be recruiting BRD4 to oncogenic condensates.

To determine the importance of FUS-CHOP DNA-binding and BRD4 condensation, we ectopically expressed our FUS-CHOP-eGFP type I and II DNA-binding deficient mutants and probed for BRD4. We observed BRD4 localizing to large FUS-CHOP-eGFP puncta (Figure 13A). We quantified the Pearson's correlation coefficient between BRD4 and FUS-CHOP-eGFP ΔDBD and observed a significant decrease in colocalization when compared to the full-length counterparts (Figure 13B). These data suggest that BRD4 and FUS-CHOP interaction is influenced by DNA binding, but is governed by phase separation that is driven by the N-terminus of FUS.

DISCUSSION

Macromolecular condensates that form via LLPS are implicated in many sub-cellular processes (Alberti and Hyman, 2021). Condensates have recently been proposed to also have roles in pathological events like oncogenic transcription (Boija et al., 2021). In such cases, oncogenesis would depend on the condensation of transcription factors, mediator complex proteins, and chromatin remodeling proteins to high density at specific SEs and promoter sequences (Boija et al., 2021). Here, we assessed the pathological FUS-CHOP fusion protein ─ which causes aberrant transcription in MLS (Joseph et al., 2014) ─ and its capacity to undergo LLPS *in vitro* and in cell models. Our data indicate

that N-terminal regions of FUS provide CHOP with novel LLPS properties. In MLS cell lines, we observed the localization of FUS-CHOP condensates at SEs, suggesting that FUS-CHOP LLPS at transcriptional start sites could be integral to oncogenic mechanisms.

FUS is a member of the FET family of proteins, along with EWS and TAF15, which can all undergo LLPS in the nucleus of cells and *in vitro* (Maharana et al., 2018). All three proteins contain an intrinsically disordered, N-terminal PrLD responsible for driving LLPS and each protein has been found in oncogenic fusions with transcription factors (Linden et al., 2019; Riggi et al., 2007). Under endogenous conditions, the FET family proteins and their fusion partners are mostly diffuse in the nucleus (Andersson et al., 2008). However, as oncogenic fusion proteins, all localize to distinct nuclear puncta (Chong et al., 2018; Thelin-Jarnum et al., 2002). The formation of dysregulated condensates, especially at SEs, is proposed to be an underlying feature of some cancers (Boija et al., 2021). We show FUS-CHOP can undergo LLPS in the nucleus and form distinct punctate structures with liquid-like dynamics. These condensates could provide an enhanced transcriptional advantage to MLS cells. Concomitant to this study, Zuo *et al* corroborated this hypothesis using an *in vitro* transcriptional model. Their data showed the formation of FUS and EWS fusion-protein condensates was disrupted with high salt, which then reduced transcriptional output (Zuo et al., 2021). These data suggest a phase-separating pathological mechanism could be common to FET-fusion oncogenic proteins.

The fusion of EWS and the transcription factor FLI1 causes Ewing's Sarcoma (Chong et al., 2018). The EWS-FLI1 fusion protein forms condensate-like hubs that are necessary for driving oncogenic transcription (Chong et al., 2018). Here, we see similar

results with FUS-CHOP phase separation in the MLS cancer cell lines. To understand how FUS-CHOP might modify the transcriptional landscape in MLS, we looked at the localization of BRD4 – a protein shown to phase separate at SEs. BRD4 has also been shown to colocalize with FUS-CHOP in MLS (Chen et al., 2019b). The C-terminal domain that drives BRD4's LLPS is necessary for its function (Wang et al., 2019), suggesting function could be linked to LLPS. Here, in MLS cancer lines, we observed FUS-CHOP nuclear condensates to localize with BRD4. Similarly, in the ectopic expression system, we observed BRD4 localization and consolidation into the large condensates composed of FUS-CHOP-eGFP. This suggests FUS-CHOP could be driving phase separation of BRD4 at oncogenic SEs in MLS. These findings provide a mechanism by which oncogenic fusion proteins, such as EWS-FLI1 and FUS-CHOP, could hijack BRD4 and other bromodomain-containing proteins to induce oncogenic SEs (Chen et al., 2019b; Gollavilli et al., 2018). FUS-CHOP has also been reported to localize to sites of chromatin remodeling, specifically interacting with the SWI/SNF chromatin remodeling complex. This interaction is dependent on FUS's PrLD, as truncation eliminates the association (Yu et al., 2019). Together, these data suggest a role of FUS-CHOP LLPS in chromatin remodeling and transcription, conferring a gain of function advantage in oncogenesis.

All FUS-CHOP fusion variants that cause MLS contain segments of FUS's PrLD (many also contain longer segments that include the entire LC region, but no fusions lack PrLD segments (Figure 14). The PrLD drives LLPS of full-length FUS *in vitro* and in cells (Burke et al., 2015; Wang et al., 2018). Our data indicate that the PrLD confers its phase-separating capacity to FUS-CHOP. The PrLD is approximately 165-residues long,

but the induction of LLPS of FUS-CHOP type I and II could still be achieved after truncating the first 50 amino acids from the N-terminus. Since the PrLD consists mostly of a few redundant amino acids (SQGY), it does not appear that any sequence feature or motif is required to induce LLPS, but simply a segment of sufficient length. Nearly all characterized FUS-CHOP variants (10 of 11) contain the entire PrLD (Figure 14) (Oikawa et al., 2012), suggesting that shorter fusions are either less probable or less likely to induce MLS transformation. Rare cases of EWS-CHOP fusions have been shown to cause MLS (Kirsanov et al., 2020; Suzuki et al., 2010). This also suggests that the addition of an IDR to CHOP, which provides for phase-separating capabilities, is sufficient to induce oncogenesis, similar to other findings showing IDR replacement approaches (Rawat et al., 2021).

The atomic-level structure of condensates appears to be non-static (Burke et al., 2015). However, rigid amyloid-like interactions have been proposed to support the architecture of condensates (Kato et al., 2012; Murray et al., 2017). A segment within FUS's PrLD (residues 39-95), forms a highly ordered amyloid structure in the recombinant protein (Murray et al., 2017). It was suggested that similar amyloid-like interactions formed by this segment could underlie the structure of the phase-separated state. However, when we deleted an internal portion of the PrLD (residues 75-125), ectopic FUS-CHOP still displayed LLPS properties. This observation suggests that LLPS is a feature that emerges from the low-complexity, intrinsically disordered nature of the PrLD and is not the consequence of a precise sequence element.

Phase separation as a mechanism of transcriptional regulation has not been definitively established (McSwiggen et al., 2019); largely because transcriptional

activation sites are small and dynamic, and thus make it challenging to design experiments that strongly support or refute an LLPS hypothesis (McSwiggen et al., 2019). Regardless, LLPS of enhancer-binding proteins, transcription factors and RNA polymerase II at transcriptional sites has been proposed by several groups (Boija et al., 2018; Cho et al., 2018; Hnisz et al., 2017). An LLPS model is attractive because it could explain the low-complexity, intrinsically disordered sequences that are common to transcription factors and coactivators as these sequences can support multivalent interactions and are prone to phase-separation. Our data do not provide an answer to the molecular-level details of FUS-CHOP-induced transcription in cancer cells. However, our data clearly show that both recombinant and ectopically expressed FUS-CHOP have the capacity to undergo LLPS, whereas this property is not observed for wild-type CHOP under identical conditions. Ectopic expression is imperfect because it may cause proteins to exceed critical concentrations that would not be normally achieved *in vivo* (McSwiggen et al., 2019). If proteins like BRD4 are indeed marking distinct liquid-phase states at transcriptional start sites, then FUS-CHOP's co-localization and capacity to undergo LLPS suggests that oncogenic transcription patterns could emerge from a phase-separated state. Recently, some cancer drugs have been shown to partition into biomolecular condensates (Klein et al., 2020), and drug concentration within condensates has been shown to influence therapeutic efficacy (Klein et al., 2020). If FUS-CHOP LLPS is integral to oncogenic cellular reprogramming, then this provides a new avenue for pharmacological exploration.

METHODS

Cell culture. NIH 3T3 (CRL-1658™, ATCC®, Manassas, VA, USA) were cultured in DMEM (D6429, Sigma-Aldrich, St. Louis, MO, USA) supplemented with 10% calf bovine serum (30-2030™, ATCC®, Manassas, VA, USA) and 1% penicillin-streptomycin (15140148, ThermoFisher, Waltham, MA, USA). DL-221 (MD Anderson cell core, Houston, TX, USA) cells were cultured in DMEM (11875093, ThermoFisher, Waltham, MA, USA) supplemented with 10% fetal bovine serum (F6178, Sigma-Aldrich, St. Louis, MO, USA) and 1% penicillin-streptomycin. MLS402-91 and MLS1765-92 (*received from Pierre Aman*, University of Gotenburg, Gotenburg, Sweden) were cultured in RPMI (11875093, ThermoFisher, Waltham, MA, USA) supplemented with 10% fetal bovine serum and 1% penicillin-streptomycin. Cells were lysed with a modified RIPA buffer (200 mM NaCl, 100 mM Tris-HCl pH 8, 0.5% sodium deoxycholate, 1% Triton X-100, 670 mM phenylmethylsulfonyl fluoride, 1250 units of benzonase nuclease (E8263, Sigma-Aldrich, St. Louis, MO, USA), 150 µL protease inhibitor cocktail (1861278, ThermoFisher, Waltham, MA, USA), and 100 µL phosphatase inhibitor (78426, ThermoFisher, Waltham, MA, USA)) for 30 minutes on ice.

Transfections. DNA was transfected into NIH 3T3 cells at ~70-80% confluency using Lipofectamine 2000 (11668027, ThermoFisher, Waltham, MA, USA) and OptiMEM (31985070, ThermoFisher, Waltham, MA, USA) in a ratio of 3-6 µg DNA to 2.5 µL Lipofectamine 2000 and incubated at 37ºC for 24 hours unless otherwise stated.

Cloning/plasmids. FUS-CHOP type I and type II genes were synthesized by Genscript (Piscataway, NJ, USA) and subcloned into pcDNA3-EGFP (Addgene #13031, deposited by Doug Golenbock) or 6xHis-MBP-FUS FL WT (Addgene #98651, deposited by Nicolas Fawzi) to produce the fusion plasmids. The FUS-CHOP truncations (Δ25, Δ50, Δ75, Δ125, and internal FUS 50-75, 75-125, 50-125 deletions) were generated through PCR cloning using the Phusion High-Fidelity DNA Polymerase (F531S, ThermoFisher, Waltham, MA, USA), designed with either BamHI/Xho or HindIII/BamHI restriction sites. The FUS-CHOP DNA binding Δ101-122 mutants were generated through Q5 site directed mutagenesis (E0554S, New England BioLabs, Ipswich, MA, USA).

Primer sequences (Integrated DNA Technologies, Coralville, IA, USA) used in the constructs were as followed:

FUS forward (CACAAGCTTATGGCCTCAAACGATTATACCCAA),

FUS Δ25 forward (CACGGATCCATGTATTCCCAGCAGAGCAG),

FUS Δ50 forward (CACGGATCCATGTATGGCCAGAGCAGC),

FUS Δ75 forward (CACGGATCCATGTATGGCTCGACTGGC),

FUS Δ125 forward (CACGGATCCATGCCCCAGAGTGGGAGC),

FUS Δ50 reverse (GTGGGATCCGCCTGAAGTGTCCGTGGA), FUS Δ75 reverse (GAGGGATCCTCCCTGGGGAGTTGACTGA)

eGFP reverse (TGCTCACCATCTCGAG), CHOP Δ101-122 forward (AAAGAACAGGAGAATGAAAGG), CHOP Δ101-122 reverse (CCCTTGGTCTTCCTCCTC)

Western blotting. Lysates were mixed with 4x NuPAGE LDS Sample Buffer (NP0008, ThermoFisher, Waltham, MA, USA) and electrophoresed through AnyKD precast gels (4569034, Bio-Rad Laboratories, Hercules, CA, USA) at 80 V for 2 hours. Gels were transferred through eBlot L1 (L00686, GenScript, Piscataway, NJ, USA) onto nitrocellulose membranes (1620112, Bio-Rad Laboratories, Hercules, CA, USA). Membranes were blocked with 6% milk (1706404, Bio-Rad Laboratories, Hercules, CA, USA) in Tris buffered saline (TBS) (J640, VWR International, Radnor, PA, USA). Primary and secondary antibodies were diluted in TBS with 0.1% Tween-20 (P7949, Sigma-Aldrich, St. Louis, MO, USA). The following primary antibodies were used to probe the blots: 1:5000 FUS (A300-302A, Bethyl Laboratories, Montgomery, TX, USA), 1:1000 CHOP (2895S, Cell Signaling Technology, Danvers, MA, USA), and 1:10,000 gamma tubulin (T6557, Sigma-Aldrich, St. Louis, MO, USA). Primary antibodies were detected with secondary antibodies conjugated to 1:20,000 IRDye fluorescent probes (926-68021, 926-32210, LI-COR Biosciences, Lincoln, NE, USA). Blots were imaged with the Odyssey CLx Imaging System (LI-COR Biosciences, Lincoln, NE, USA). Blot processing was done using Image Studio software (Li-COR Biosciences, Lincoln, NE, USA).

Microscopy (fixed & live cell imaging techniques). For fixed cell imaging, cells were grown on glass coverslips for 24 hours and fixed with 4% paraformaldehyde (P6148, Sigma-Aldrich, St. Louis, MO, USA). The cells were permeabilized in cold methanol (-20ºC) and blocked with 5% normal goat serum (ab7481, Abcam, Cambridge, United Kingdom) with 0.05% sodium azide (S2002, Sigma-Aldrich, St. Louis, MO, USA). The following antibodies were used to probe the fixed cells: 1:5000 FUS (A300-302A, Bethyl

Laboratories, Montgomery, TX, USA), 1:1000 CHOP (2895S, Cell Signaling Technology, Danvers, MA, USA), and 1:750 BRD4 (ab128874, Abcam, Cambridge, United Kingdom). Secondary antibodies used to detect primary antibodies were 1:2500 AlexaFluors AF488 and AF568 (A-11001, A-11011, ThermoFisher, Waltham, MA, USA). Nuclei were stained using Prolong mounting media with DAPI (P36931, ThermoFisher, Waltham, MA, USA). Slides were imaged using the Nikon A1R (Melville, NY, USA) and the Zeiss 980 with Airyscan (Oberkochen, Germany). Airyscan images were taken using the smart setup settings. Images were directly processed using the Zeiss system. All fixed cell images were further processed using ImageJ and Photoshop. Pearson's correlation coefficient was calculated using the EzColocalization plug-in in Fiji (Stauffer et al., 2018).

For live cell imaging, cells were grown in glass bottom microwell dishes 24 hours prior to transfection. The cells were incubated at 37ºC for 24 hours post transfection. Before imaging, the media was changed to dye-free DMEM (21063029, ThermoFisher, Waltham, MA, USA). To analyze dynamics and fusion events of FUS-CHOP spheres, time-lapse, 3-dimensional confocal imaging was carried out using the resonant scanner and Piezo Z-stage controller of the Nikon A1R microscope. Z-stacks with an interval of 0.5 μm that encompassed the nucleus of a single cell were acquired every 2 seconds over a 4 minute time period. The Z-stacks were then processed to generate 3-dimensional renderings using Nikon Elements software, and time lapse renderings were converted to video files. FRAP experiments were also carried out on the Nikon A1R. The center of a granule, marked by a 0.3 μm region of interest, was bleached at 50% power for 1.9 seconds using the 488 nm laser. The recovery was analyzed for 98 seconds (~1.5

minutes) with image acquisitions every second. The recovery was quantified using the time series analyzer V3 plugin on Fiji. The bleached pixel intensity was subtracted from each data point and then data points were normalized to the pixel intensity before the bleaching occurred.

***In vitro* expression and purification of FUS-CHOP fusion and CHOP.** N-terminally MBP-tagged (pTHMT) FUS-CHOP fusion type II and CHOP oncogene were expressed in *Escherichia coli* BL21 Star (DE3) cells (C600003, ThermoFisher, Waltham, MA, USA). Bacterial cultures were grown to an optical density of 0.7–0.9 before induction with 1 mM isopropyl-b-D-1-thiogalactopyranoside (IPTG) for 4 hours at 37ºC. Cell pellets were harvested by centrifugation and stored at -80ºC. Cell pellets were resuspended in approximately 20 mL of 20 mM sodium phosphate, 1 M NaCl, 10 mM imidazole, pH 7.4 with one Roche EDTA-free protease inhibitor tablet (11697498001, Sigma-Aldrich, St. Louis, MO, USA) for approximately 2 g cell pellet and lysed using the Avestin Emulsiflex C3 (Ottawa, Ontario, Canada). The lysate was cleared by centrifugation at 47,850 x *g* for 50 min at 4ºC, filtered using a 0.2 μm syringe filter, and loaded onto a HisTrap HP 5 mL column (17524701, Cytiva, Marlborough, MA, USA). The protein was eluted with a gradient from 10 to 300 mM imidazole in 20 mM sodium phosphate, 1 M NaCl, pH 7.4. Fractions containing MBP-tagged FUS-CHOP fusion type II or CHOP were loaded onto a HiLoad 26/600 Superdex 200 pg column (28-9893-36, Cytiva, Marlborough, MA, USA) equilibrated in 20 mM sodium phosphate, 1.0 M NaCl. Fractions with high purity were identified by SDS–PAGE and concentrated using a centrifugation filter with a 10 kDa cutoff filter (ACS501024, MilliporeSigma, Burlington,

MA, USA). MBP-FUS-CHOP fusion type II and MBP-CHOP proteins were then flash frozen in 25% glycerol.

Turbidity measurements. Turbidity was used to evaluate phase separation of 50 μM MBP-FUS-CHOP fusion type II and MBP-CHOP in the presence of 0.01 mg mL^{-1} TEV protease (~ 0.3 mg mL^{-1} in 50 mM Tris, 1 mM EDTA, 5 mM DTT pH 7.5, 50% glycerol, 0.1% Triton-X-100). The experiment was performed in 50 mM Tris, 150 mM NaCl pH 7.4. Turbidity experiments were performed in a 96-well clear plate with 70 μL samples sealed with optical adhesive film to prevent evaporation (4311971, ThermoFisher, Waltham, MA, USA). The absorbance at 600 nm was monitored over time using a Cytation 5 Cell Imaging Multi-Mode Reader (BioTek Instruments, Winooski, VT, USA) at 5 minute time intervals for up to 12 hours with mixing and subtracted from a blank buffer with no turbidity.

DIC microscopy. For 50 μM MBP-FUS-CHOP type II fusion and MBP-CHOP, the samples were incubated with 0.03 mg mL^{-1} TEV protease for ~ 20 minutes before visualization. Samples were spotted onto a glass coverslip and droplet formation was evaluated by imaging with differential interference contrast on an Axiovert 200M microscope (Zeiss, Oberkochen, Germany).

ACKNOWLEDGMENTS

We thank Dennis McDaniel for his assistance with confocal microscopy. We also thank Pierre Åman for sharing the myxoid liposarcoma cell lines with our lab. This project was supported by the National Institute of General Medical Sciences (Award Numbers R35GM119790 (to F.S.) and R01GM118530 (to N.L.F.)) and the National

Institute of Neurological Diseases and Stroke (Award R01NS116176 (to N.L.F.)). The authors declare no competing financial interests.

ABBREVIATIONS

Bromodomain containing protein 4 (BRD4), CCAAT/Enhancer Binding Protein (C/EBP), CCAAT/Enhancer Binding Protein Homologous Protein (CHOP), Fluorescence recovery after photobleaching (FRAP), Fused in Sarcoma (FUS), Intrinsically disordered region (IDRs), Liquid-liquid phase separation (LLPS), Low complexity (LC), Maltose binding protein (MBP), Myxoid Liposarcoma (MLS), Prion-like Domain (PrLD), Soft tissue sarcoma (STS), Super Enhancers (SEs)

FIGURES

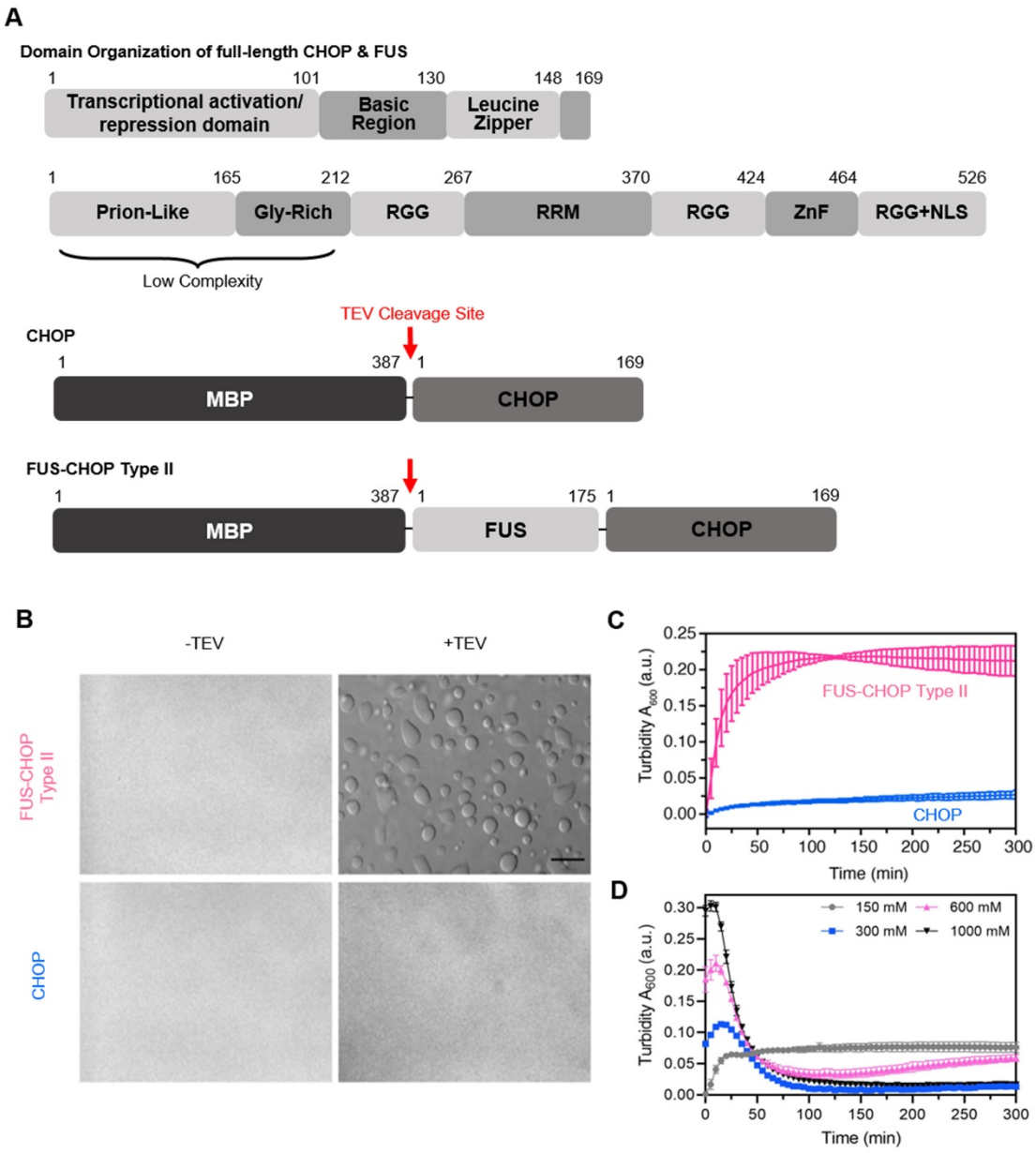
A
Domain Organization of full-length CHOP & FUS
1
101
130
148
169
Transcriptional activation/ repression domain
Basic Region
Leucine Zipper
1
165
212
267
370
424
464
526
Prion-Like
Gly-Rich
RGG
RRM
RGG
ZnF
RGG+NLS
Low Complexity
TEV Cleavage Site
CHOP
1
387
1
169
MBP
CHOP
FUS-CHOP Type II
1
387
1
175
1
169
MBP
FUS
CHOP
B
-TEV
+TEV
FUS-CHOP Type II
CHOP
C
Turbidity A600 (a.u.)
FUS-CHOP Type II
CHOP
Time (min)
D
Turbidity A600 (a.u.)
150 mM
600 mM
300 mM
1000 mM
Time (min)

Fig 6. FUS-CHOP Type II undergoes LLPS *in vitro*

(A) Schematic of full length CHOP (aa1-169) and FUS (aa1-526) as well as purified recombinant MBP-CHOP and MBP-FUS-CHOP. TEV protease cleavage site indicated by red arrow. (B) DIC micrographs of 50 μM FUS-CHOP Type II fusion (top) and CHOP protein alone (bottom) in 50 mM Tris, 150 mM NaCl, pH 7.4 without and with TEV protease to cleave the N-terminal maltose binding protein (MBP) solubilizing tag. Scale bar represents 80 μm. (C) Corresponding turbidity measurements of FUS-CHOP type II fusion (pink) and CHOP protein alone (blue) after initiating cleavage of the MBP tag by addition of TEV protease. (D) Error bars represent the s.d. of measurements from three experimental replicates.

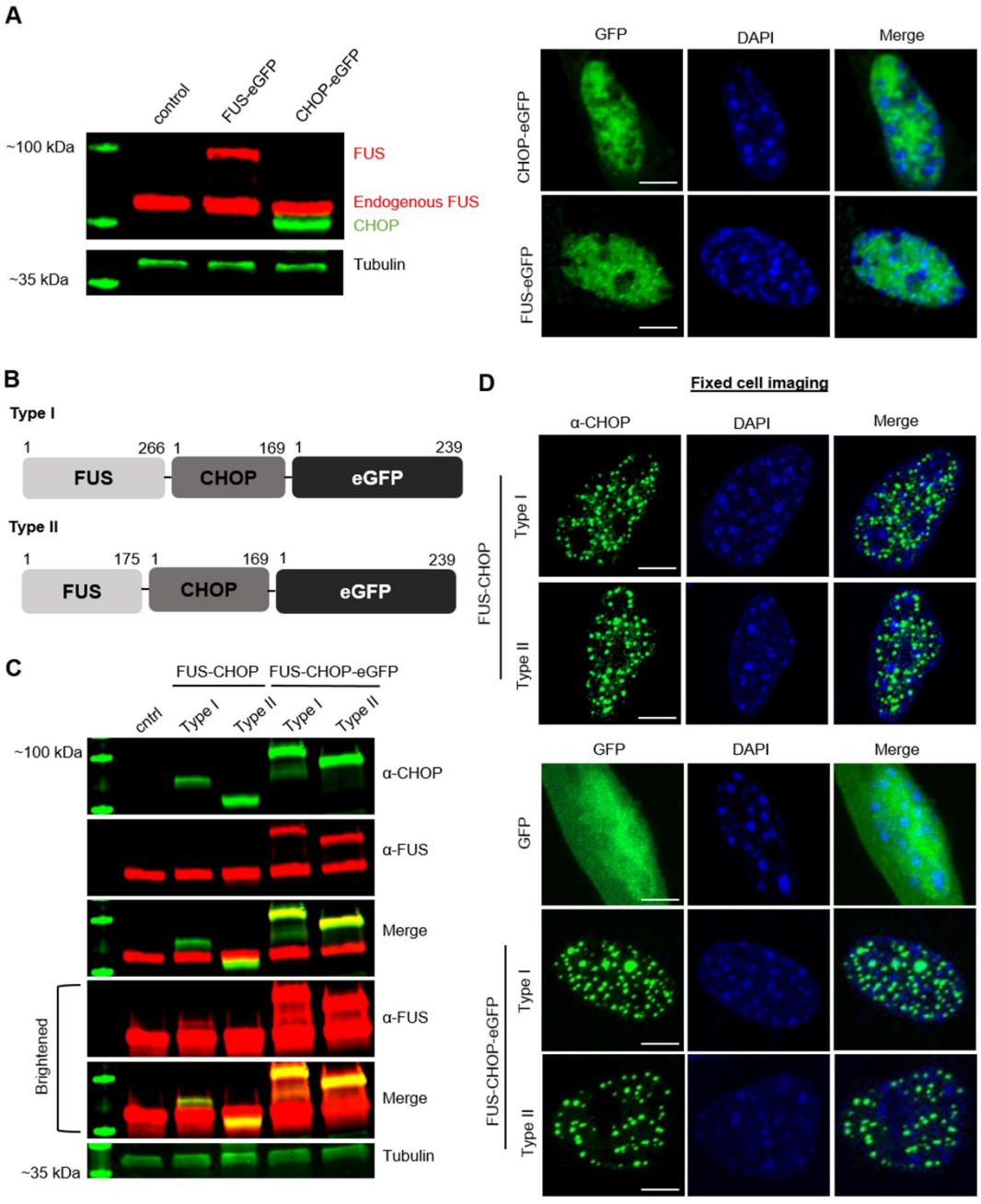
A
control
FUS-eGFP
CHOP-eGFP
~100 kDa
FUS
Endogenous FUS
CHOP
~35 kDa
Tubulin
GFP
DAPI
Merge
CHOP-eGFP
FUS-eGFP
B
Type I
1
266
1
169
1
239
FUS
CHOP
eGFP
Type II
1
175
1
169
1
239
FUS
CHOP
eGFP
C
FUS-CHOP
FUS-CHOP-eGFP
cntrl
Type I
Type II
Type I
Type II
~100 kDa
α-CHOP
α-FUS
Merge
α-FUS
Merge
Tubulin
~35 kDa
Brightened
D
Fixed cell imaging
α-CHOP
DAPI
Merge
FUS-CHOP
Type I
Type II
GFP
DAPI
Merge
FUS-CHOP-eGFP
Type I
Type II

Fig 7. Ectopically expressed FUS-CHOP localizes to sphere shaped puncta in the nucleus

(A) Western Blot and immunofluorescent images of ectopically expressed FUS-eGFP and CHOP-eGFP. (B) Schematic of FUS-CHOP-eGFP fusion proteins. (C) Western Blot of ectopically expressed untagged FUS-CHOP and FUS-CHOP-eGFP in NIH 3T3 cells. The bottom panels have been brightened to show all FUS antibody binding. (D) Confocal images of nuclear puncta formed by ectopically expressed FUS-CHOP (with and without eGFP tag) in NIH 3T3 cells. Scale bar represents 5 μm. Representative data from three experimental replicates.

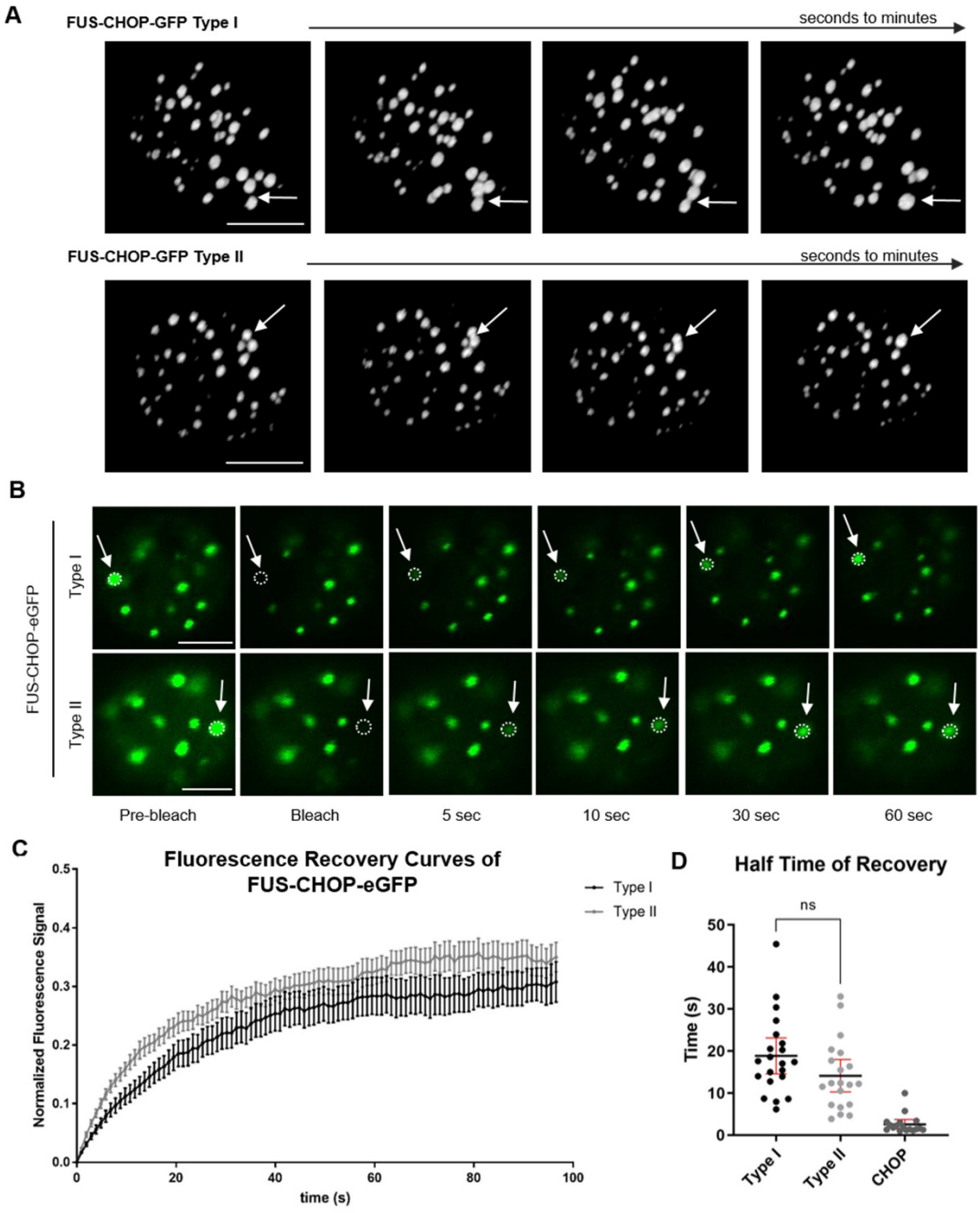
A
FUS-CHOP-GFP Type I
seconds to minutes
FUS-CHOP-GFP Type II
seconds to minutes
B
FUS-CHOP-eGFP
Type I
Type II
Pre-bleach
Bleach
5 sec
10 sec
30 sec
60 sec
C
Fluorescence Recovery Curves of FUS-CHOP-eGFP
Type I
Type II
Normalized Fluorescence Signal
time (s)
D
Half Time of Recovery
ns
Time (s)
Type I
Type II
CHOP

Fig 8. FUS-CHOP-eGFP puncta have liquid-like characteristics.

(A) Still frames from time course movies imaged by confocal microscopy of FUS-CHOP-eGFP type I and type II puncta fusing upon touching**.** Videos are available in Supplementary Data. (B) FUS-CHOP-eGFP type I and type II puncta recover on the time scale of seconds following fluorescence bleaching. Scale bar represents 5 μm. Representative data from three experimental replicates. (C) Average fluorescence recovery curves of FUS-CHOP-eGFP type I and type II. (D) Half time of recovery of FUS-CHOP-eGFP type I and II puncta. FRAP half-time data was statistically analyzed using an upaired t-test (P value = 0.0953). Error bars represent the mean with 95% c.i. of measurements from three experimental replicates (total of 20 cells bleached per experimental group) (B, C, D).

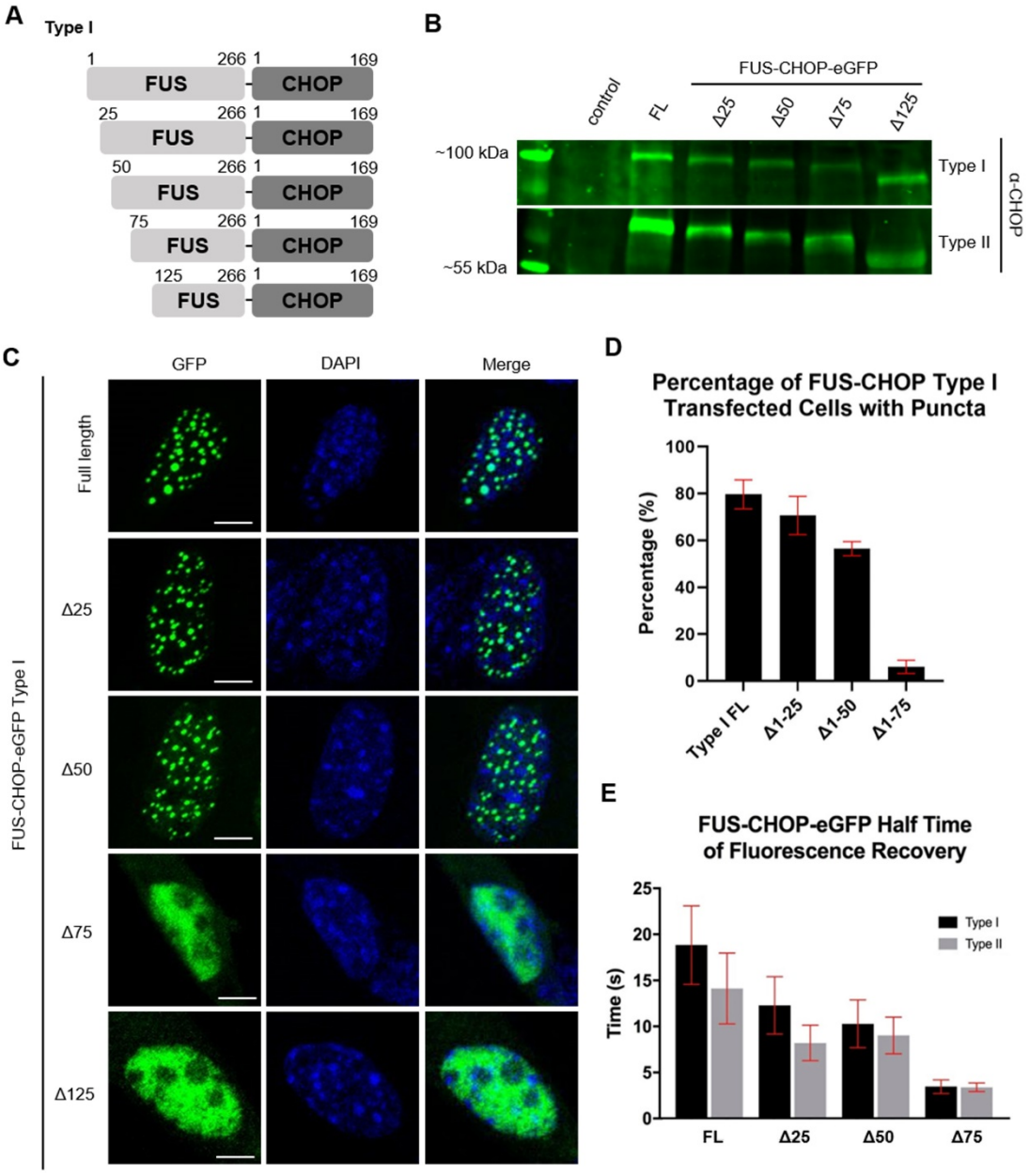
A
Type I
1
266
1
169
FUS
CHOP
25
266
1
169
FUS
CHOP
50
266
1
169
FUS
CHOP
75
266
1
169
FUS
CHOP
125
266
1
169
FUS
CHOP
B
control
FL
FUS-CHOP-eGFP
Δ25
Δ50
Δ75
Δ125
~100 kDa
~55 kDa
Type I
Type II
α-CHOP
C
GFP
DAPI
Merge
FUS-CHOP-eGFP Type I
Full length
Δ25
Δ50
Δ75
Δ125
D
Percentage of FUS-CHOP Type I Transfected Cells with Puncta
Percentage (%)
100
80
60
40
20
0
Type I FL
Δ1-25
Δ1-50
Δ1-75
E
FUS-CHOP-eGFP Half Time of Fluorescence Recovery
Time (s)
25
20
15
10
5
0
Type I
Type II
FL
Δ25
Δ50
Δ75

Fig 9. FUS-CHOP-eGFP liquid-liquid phase separation is dependent on the N-terminus of FUS.

(A) Schematic of truncations made to FUS-CHOP-eGFP type I. (B) Western blot of NIH 3T3 cells transfected with full-length (FL) or truncated FUS-CHOP-eGFP constructs. NIH 3T3 cell lysates were probed with anti-CHOP antibody. (C) Full-length or truncated FUS-CHOP-eGFP type I ectopically expressed in NIH 3T3 cells and imaged by confocal microscopy. Scale bar represents 5 μm. Representative data from three experimental replicates. Type II images are shown in Supplementary Data. (D) The percentage of eGFP positive cells containing nuclear puncta were quantified following a 24 hour transfection. (E) Half-time of recovery of FUS-CHOP-eGFP type I and type II full length or truncated constructs. Error bars represent the mean with 95% c.i. of measurements from three experimental replicates.

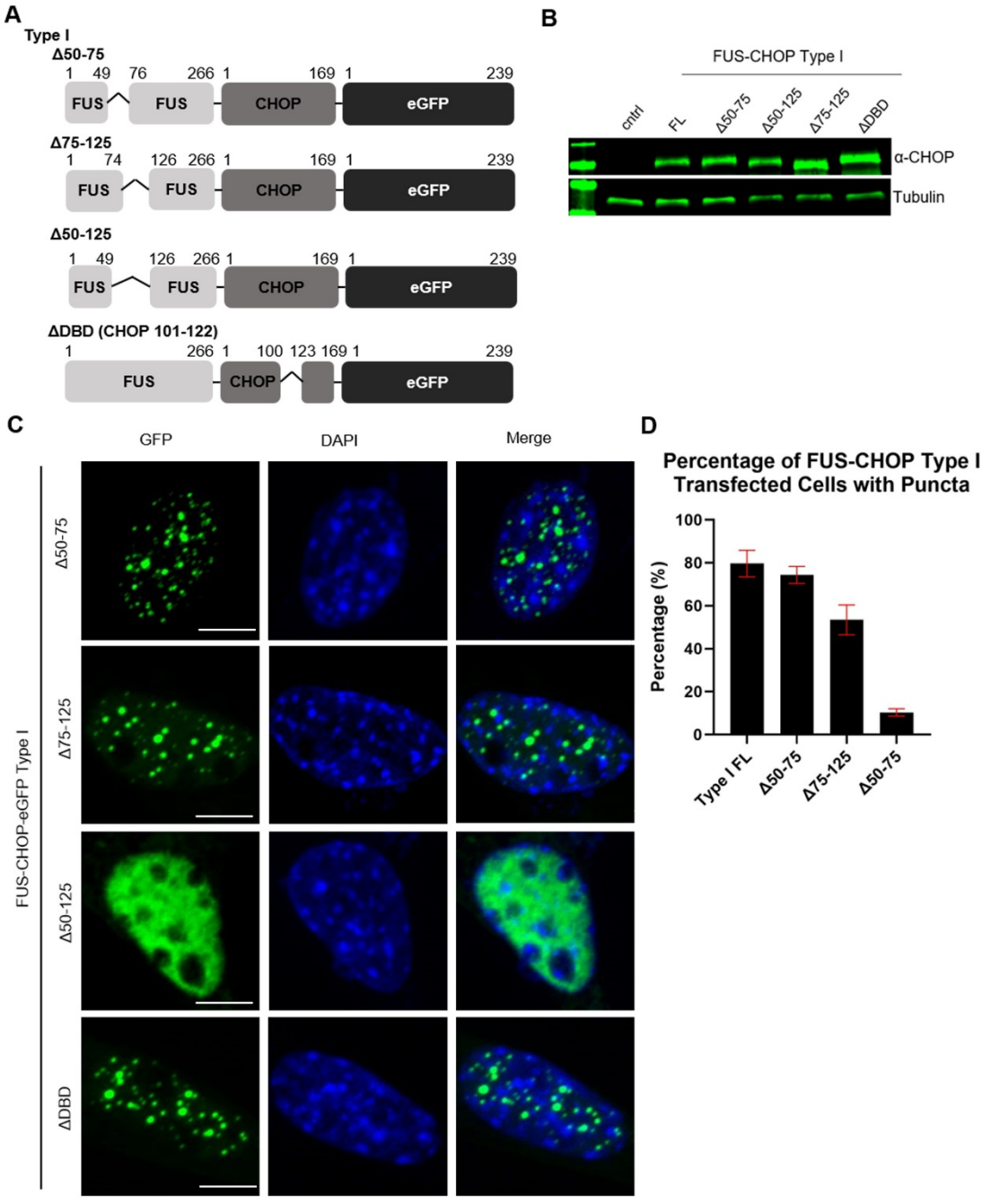
A
Type I
Δ50-75
1 49 76 266 1 169 1 239
FUS FUS CHOP eGFP
Δ75-125
1 74 126 266 1 169 1 239
FUS FUS CHOP eGFP
Δ50-125
1 49 126 266 1 169 1 239
FUS FUS CHOP eGFP
ΔDBD (CHOP 101-122)
1 266 1 100 123 169 1 239
FUS CHOP eGFP
B
FUS-CHOP Type I
cntrl
FL
Δ50-75
Δ50-125
Δ75-125
ΔDBD
α-CHOP
Tubulin
C
GFP
DAPI
Merge
FUS-CHOP-eGFP Type I
Δ50-75
Δ75-125
Δ50-125
ΔDBD
D
Percentage of FUS-CHOP Type I Transfected Cells with Puncta
Percentage (%)
100
80
60
40
20
0
Type I FL
Δ50-75
Δ75-125
Δ50-75

Fig 10. Phase separation of FUS-CHOP is not dependent on a central core region within FUS's prion-like domain.

(A) Schematic of FUS-CHOP-eGFP type I internal truncations. (B) NIH 3T3 cells transfected with full-length (FL) or truncated (Δ 50-75, Δ75-125, Δ50-125, or ΔDBD) FUS-CHOP-eGFP type I. Cell lysates were analyzed by Western Blot and probed with anti-CHOP and anti-tubulin antibodies. (C) Confocal images of internally truncated FUS-CHOP-eGFP type I nuclear puncta. Scale bar represents 5 μm. Type II images are shown in Supplementary Data. (D) The percentage of eGFP positive cells containing nuclear puncta were quantified following a 24 hour transfection. Error bars represent the mean with 95% c.i. of measurements from three experimental replicates.

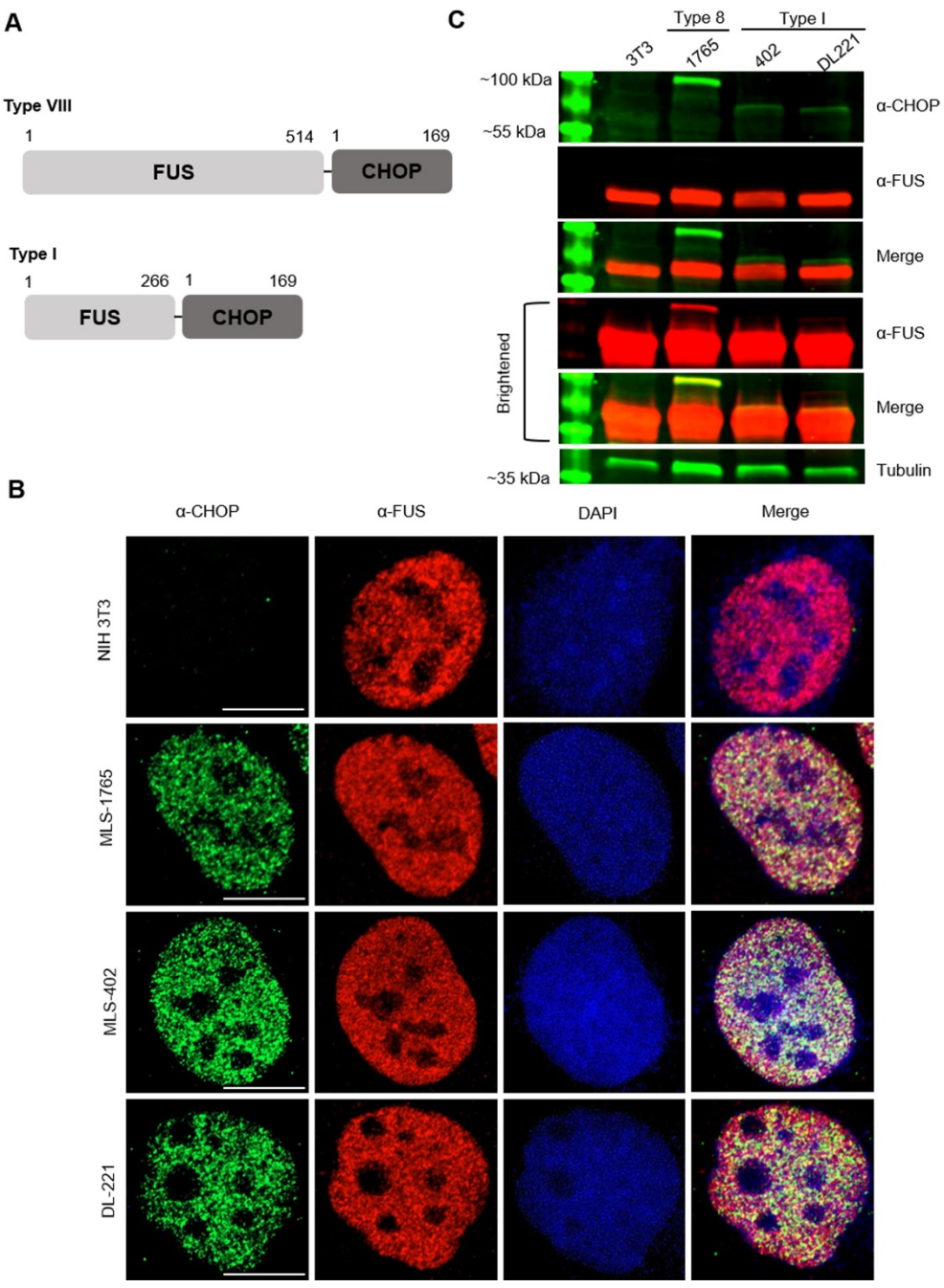
A
Type VIII
1
514
1
169
FUS
CHOP
Type I
1
266
1
169
FUS
CHOP
C
Type 8
Type I
3T3
1765
402
DL221
~100 kDa
~55 kDa
α-CHOP
α-FUS
Merge
Brightened
α-FUS
Merge
~35 kDa
Tubulin
B
α-CHOP
α-FUS
DAPI
Merge
NIH 3T3
MLS-1765
MLS-402
DL-221

Fig 11. FUS-CHOP forms nuclear puncta in Myxoid Liposarcoma cell lines.

(A) Schematic of FUS-CHOP fusions. MLS-1765 encodes a type VIII FUS-CHOP fusion protein while MLS-402 and DL-221 contain a type I fusion protein (diagram in Supplementary Figures). (B) MLS cell lines were probed with anti-CHOP and anti-FUS antibodies and imaged using confocal microscopy with Airyscan. (C) Cancer cell lysates analyzed by Western Blot. Brightened Blot shows FUS antibody binding. Representative data from three experimental replicates.

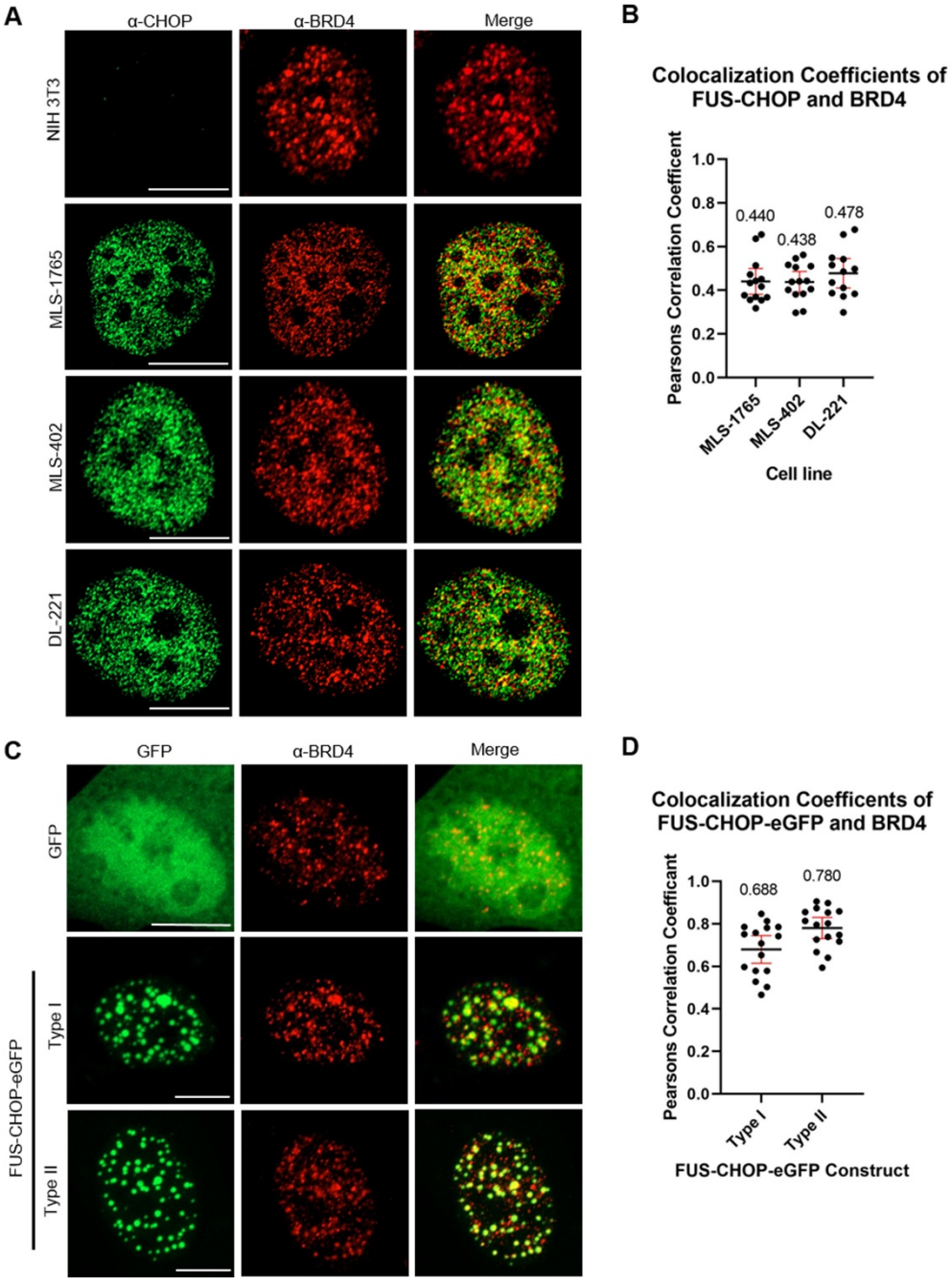
A
α-CHOP
α-BRD4
Merge
NIH 3T3
MLS-1765
MLS-402
DL-221
B
Colocalization Coefficients of FUS-CHOP and BRD4
Pearsons Correlation Coefficent
1.0
0.8
0.6
0.4
0.2
0.0
0.440
0.438
0.478
MLS-1765
MLS-402
DL-221
Cell line
C
GFP
α-BRD4
Merge
GFP
FUS-CHOP-eGFP
Type I
Type II
D
Colocalization Coefficents of FUS-CHOP-eGFP and BRD4
Pearsons Correlation Coefficant
1.0
0.8
0.6
0.4
0.2
0.0
0.688
0.780
Type I
Type II
FUS-CHOP-eGFP Construct

Fig 12. FUS-CHOP localizes with phase-separating super-enhancer protein BRD4.

(A) MLS-1765, MLS-402, and DL-221 cells were probed with anti-CHOP and anti-BRD4 antibodies and analyzed by confocal microscopy with Airyscan. (B) Pearson's correlation coefficient between FUS-CHOP and BRD4 was calculated using the EzColocalization plug-in in Fiji (total of 13 cells analyzed from each experimental group). (C) NIH 3T3 cells were transfected with FUS-CHOP-eGFP type I or type II for 24 hours. Following transfection, cells were probed with anti-BRD4 and assessed by confocal microscopy with Airyscan. Representative data from three experimental replicates. (D) Pearson's correlation coefficient between FUS-CHOP and BRD4 was calculated using the EzColocalization plug-in in Fiji (total of 14 cells analyzed from each experimental group).

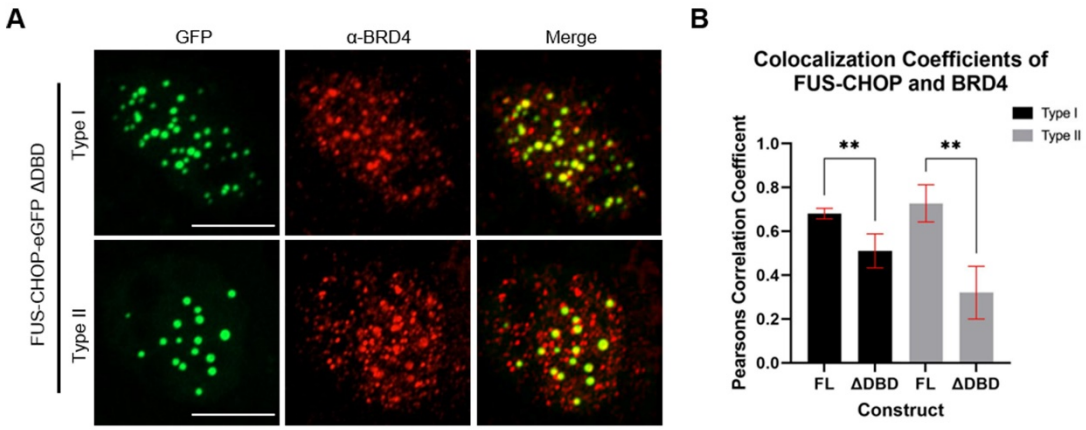

Fig 13. Phase separation with BRD4 is influenced by FUS-CHOP DNA binding.

(A) NIH 3T3 cells were transfected with FUS-CHOP-eGFP type I or type II DNA-binding deficient mutants for 24 hours. Following transfection, cells were probed with anti-BRD4 and assessed by confocal microscopy with Airyscan. Representative data from three experimental replicates. (B) Pearson's correlation coefficient between FUS-CHOP and BRD4 was calculated using the EzColocalization plug-in in Fiji. Colocalization data was statistically analyzed using an upaired t-test (Type I P value = 0.0081, Type II P value = 0.0031). Error bars represent the mean with s.d. of measurements from three experimental replicates (total of 14 cells were analyzed per experimental group).

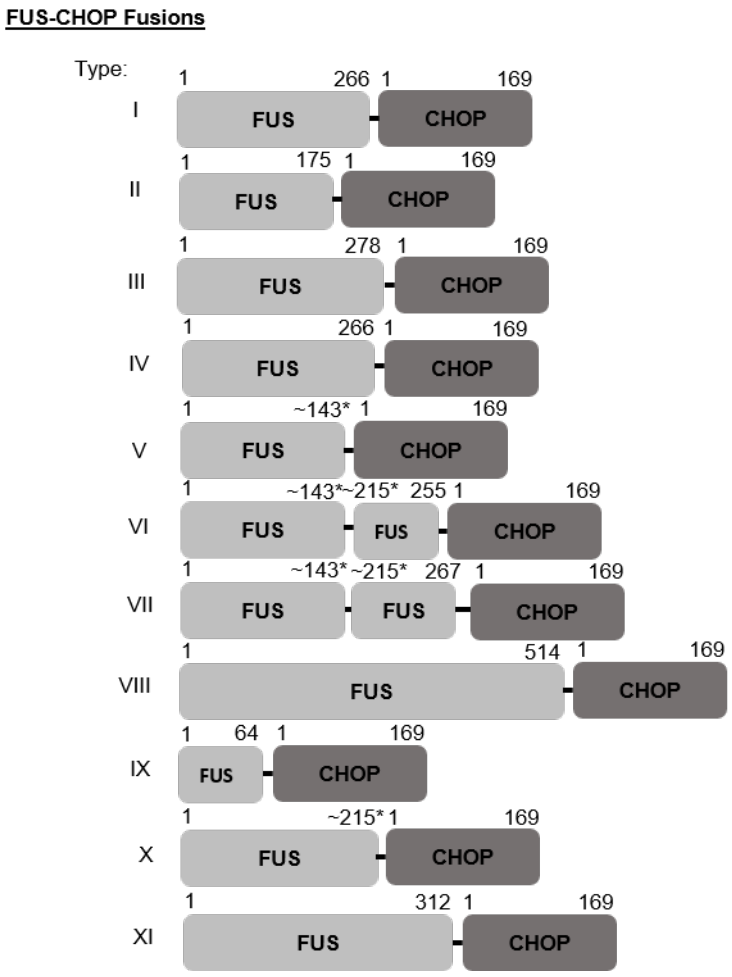

Fig 14. FUS-CHOP fusions.

Schematic of the 11 different types of FUS-CHOP fusions. *Approximations based on reporting of FUS exon fusions/truncations but not precise codon sites.

Construct	# of FUS PrLD tyrosine motifs removed
FUS-CHOP Δ25	3
FUS-CHOP Δ50	7
FUS-CHOP Δ75	11
FUS-CHOP Δ125	18
FUS-CHOP Δ50-75	5
FUS-CHOP Δ75-125	8
FUS-CHOP Δ50-125	11

Table 1. FUS PrLD tyrosine motifs removed by truncation.

Table denoting the number of tyrosine motifs removed in the FUS prion-like domain portion of FUS-CHOP truncations and internal deletions.

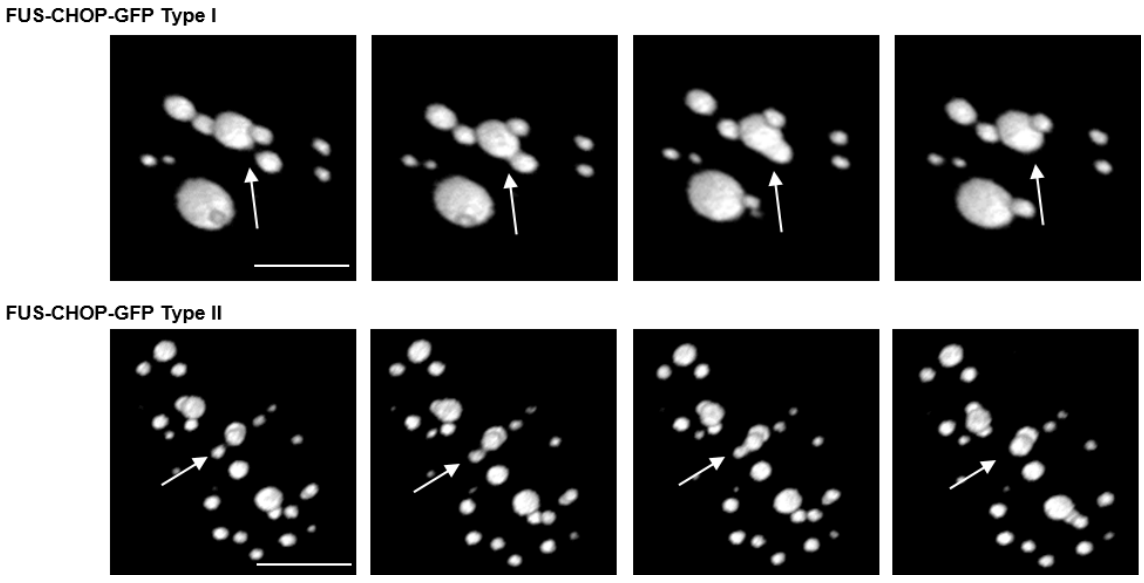

Fig 15. FUS-CHOP-eGFP puncta have liquid-like characteristics

Still frames from time course movies imaged by confocal microscopy of FUS-CHOP-eGFP type I and type II puncta fuse upon touching.

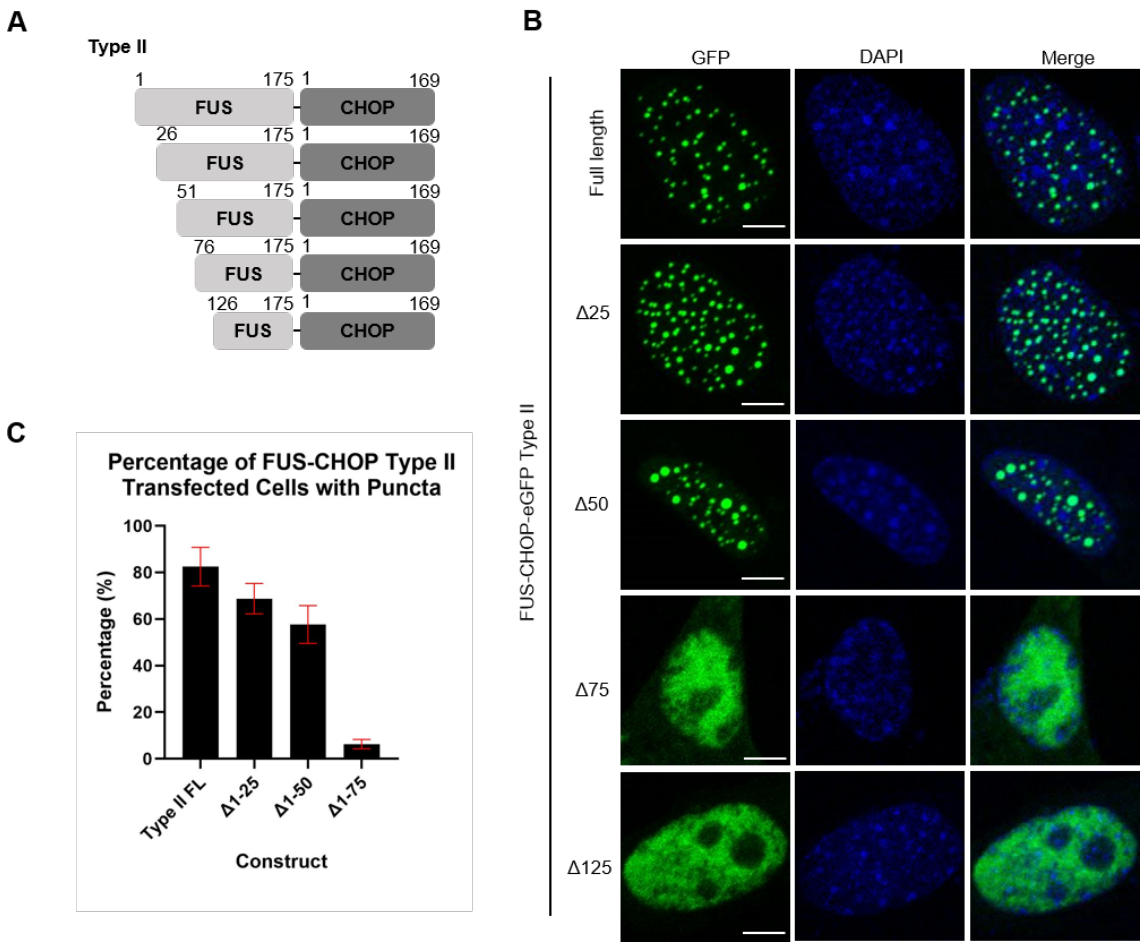

Fig 16. FUS-CHOP-eGFP Type II liquid-liquid phase separation is dependent on the N-terminus of FUS.

(A) Schematic of truncations made to FUS-CHOP-eGFP type II. (B) Full-length or truncated FUS-CHOP-eGFP type II ectopically expressed in NIH 3T3 cells and imaged by confocal microscopy. Scale bar represents 5 μm. Representative data from three experimental replicates. (C) Quantification of the percentage of transfected cells with nuclear puncta. Error bars represent the mean with 95% c.i. of measurements from three experimental replicates.

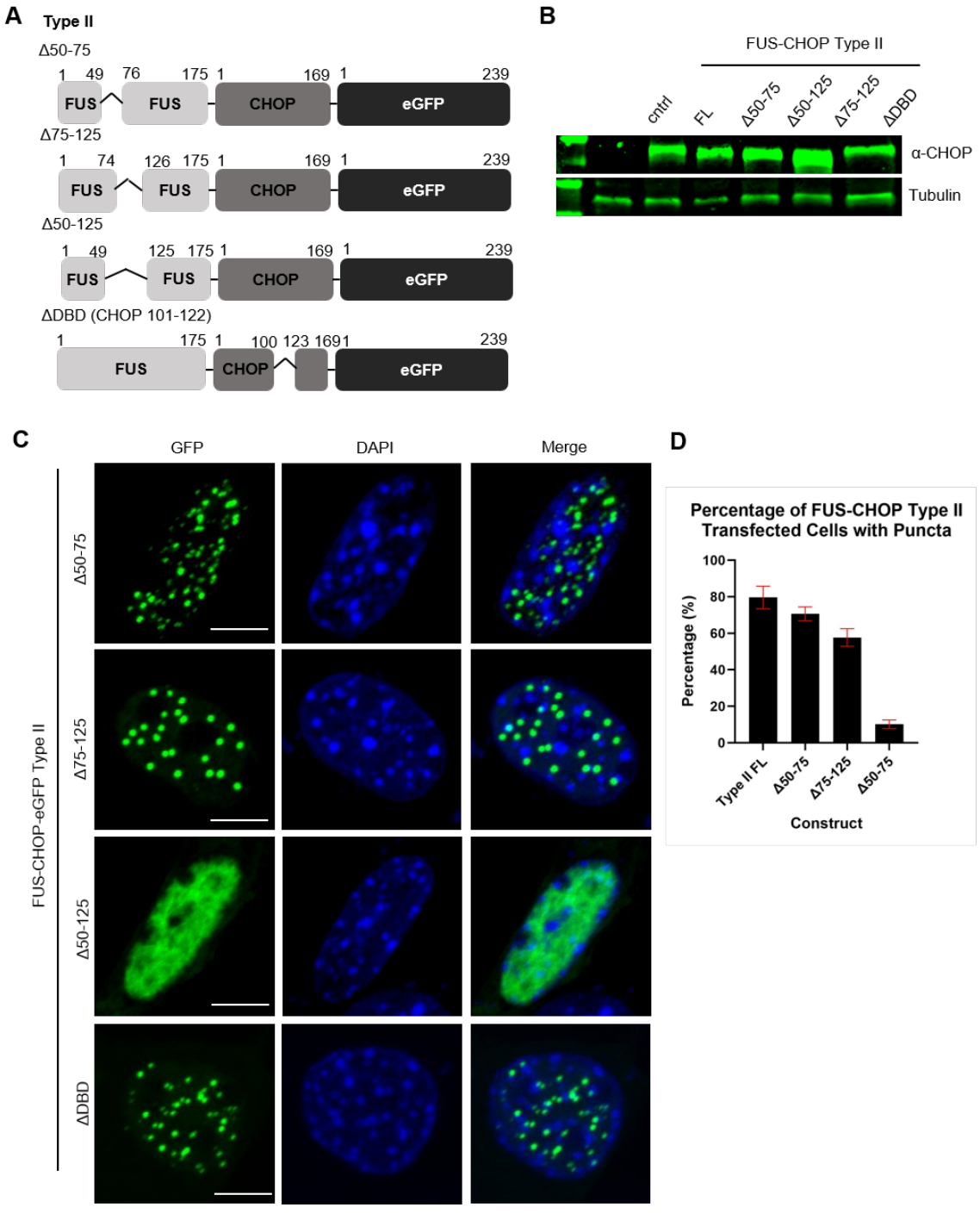
A
Type II
Δ50-75
1 49 76 175 1 169 1 239
FUS FUS CHOP eGFP
Δ75-125
1 74 126 175 1 169 1 239
FUS FUS CHOP eGFP
Δ50-125
1 49 125 175 1 169 1 239
FUS FUS CHOP eGFP
ΔDBD (CHOP 101-122)
1 175 1 100 123 169 1 239
FUS CHOP eGFP
B
FUS-CHOP Type II
cntrl
FL
Δ50-75
Δ50-125
Δ75-125
ΔDBD
α-CHOP
Tubulin
C
GFP
DAPI
Merge
FUS-CHOP-eGFP Type II
Δ50-75
Δ75-125
Δ50-125
ΔDBD
D
Percentage of FUS-CHOP Type II Transfected Cells with Puncta
Percentage (%)
100
80
60
40
20
0
Type II FL
Δ50-75
Δ75-125
Δ50-75
Construct

Fig 17. Phase separation of FUS-CHOP is not dependent on a central core region within FUS's prion-like domain.

(A) Schematic of FUS-CHOP-eGFP type II internal truncations. (B)NIH 3T3 cells transfected with full-length (FL) or truncated (Δ 50-75, Δ75-125, Δ50-125, or ΔDBD) FUS-CHOP-eGFP type II. Cell lysates were analyzed by Western Blot and probed with anti-CHOP and anti-tubulin antibodies. (C) Confocal images of internally truncated FUS-CHOP-eGFP nuclear puncta type I or type II. Scale bar represents 5 μm. (D) Percentage of transfected cells with nuclear puncta were quantified for each FUS-CHOP-eGFP construct. Error bars represent the mean with 95% c.i. of measurements from three experimental replicates.

CHAPTER 3:The prion-like domain of FUS is phosphorylated by multiple kinases affecting liquid- and solid-phase transitions

Izzy Owen[1], Shannon Rhoads[1], Debra Yee[1], Hala Wyne[1], Kevin Gery[1], Isabelle Hannula[1], Meena Sundrum[1], and Frank Shewmaker[1]

[1]Department of Biochemistry and Molecular Biology, Uniformed Services University, Bethesda, MD, USA

Published in *Molecular Biology of the Cell*, September 2020 (Vol. 31, No. 23).

ABSTRACT

Fused in Sarcoma (FUS) is a ubiquitously expressed protein that can phase-separate from nucleoplasm and cytoplasm into distinct liquid-droplet structures. It is predominately nuclear and most of its functions are related to RNA and DNA metabolism. Excessive persistence of FUS within cytoplasmic phase-separated assemblies is implicated in the diseases amyotrophic lateral sclerosis (ALS) and frontotemporal dementia (FTD). Phosphorylation of FUS's prion-like domain (PrLD), by nuclear PIKK-family kinases following DNA damage, was previously shown to alter FUS's liquid-phase and solid-phase transitions in cell models and *in vitro*. However, proteomic data suggest FUS's PrLD is phosphorylated at numerous additional sites and it is unknown if other non-PIKK and non-nuclear kinases might be influencing FUS's phase transitions. Here we evaluated disease mutations and stress conditions that increase FUS accumulation into cytoplasmic phase-separated structures. We observed that cytoplasmic liquid-phase structures contain FUS phosphorylated at novel sites, which occurs independently of PIKK-family kinases. We engineered phosphomimetic substitutions within FUS's PrLD and observed that mimicking a few phosphorylation sites strongly inhibited FUS solid-phase aggregation, while minimally altering liquid-phase condensation. These effects occur independently of the exact location of the phosphomimetic substitutions, suggesting that modulation of PrLD phosphorylation may offer therapeutic strategies that are specific for solid-phase aggregation observed in disease.

INTRODUCTION

Amyotrophic lateral sclerosis (ALS) and frontotemporal dementia (FTD) are progressive neurodegenerative diseases with overlapping histopathological features (Ferrari et al., 2011; Karch et al., 2018). Subtypes of both diseases can be categorized by the specific proteins that accumulate into neuronal proteinaceous inclusions (Irwin et al., 2015) (Saberi et al., 2015). A small percentage of ALS and FTD subtypes feature neuronal inclusions enriched for the fused in sarcoma protein (FUS) (Kwiatkowski et al., 2009; Vance et al., 2009) (Snowden et al., 2011). The pathological causes and consequences of FUS aggregation are incompletely known, and there are no drugs that prevent FUS-linked neurodegeneration.

FUS is a 526-amino acid, ubiquitously expressed, predominantly nuclear protein that supports numerous DNA/RNA-related functions, including transcription, RNA transport, RNA splicing, and the DNA damage response (Zinszner et al., 1997; Yang et al., 1998; Tan et al., 2012; Mastrocola et al., 2013; Yang et al., 2014). FUS consists of an N-terminal low-complexity prion-like domain (PrLD), three RGG repeat motifs, a zinc-finger, an RNA recognition motif, and a C-terminal nuclear localization signal (NLS). The PrLD is ~160 amino acids and is named for its sequence similarity to yeast prion domains (Gitler and Shorter, 2011), which are typically intrinsically disordered and lack sequence complexity (*i.e.* they are abundant in a few polar residues, with very few charged or hydrophobic residues) (Ross and Toombs, 2010). These domains (and similar so-called “prion-like” domains) can facilitate proteins to self-associate and undergo liquid- and/or solid-phase transitions (Franzmann and Alberti, 2019). Conversion into solid aggregates is usually considered a stochastic, pathological event (Wickner et al.,

2011), whereas the liquid-phase transitions are considered integral to function (Shin and Brangwynne, 2017). FUS's PrLD enables the protein to condense into liquid-droplet structures that are distinct from the bulk solvent in a process frequently described as liquid-liquid phase separation (LLPS) (Burke et al., 2015; Lin et al., 2017). However, FUS's PrLD can also form solid amyloid-like aggregates *in vitro* (Murray et al., 2017).

The condensation of macromolecules like FUS into distinct liquid phases allows for temporal and spatial control of specific cellular functions (Owen and Shewmaker, 2019). Examples of these liquid-phase structures include Cajal bodies, stress granules, and the nucleolus. These diverse condensates are thought to be partially stabilized by proteins with intrinsically disordered domains—such as FUS's PrLD—that have the capacity to form numerous non-specific, transient, multivalent interactions (Banani et al., 2017). However, an emerging hypothesis in disease is that the high concentrations of these unstructured domains within liquid condensates can potentiate the formation of intractable pathological solid aggregates (March et al., 2016). In the case of FUS, persistent condensation and/or mislocalization may initiate its solid-phase aggregation along neuroanatomical pathways (Armstrong, 2017). Once in the solid phase, both gain-of-function and loss-of-function mechanisms may contribute to neuronal degeneration (Sharma et al., 2016; Ishigaki and Sobue, 2018). Disrupting the formation of FUS-enriched neuronal inclusions is a therapeutic strategy for FUS-specific subtypes of ALS and FTD.

Post-translational modifications (PTMs) can regulate LLPS (Soding et al., 2020) (Owen and Shewmaker, 2019). Low-complexity sequences, like FUS's PrLD, are common to phase-separating proteins and are especially susceptible to enzymatic

modification due to their relatively open conformational ensembles (Bah and Forman-Kay, 2016). We previously reported FUS's PrLD is highly post translationally modified under DNA-damaging conditions. Based on our and others' work, 32 putative phosphorylation sites have been identified (Rhoads et al., 2018b). Twelve of these sites are serine or threonine followed by a glutamine (S/TQ), the consensus sequence for the phosphatidylinositol 3-kinase-related kinases (PIKKs). PIKKs, which include the kinases DNA-PK, ATM, and ATR, are activated during the DNA damage response and have been confirmed to phosphorylate FUS's PrLD (Gardiner et al., 2008; Deng et al., 2014; Monahan et al., 2017; Rhoads et al., 2018a). Our findings demonstrated phosphorylation or phosphomimetic substitutions of PIKK consensus sites inhibited FUS's propensity to undergo solid-phase transitions into amyloid-like aggregates (Monahan et al., 2017); *in vitro* suppression of LLPS was also observed. However, most of FUS's putative phosphorylation sites are not PIKK consensus sites and it is unknown if these sites are actually phosphorylated in cells and if they alter FUS's state transitions.

In addition to DNA-damaging conditions, FUS has also been shown to respond to oxidative and osmotic stress (Sama et al., 2013). With hyperosmolar stress, wild-type FUS extensively accumulates into cytoplasmic granules, whereas with oxidative stress, ALS-mutant FUS accumulates into stress granules (Vance et al., 2013). However, specific phosphorylation of FUS's PrLD has not been characterized under these conditions. In this study, we produced phospho-specific antibodies to evaluate phosphorylation of PIKK and non-PIKK consensus sites within FUS's PrLD following different types of stress in human cell models. We also evaluated ALS-mutant FUS to determine if there was an association between pathological cytoplasmic aggregation and

FUS PrLD phosphorylation. We then determined if phosphomimetic substitutions within FUS's PrLD could alter FUS phase transitions in a non-site-specific manner. Our results suggest non-PIKK kinases act upon FUS's PrLD and are capable of modifying FUS's aggregation propensity. This suggests that FUS pathological aggregation in FTD and ALS could be ameliorated by altering post-translational modifications.

RESULTS

The FUS prion-like domain is phosphorylated at multiple non-PIKK sites.

We previously confirmed and evaluated phosphorylation at PIKK sites (S/TQ) within FUS's PrLD following DNA damaging stress (Rhoads et al., 2018a). Our preliminary mass spectrometry experiments suggested that non-PIKK consensus sites within the PrLD were also being phosphorylated. We selected 3 potential non-PIKK sites for corroboration with custom polyclonal antibodies: S57, T71, and S96. Sites 57 and 96 were of interest because they are putative ALS-mutation sites (Rhoads et al., 2018b). Custom antibodies (α-pS57, α-pT71, and α-pS96) that are specific to phosphorylated FUS (pFUS) were produced in rabbits (ThermoFisher and Genscript). Specificity for the phosphorylated epitope, relative to the non-phosphorylated epitope, was confirmed by immuno-blotting (Figure 26A). Also, antibodies were confirmed to not cross-react with other phospho-epitopes (Figure 26B).

Antibody specificity to full-length FUS from human H4 neuroglioma cells was tested by Western blotting. H4 cells were treated with the DNA-damaging agent calicheamicin, as previously described (Rhoads et al., 2018a). From treated cells, the pFUS antibodies reacted with protein species that migrated similarly to species

recognized by commercial FUS antibodies (Figure 18A). The custom antibodies gave no signal at the same position as FUS in the no-treatment control; however, nonspecific bands of different molecular weights were present (Figure 26C). To ensure the phospho-specific antibodies were identifying FUS species, knockdown experiments (siRNA) were performed. Quantification of Western blot signals revealed similar knockdown efficiency of FUS and pFUS signals using the same FUS-specific siRNA (Figure 18B). The custom antibodies were analyzed using immunofluorescence microscopy of H4 cells to verify their specificity to FUS, which is predominantly a nuclear protein. After calicheamicin treatment, the pFUS antibodies yielded strong nuclear signals (Figure 18C) that were eliminated, similarly to FUS signal, by FUS siRNA (Figure 18D).

Our previous work found that low concentrations of calicheamicin (~0.5 nM) induced PIKK-kinase phosphorylation of the FUS PrLD at two PIKK consensus sites: S26 and S30 (Rhoads et al., 2018a). When H4 cells were treated with a calicheamicin dose series, the α-pS57, α-pT71, and α-pS96 antibodies detected FUS species at and above approximately 10 nM calicheamicin (Figure 19A). This phosphorylation was completely inhibited with a PIKK-kinase inhibitor (discussed further below; Figure 21A). The phospho-bands detected by α-pS57, α-pT71, and α-pS96 overlapped with the higher apparent molecular weight commercial α-FUS bands; this slower electrophoretic migration occurs when FUS is multi-phosphorylated (Deng et al., 2014; Monahan et al., 2017) (Figure 19A). The antibodies specific to PIKK consensus sites (pS26 and pS30) identify FUS prior, during, and after its shift to higher molecular weight, which could indicate that phosphorylation occurs at PIKK sites first. The potential for PIKK kinases to phosphorylate these non-PIKK-consensus sites (S57, T71 and S96) in FUS's PrLD were

corroborated by *in vitro* assays using recombinant PIKK kinase (DNA-PK) and maltose-binding-protein-tagged FUS (MBP-FUS; Figure 19B).

Phosphorylation of FUS occurs independently of PIKK-family kinases following osmotic and oxidative stress

Since each custom antibody was specific to its unique epitope in cross-reactivity assays (Figure 26B), we concluded that the phosphorylation of FUS's PrLD is not limited to the 12 S/TQ consensus sites, and other non-PIKK kinases may also act upon this domain. However, because of the low sequence complexity of FUS's PrLD, it could not be ruled out that phospho-specific antibodies cross-react to other PIKK-site phospho-epitopes non-specifically. We therefore asked if other stress conditions that affect FUS cell biology would reveal distinct phosphorylation patterns that would be independent of PIKK kinase activity.

Previous work demonstrated both sorbitol (osmotic stress) and sodium arsenite (oxidative stress) affect mutant or wild-type FUS subcellular localization (Andersson et al., 2008; Sama et al., 2013). We analyzed the phosphorylation status of FUS's PrLD at PIKK and non-PIKK sites following treatment of H4 cells with these stressors (Figure 20A). Western blotting indicated S30, T71, and S96 are phosphorylated following both treatments, whereas S26 and S57 are unchanged. For the α-pS30, α-pT71, and α-pS96 antibodies, higher and lower molecular weight bands were also evident following treatment, but FUS siRNA knockdown confirmed these bands were not specific to FUS (Figure 26D). Quantification of the Western blot signals showed an immediate increase in phosphorylation at S30, T71, and S96 within 15 minutes following sorbitol treatment

(Figure 20B). Comparatively, there was a gradual increase in phosphorylation following sodium arsenite treatment that did not plateau until approximately 45 minutes (Figure 20B).

FUS remains nuclear following PIKK-kinase phosphorylation (Rhoads et al., 2018a). However, since osmotic and oxidative stress can cause FUS to accumulate into cytoplasmic granules (Andersson et al., 2008; Sama et al., 2013), we asked if phospho-FUS species could be seen in these structures by immunofluorescence microscopy. H4 cells were treated with sodium arsenite or sorbitol as before and then immuno-stained with the custom FUS antibodies. Figure 20C shows representative images using commercial and α-pS30 FUS antibodies. Both pFUS and FUS co-localize in cytoplasmic inclusions. The α-pT71, and α-pS96 antibodies also stain cytoplasmic structures (Figure 28) but are inconclusive due to cross-reactivity with other species (Figure 26B). To determine if the pFUS-positive cytoplasmic granules were stress granules, immuno-staining was performed with α-G3BP and α-TIA1 (Figure 20D, 29); both markers co-localized with phospho-FUS antibodies, suggesting that stress granules contain phosphorylated FUS.

In previous work we showed that PIKK kinases phosphorylate the FUS PrLD following DNA damage, but phosphorylation could be eliminated with the addition of PIKK-specific inhibitors (Rhoads et al., 2018a). To determine if phosphorylation following osmotic and oxidative stress is facilitated by PIKK kinases, here we used the PIKK-specific inhibitor torin 2 (Blackford and Jackson, 2017; Udayakumar et al., 2016), which we confirmed to be a broadly acting PIKK kinase inhibitor (Figure 27A). Torin 2 treatment completely abrogated DNA damage-induced (calicheamicin (CLM))

phosphorylation at all PIKK and non-PIKK sites, but only had a small effect on osmotic stress-induced phosphorylation and essentially no effect on oxidative stress-induced phosphorylation (Figure 21A, B).

When we pre-treated cells with torin 2, the morphology of FUS-positive granules did not change and still reacted with the phospho-antibodies (Figure 21C). At the three sites analyzed, we see torin 2 dramatically reduces nuclear phospho-FUS signal when cells were treated with calicheamicin, but not with sorbitol or sodium arsenite (Figure 21D, 27B). Cytoplasmic phospho-FUS levels under all conditions are not significantly reduced by torin 2 (Figure 21D, 27B). The above data suggest that phosphorylated FUS is present in cytoplasmic granules and may be modified by an unidentified nuclear or cytoplasmic kinase(s).

Phosphorylated ALS-mutant FUS is present in cytoplasmic inclusions

ALS-associated mutations that disrupt FUS's C-terminal NLS cause FUS to accumulate in the cytoplasm, which is hypothesized to be part of the pathological mechanism causing FUS-linked ALS (Dormann et al., 2010). Since we observed that FUS's PrLD is capable of being phosphorylated at non-PIKK sites and by non-PIKK kinases, we asked if mutant cytoplasm-confined FUS can be phosphorylated. We expressed an N-terminal GFP-tagged FUS containing an ALS-causing nonsense mutation that eliminates FUS's NLS (FUS(R495X)) in H4 cells. Expression of FUS(R495X) in H4 cells, followed by immunoprecipitation and Western blotting with phospho-specific antibodies indicated that mutant FUS's PrLD was being phosphorylated in the cytoplasm (Figure 22A, 30A).

Using immuno-fluorescence microscopy, we characterized cytoplasmic mutant FUS expression patterns. Expression of GFP-FUS(495X) for 6, 8, or 24 hours yielded diffuse, granular, or aggregated cytoplasmic patterns (Figure 22B, C). To confirm these results, we also used a C-terminal GFP-tagged FUS (FUS(1-494-GFP)). Both N-terminal and C-terminal GFP-FUS constructs showed similar cytoplasmic accumulation (Figure 22B). At 6 hours post transfection, the majority of mutant FUS was in a diffuse or granular state. By 24 hours, the aggregated pattern was more prevalent. We assessed the phosphorylation of diffuse, granular, and aggregated FUS(R495X) at 24 hours post-transfection and quantified phosphorylation at both PIKK and non-PIKK consensus sites ((Figure 22A, D; 29). The phospho-signal had the highest correlation coefficient with the GFP-signal in the aggregated inclusion state, and decreased as the expression became more diffuse.

To determine if phosphorylation of mutant FUS's PrLD is dependent on PIKK-family kinases, H4 cells were treated with torin 2 after 6 hours of transfection – prior to when aggregation was observed. The inhibition of PIKK-family kinases did not significantly affect mutant FUS phosphorylation at any residues analyzed (Figure 22E, 30). These data indicate that ALS-mutant FUS can be phosphorylated by cytoplasmic kinases and phospho-FUS is enriched within cytoplasmic foci.

Mutant FUS—with or without phosphomimetic substitutions at non-PIKK sites—forms cytoplasmic inclusions with liquid-like properties

In our previous work, we found that phosphomimetic substitutions (S/T→E) of all twelve PIKK consensus sites within the PrLD dramatically decreased cytoplasmic

aggregation of ALS-mutant FUS(495X) in cell culture (Monahan et al., 2017). We asked if phosphomimetic substitution (S/T→E) at four non-PIKK consensus sites (4Ev3 and 4Ev4; diagrammed in Figure 24A) would alter cytoplasmic inclusion formation of mutant FUS(1-494-GFP) in H4 cells. For controls we used constructs with all the PIKK sites substituted to alanine or glutamate (12A or 12E), as well as a construct with no substitutions (0E). We analyzed the expression patterns 24 hours post-transfection using live cell imaging (Figure 23A).

Expression of FUS(1-494)-GFP (0E) resulted in the formation of numerous cytoplasmic inclusions with different morphologies, from smooth to amorphous (Figure 23A). The 12A construct produced amorphous, relatively small puncta throughout the cytoplasm of cells. The expression of the 12E variant had the most profound effect, with noticeably more soluble protein. The 4E phosphomimetic constructs resulted in patterns like the 0E control. We counted the number of granules in cells transfected with each construct (Figure 23B). There was a significant decrease in the number of granules present in cells containing the 12E construct when compared to all other constructs, as previously observed (Monahan et al., 2017). However, the 4E constructs appeared much like 0E.

Different variants of mutant FUS have previously been shown to form condensates with liquid-like characteristics (Niaki et al., 2020). We asked if the FUS(1-494) inclusions would have liquid-like behavior and if phosphomimetic substitutions would alter their dynamics. We used fluorescence recovery after photobleaching (FRAP) to assess the dynamics of mutant FUS cytoplasmic inclusions (Alberti et al., 2019). All FUS constructs had similar mobile fractions and half times of recovery, suggesting

similar dynamics (Figure 23C). Each construct also displayed liquid-like characteristics with recovery on the time scale of seconds. We also performed FRAP with cells treated with sodium arsenite, since it is reported to drive cytoplasmic FUS into granules; the fluorescence recovery times were similar for all variants (Figure 31) These data suggest a few phosphomimetic substitutions in the PrLD do not dramatically alter FUS's LLPS in cells, which could be because a percentage of FUS is typically phosphorylated at sites within the PrLD when contained within liquid-like cytoplasmic inclusions.

FUS toxicity and aggregation can be altered by non-PIKK phosphomimetic substitution

Our previous work in yeast models revealed a link between human FUS's cytoplasmic aggregation and toxicity when ectopically expressed (Kryndushkin et al., 2011; Monahan et al., 2017; Monahan et al., 2018). FUS expressed in yeast models displays detergent resistance and dye-binding properties more typical of solid-phase aggregates (Fushimi et al., 2011; Kryndushkin et al., 2011). In yeast, we previously found that phosphomimetic substitutions (S/T→E) of the PrLD's 12 PIKK-kinase consensus sites reduced FUS's aggregation propensity and caused a concomitant reduction in its toxicity (Monahan et al., 2017). However, it was not known if the PIKK consensus sites were special, or if other potential phosphorylation sites within the PrLD could likewise inhibit aggregation and toxicity.

We compared the effect of PIKK versus non-PIKK consensus site phosphomimetic substitution by using five full-length FUS variants that each had four unique S/T→E substitutions (Figure 24A). The constructs contained substitutions at

PIKK consensus sites (4Ev0, v1, v2), non-PIKK consensus sites (4Ev3, v4), or both (4Ev5). The different combinations of 4E substitutions were expressed at similar levels and significantly decreased toxicity regardless of the specific substitutions being PIKK or non-PIKK consensus sites (Figure 24B; 32A, B). Substitutions that overlapped a core region (aa39-95), previously defined by solid-state NMR as being important for solid-phase aggregation (Murray et al., 2017) appeared to have a slightly greater suppression of toxicity, although not statistically significant (Figure 32C). We used structured illumination microscopy of yeast cells expressing GFP-tagged FUS (4Ev3 and 4Ev4) and found that phosphomimetic substitutions at non-PIKK sites could cause FUS to have a more diffuse expression pattern than WT FUS (Figure 24C, D), which is consistent with previous results in which all the PIKK sites were substituted (Monahan et al., 2017).

Phosphomimetic substitutions in the core of FUS's PrLD inhibit prion-like behavior in a yeast model

FUS's PrLD is compositionally similar to the naturally occurring prion proteins that form self-propagating, toxic amyloid in yeast (Kryndushkin et al., 2011; McGlinchey et al., 2011). Human disease proteins that resemble yeast prion proteins have previously been evaluated using quantitative prion scoring methods that exploit well-characterized prion assays. With these methods, human prion-like sequences are substituted for segments within the yeast prion protein Sup35 (Kim et al., 2013). The sequences can then be scored for how well they support prion-like aggregation, which is phenotypically reported by growth on media lacking adenine (essentially, the prion-like aggregation of the fusion protein results in its loss of function) (Tuite et al., 2015).

We replaced the nucleating portion of the Sup35 prion domain (aa 3-40) with a section of the FUS PrLD (aa 25-109). We also engineered a variant (4Ev6; Figure 24A) with 4 phosphomimetic substitutions within the region that appeared to best protect against FUS toxicity. The WT and 4Ev6 fusions with Sup35 were both able to compliment a sup35Δ strain (Figure 24E, top 2 rows). Both fusions were able to perform normal translational termination by not permitting read-through of the *ade-1* gene with an internal nonsense codon (non-growth on media lacking adenine; Figure 24E, rows 3-4). Transient expression of Sup35NM, which is a non-functional amino-terminal fragment of Sup35, can promote prion formation of the full-length protein (Ter-Avanesyan et al., 1994). After Sup35NM was transiently over-expressed, the FUS-Sup35 fusions gained the ability to grow on media lacking adenine. However, induction of growth for 4Ev6 was reduced by about 1 log relative to the non-mimetic fusion. This suggests phosphorylation within a few sites (either PIKK or non-PIKK) of FUS's PrLD may be able to inhibit prion-like aggregation.

Non-PIKK phosphomimetic substitutions inhibit FUS solid-phase aggregation *in vitro*

We, and others, previously showed that recombinant FUS can undergo liquid- and solid-phase transitions into dynamic droplet or solid aggregate structures *in vitro* (Monahan et al., 2017; Patel et al., 2015). Wild-type full-length FUS will undergo LLPS and form liquid droplets observable by differential interference contrast (DIC) microscopy, but after prolonged agitation solid amorphous aggregates form (Monahan et al., 2017). We created two FUS-MBP phosphomimetic constructs with the same 4 non-

PIKK S/T→E substitutions described above (Figure 24A; 4Ev3 and 4Ev4). We examined phase separation of these two non-PIKK phosphomimetic constructs using DIC. We also included a control with phosphomimetic substitutions at all 12 PIKK sites (12E), which were previously found to be sufficient to inhibit the formation of solid aggregates when FUS was subjected to overnight agitation. We found that the FUS constructs that contained 4 non-PIKK phosphomimetic substitutions in the PrLD were able to form droplet structures, but failed to form solid aggregates with prolonged agitation (Figure 25A, 33A). Amorphous aggregates of FUS start to form within 6 hours of agitation, while the droplet structures formed by the phosphomimetic variants persist up to 48 hours with agitation (Figure 33A). To ensure these droplets were in a liquid-phase separated state we treated the agitated proteins with 1,6-hexanediol, a chemical probe used to disrupt weak hydrophobic interactions (Sonja Kroschwald, 2017). Wild-type full-length FUS solid aggregates were unaffected by 1,6-hexanediol treatment, while the phosphomimetic FUS droplets dissolved upon exposure (Figure 33B).Using turbidity as a reporter for LLPS, we also found that high salt could significantly suppress phase separation for both FUS-4Ev3 and FUS-4Ev4 when compared to the baseline condition (150 mM NaCl; Figure 25B), which is similar to results observed for phosphomimetic substitutions at 6 or 12 PIKK consensus sites (Monahan et al., 2017). These results suggest that non-PIKK kinases that act upon a few sites within the PrLD could have dramatic effects on FUS's phase separation, especially in preventing irreversible solid aggregate formation.

DISCUSSION

Post-translational modifications of FUS have been proposed to regulate its inclusion and function in membraneless organelles (Owen and Shewmaker, 2019). Aberrant formation of membraneless organelles has also been linked to FUS-associated neurodegenerative disease (Shin and Brangwynne, 2017). To better understand the link between PTMs and FUS phase transitions, we analyzed both PIKK and non-PIKK consensus site phosphorylation of wild-type FUS's PrLD under cellular stress conditions and ectopically expressed mutant FUS. Our data suggest that the FUS PrLD is differentially phosphorylated depending on the stress condition within the cell. We evaluated how phosphomimetic substitutions at PIKK and non-PIKK sites affected FUS's phase separation and aggregation. Our data suggest that phosphorylation at non-PIKK sites can have similar inhibitory effects on phase separation and aggregation as previously observed with PIKK sites (Monahan et al., 2017); however, phosphomimetic substitutions in FUS's PrLD appear to be particularly detrimental to solid-phase transitions.

Previous mass spectrometry analysis of FUS indicated 32 putative phosphorylation sites in the PrLD of FUS (Rhoads et al., 2018a). We and others previously confirmed phosphorylation of three PIKK consensus sites by PIKK-family kinases following DNA damage (Deng et al., 2014; Gardiner et al., 2008; Rhoads et al., 2018a). In this study we provide data that three non-PIKK consensus sites (S57, T71, and S96) are phosphorylated following different types of cellular stress. The inhibition of PIKK-family kinases did not prevent phosphorylation of FUS's PrLD following osmotic or oxidative stress, suggesting that other kinases may regulate this domain. The NetPhos

algorithm predicts protein kinase C (PKC) is the most likely candidate kinase for sites S57 and S96, and cyclin dependent kinase 5 (cdk5) is the most likely for T71. Our preliminary experiments using pharmacological inhibitors of these kinases were inconclusive. We also evaluated ALS-mutant FUS that was confined to the cytoplasm due to defects in its NLS. Mutant cytoplasmic FUS was phosphorylated by one or more presumably cytoplasmic kinase(s) that were not affected by PIKK inhibition.

We also observed that PIKK-family kinases have the potential to phosphorylate non S/TQ consensus sites within the PrLD following DNA damage, which is consistent with bioinformatic data on PIKK substrates that indicates non-canonical phosphorylation is not uncommon (kinaseNET). However, non-PIKK sites appeared to be phosphorylated subsequently to PIKK sites. In conclusion, we observed differential phosphorylation of PIKK and non-PIKK consensus sites depending on the type and extent of stress response elicited from mutations, DNA-damage, oxidative stress, or osmotic stress. This suggests that FUS's phospho-proteoform can change according to the specific function it is performing or the stress it responding to.

Previous work shows that cytoplasmic FUS phase separates into stress granules. Here we found that under stress conditions that caused FUS accumulation into cytoplasmic granules, phospho-FUS was detectable in G3BP-positive stress granules. The rates of phosphorylation observed by Western blotting were stress-dependent and correlated with the dynamics previously reported for stress granule formation under different stress conditions (Wheeler et al., 2016). These data suggest a role for site-specific phosphorylation of FUS that could be important for its function or localization

within stress granules (both into or out of). However, the temporal relationship between phosphorylation and granule dynamics requires further characterization.

A recent study showed numerous mutant FUS constructs can separate into droplets *in vitro* (Niaki et al., 2020). The liquid-like dynamics of FUS varied depending on the type or location of the mutation. Here, we corroborated these findings and observed that NLS-mutant FUS (FUS(R495X)) can liquid-phase separate in cells. We biophysically characterized mutant FUS and determined that it is in a liquid-like state in cytoplasmic granules. When 4 phosphomimetic substitutions were introduced into the PrLD, no differences in FUS dynamics within granules were observed by FRAP. The dynamics were similar regardless of where the phosphomimetic substitutions occurred. When 12 substitutions were introduced, the effect was largely observed as more diffuse FUS, but FRAP dynamics of cytoplasmic granules remained largely the same. Likewise, mutant FUS-positive cytoplasmic granules did not have altered FRAP dynamics even when cells were treated with sodium arsenite to induce PrLD phosphorylation. Thus, FUS dynamics within these structures appears to not be greatly altered by PrLD phosphorylation. This may be because cytoplasmic liquid-state granules are complex heterogeneous structures, of which FUS might be a minority species and subject to many other overriding interactions.

Phosphorylation of FUS's PrLD may be more critical for preventing pathological solid-state transitions. A current hypothesis suggests a link between membraneless organelle dynamics and formation of toxic cytoplasmic inclusion in neurodegenerative disorders like ALS (Wolozin and Ivanov, 2019). The high concentrations of proteins like FUS within condensates may potentiate molecular interactions that lead to

solid/irreversible aggregate formation (Shin and Brangwynne, 2017). Our *in vitro* data with recombinant FUS suggests phosphorylation of the PrLD can have profound inhibition on solid-phase transition while minimally affecting LLPS. Also, these effects are non-specific; phosphomimetic substitutions had similar effects regardless of their exact locations within the PrLD. In yeast, we observed similarly that 4 phosphomimetic substitutions were enough to suppress prion/amyloid-like aggregation and proteotoxicity. Toombs *et al.* previously discovered that amino acid composition of prion domains can be more important for amyloid-like solid-phase aggregation than the specific order of the amino acids; charged groups are especially unfavorable (Toombs et al., 2010). Likewise, the in-register parallel cross-β structural model of FUS PrLD proposed by Murray *et al.* would be strongly disfavored by the introduction of charged groups (Murray et al., 2017). Our phosphomimetic data is consistent with these findings by suggesting substitution at specific PIKK sites is not required to have a general anti-aggregation effect on the solid phase.

In the case of NLS-deficient mutant FUS (FUS(R495X)), which localizes to the cytoplasm in either a diffuse, granular, or aggregated state, we observed that punctate FUS appears to have greater PrLD phosphorylation. A possibility is the environment of some liquid-phase-separated environments favors more phosphorylation (Rai et al., 2018), which could have protective effects against solid-phase aggregation. Hyperphosphorylation of some neurodegenerative-associated proteins within pathological inclusions could be the marks of failed solubilization mechanisms, rather than promoters of aggregation (Hergesheimer et al., 2019; Li et al., 2011).

While FUS's PrLD has 12 PIKK consensus and numerous other putative phosphorylation sites, in our observations, the FUS proteoform generally consists of protein with only a few phosphorylation events following most stress. This is evident because when FUS is highly phosphorylated it visibly migrates slower by Western blot (Deng et al., 2014; Monahan et al., 2017). We observed a few phosphomimetic substitutions could have dramatic effects on solid-state aggregation, regardless of their exact position in the PrLD. Phosphomimetic substitutions are not perfect substitutes for phospho-serine and phospho-threonine, and are more subtle than the addition of phosphate groups to amino acids, so possibly the phosphomimetic effects understate the inhibitory effects of phosphorylation. Tilting the balance towards slightly greater phosphorylation of the FUS proteoform in vivo could be a therapeutic strategy for ALS and FTD subtypes. Further research into the kinase and phosphatase regulation of FUS is required.

METHODS

Cell culture / transfections / FUS knockdowns. H4 neuroglioma (ATCC HTB-148) cells were cultured in DMEM (Sigma D6429) supplemented with 10% fetal bovine serum (Sigma F6178) and 1% penicillin-streptomycin (Corning 30-002-Cl). Cells were lysed with a modified RIPA buffer (200 mM NaCl, 100 mM Tris-HCl pH 8, 0.5% sodium deoxycholate, 1% Triton X-100, 670 mM phenylmethylsulfonyl fluoride, 1250 units of benzonase nuclease (Sigma E8263), 150 μL protease inhibitor cocktail (Thermo 1861278), and 100 μL phosphatase inhibitor (Thermo 78426)) for 30 minutes on ice.

DNA was transfected into H4 cells at ~70-80% confluency using Lipofectamine 2000 (Thermo 11668027) and OptiMEM (Gibco 31985070) in a ratio of 3 μg DNA to 2.5 μL Lipofectamine 2000 and incubated at 37 C for 24 hours unless otherwise stated. FUS knockdowns were done with Lipofectamine RNAiMAX (Thermo 13778075) and 30 pmol siRNA (FUS (Thermo 4392420) and negative control (Thermo 4390843)) for 48 hours at 37 C.

H4 cells were treated with the following reagents for 1 hour at 37 C unless otherwise stated: 15 nM or 50 nM calicheamicin-γ (generous gift from Pfizer), 0.4 M sorbitol (Sigma S1876), 500 μM sodium arsenite (Chem Cruz 301816), and 200 nM torin 2 (Selleckchem S2817).

Cloning/Plasmids. WT FUS, FUS 12E, and GFP-FUS 495X plasmids were obtained from Monahan et al (2017). Plasmids were generated through either PCR cloning (Thermo F531S) genes into *appropriate parent vectors at multiple cloning sites* or through site directed mutagenesis (New England Biolabs E0552S), with the exception of FUS 12A which was synthesized by GenScript (Piscataway, NJ). Plasmids used for protein purification were derived from 6xHis-MBP-FUS (source – Addgene 98651); plasmids used for immunofluorescence and live-cell imaging were derived from C1-eGFP (source – Addgene 54759); plasmids used for yeast toxicity were derived from pH317 (*2μ LEU2* P_{GAL}; source – Shewmaker lab); plasmids used for yeast SIM imaging were derived from pH316 (*CEN LEU2* P_{GAL}; source – Shewmaker lab).

Custom antibodies and peptide specificity. Production of Serine 26 and Serine 30 phospho-antibodies were previously described in Rhoads et al 2018 by GenScript (Piscataway, NJ). Serine 57, Threonine 71 and Serine 96 were produced similarly using synthetic peptides FUS 51-63 GQSSYS(p-S)YGQSQN, FUS 65-79 GYGTQS{p-T}PQGYGSTC, and FUS 91-105 YGQQS{p-S}YPGYGQQPC as immunogens for antibody production in rabbits, respectively. T71 and S96 peptide synthesis and antibody production was performed by Genscript, while S57 production was performed by ThermoFisher (Lafayette, CO)

Specificity of phospho-antibodies were verified through FUS knockdowns and peptide dilutions. FUS knockdowns were analyzed through Western blot and immunocytochemistry procedures. Nitrocellulose membranes (BioRad 1620112) were saturated with 8 M urea before being loaded on the Hybri-Slot Manifold blotting apparatus (BRL 1052MM). Unmodified and phosphorylated FUS peptides were blotted and probed with respective antibodies following Western blotting protocol.

Immunocytochemistry and FRAP. For fixed cell imaging, cells were grown on glass coverslips for 24 hours prior to any treatments and fixation with 4% paraformaldehyde (Sigma P6148). The cells were permeabilized with -20 C methanol and blocked with 5% normal goat serum (Abcam ab7481) with 0.05% sodium azide (Life Technologies 50062Z). The following antibodies were used to probe the fixed cells: FUS antibodies (Abcam ab154141, custom rabbit phospho-FUS antibodies), G3BP (BD 61112), and TIA1 (Santa Cruz 166247). Secondaries used to detect primary antibodies were AlexaFluors AF488 and AF568 (ThermoFisher A-11001, A-11011). Nuclei were stained

using the Mounting media with DAPI (ThermoFisher P36931). Slides were imaged using Zeiss 700 and the Nikon A1R. Immunofluorescence quantification was done using the raw integral density in Fiji (Schindelin et al., 2012). Values were normalized to the highest intensity in the data set. Mutant FUS(495X) phosphorylation was quantified using Pearson's correlation coefficient to the GFP signal. FUS(494)-GFP granule area and number was quantified using particle analysis on ImageJ.

For live cell imaging, cells were grown in glass bottom microwell dishes 24 hours prior to transfection. The cells were incubated at 37 C for either 12 or 24 hours post transfection. After either time point, the medium was changed to dye-free DMEM (Thermo #21063029). The FRAP data was collected on the Nikon A1R. The center of a granule, marked by a 0.3 μm region of interest, was bleached at 100% power for 1.9 seconds. The recovery was analyzed for 98 seconds (~1.5 minutes). The recovery was quantified using the time series analyzer V3 plugin on Fiji. The bleached pixel intensity was subtracted from each data point and then data points were normalized to the pixel intensity before the bleaching occurred.

Western blotting. Lysates were mixed with 4x NuPAGE LDS Sample Buffer (Thermo NP0008) and ran through AnyKD precast gels (BioRad 4569034) for 80 V for 2 hours. Gels were transferred through either Trans-Blot Turbo Transfer System (Bio-Rad 1704150) or eBlot L1 (GenScript L00686) onto nitrocellulose membranes (BioRad 1620112). Membranes were blocked with 6% milk (BioRad 1706404) in Tris buffered saline (TBS). Primary and secondary antibodies were diluted in TBS with 0.1% Tween-20 (Sigma P7949). The following primary antibodies were used to probe the blots: FUS

antibodies (Santa Cruz 373698, Abcam ab154141, Bethyl A300-293A, custom rabbit phospho-FUS antibodies), gamma tubulin (Sigma T6557), GFP (Roche 11814460001). Primary antibodies were detected with secondaries conjugated to IRDye fluorescent probes (LI-COR 926-68021, 926-32210). Blots were imaged with the Odyssey CLx Imaging System (LI-COR). Band densitometry quantification was done using Image Studio software (Li-COR). Phospho-bands were normalized to endogenous FUS band intensity.

***In vitro* DNA-PK phosphorylation** (2B). A plasmid encoding for 6xHis-MBP-FUS (Addgene 98651) was transformed into NiCo(DE3) competent *Escherichia coli* (New England BioLabs C2529H). Cell pellets were collected from 1 liter cultures induced with 0.5 mM IPTG after continued growth at 37 C for 4 hours. Pellets were sonicated in 20 mM NaPi pH 7, 1 M NaCl, 10 mM imidazole with a protease inhibitor tablet (Roche 11836170001) and spun down at 20,000 x g for one hour at 4 C. The supernatant was filtered through 0.8 μm surfactant-free cellulose acetate syringe filters (Corning 431221) before being run through a nickel column (GE 17-5286-01). The column was washed with 20 mM NaPi pH 7, 1 M NaCl, 30 mM imidazole prior elution with 20 mM NaPi pH 7, 1 M NaCl, 300 mM imidazole. The eluate was collected and spun down with 50 kDa centrifuge filters (Millipore UFC505024) and stored in 75% 20 mM NaPi pH 7, 1 M NaCl, 25% glycerol.

In vitro DNA-PK reactions were done using a DNA-PK kinase enzyme system (Promega V4106) in a reaction following the manufacturer's protocol containing 5 μg recombinant MBP-FUS, 200 μM ATP, and varying doses of DNA-PK. The reactions

were incubated at room temperature for one hour before being prepped for Western blotting.

Phase separation and turbidity. A plasmid encoding for 6xHis-MBP-FUS (Addgene 98651) and phosphomimetic derivatives were transformed into BL21(DE3) competent *Escherichia coli* (New England BioLabs C2529H). Cell pellets were collected from 1 liter cultures induced with 0.5 mM IPTG after continued growth at 37 C for 4 hours. Pellets were sonicated in 20 mM Tris-HCl, 1 M NaCl, 1 mM EDTA, pH 7.4, with a protease inhibitor tablet (Roche 11836170001) and spun down at 20,000 x g for one hour at 4 C. The supernatant was filtered through 0.8 μm surfactant-free cellulose acetate syringe filters (Corning 431221) before being run through a MBPTrap column (GE 17-5286-01). The column was washed with 20 mM Tris-HCl, 1 M NaCl, 1 mM EDTA, pH 7.4 prior elution with 10 mM maltose in the buffer. The eluate was collected and spun down with 50 kDa centrifuge filters (Millipore UFC505024) and stored with 25% glycerol.

Phase separation samples were prepared in 20 mM Tris HCl, 150 mM NaCl, pH 7.4 with 5 uM of MBP-FUS and 5 units of ProTEV Plus (Promega 20200703) and agitated at 1200 rpm at 25 C overnight. Samples were aliquoted onto glass slides and imaged through differential interference microscopy (Olympus IX73). Phase-separated, agitated protein samples were subjected to 10% 1,6-hexanediol (Sigma 629118). Protein samples were aliquoted into a glass microscopy dish and 10% 1,6-hexanediol (final concentration) was added. Images were taken using differential interference microscopy (Leica DMi1) before treatment and at 5, 10 and 30 minutes during treatment. Turbidity

measurements were done with 5 uM MBP-FUS in 20 mM Tris HCl and varying concentrations of NaCl ranging from 150 mM to 1 M. Samples were incubated with 10 units of ProTEV Plus (Promega) for 45 minutes at 30 C, and absorbance at 600 nm was measured using a BioTek Cytation 5 imaging reader.

Yeast. Yeast strain BY4741 (*his3D1 leu2D0 met15D0 ura3D0 PIN+)* was used for toxicity and aggregation assays. For the toxicity assay, single colonies were grown overnight at 30 C and dilution spotted on glucose and galactose plates. For structured illumination microscopy, overnight cultures were induced with galactose for 8 hours at 30 C before being fixed with 4% PFA and washed with 0.1 M KPO_4 and 0.1 M KPO_4/1.2 M sorbitol buffer. The cells were treated with 100T zymolyase (Zymo Research E1005) to form spheroplasts. Glass slides were treated with 0.1% poly-D-lysine and the spheroplasts settled on the slide before permeabilized with -20 C methanol. Slides were blocked with PBS-BSA and probed with rabbit anti-FUS polyclonal antibody (Bethyl 300-293A). Alexa Fluor 488 Conjugate #4412 secondary was used to detect the FUS antibody before being mounted with Prolong mounting media with DAPI (ThermoFisher P36931) and covered with a glass coverslip. Samples were imaged using the Zeiss Elyra PS.1 with three rotated gratings.

Yeast Sup35 knockout strain (*kar1-1, SWQ5, ade2-1, his3, leu2, trp1, ura3, sup35::KanMx*) was complemented by Sup35 or Sup35-FUS fusion plasmids. A galactose-inducible Sup35NM plasmid was transformed into the yeast strains and induced for 16 hours at 30 C before being plated on synthetic complete media and media lacking adenine.

FIGURES

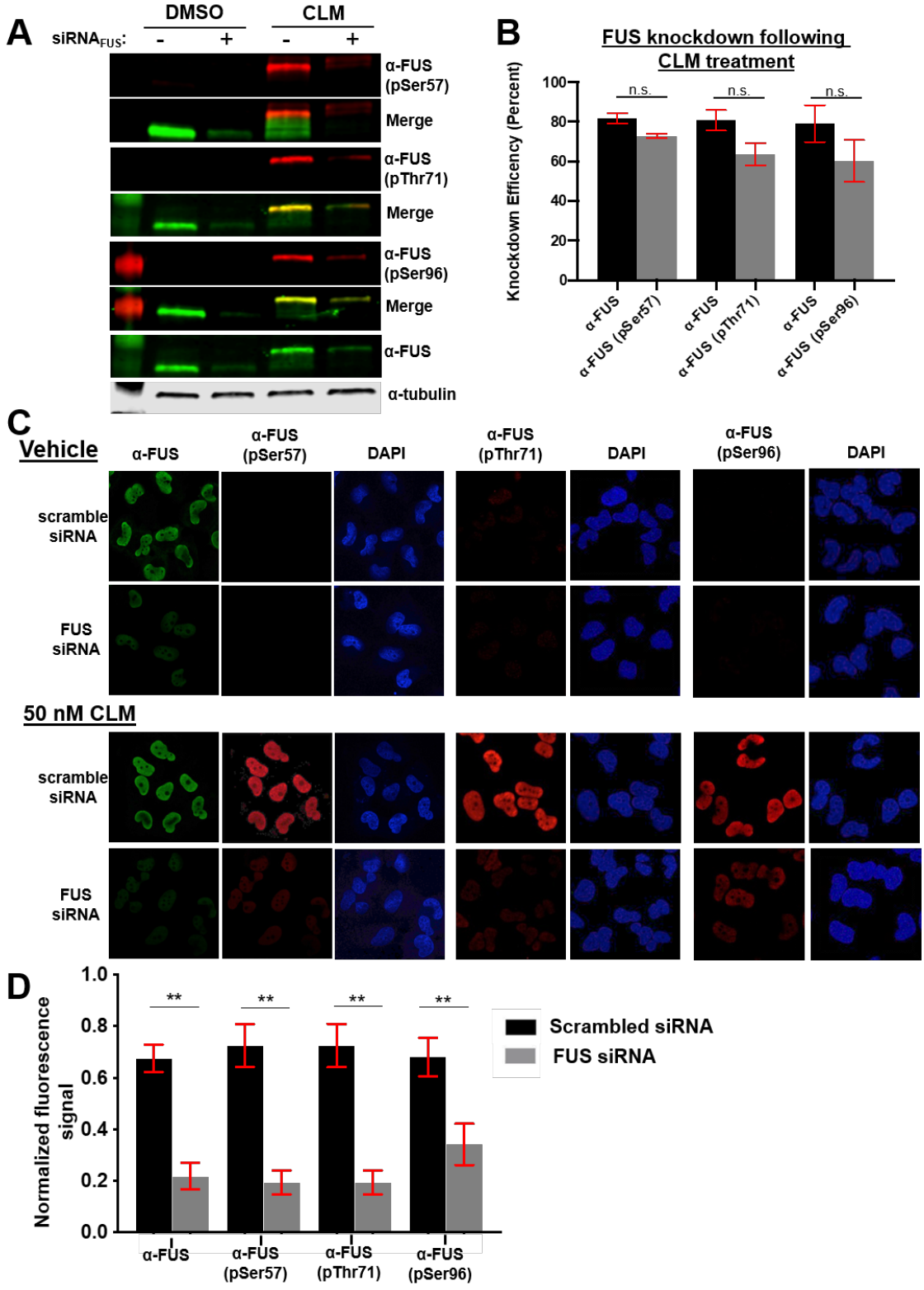
A
siRNA$_{FUS}$:
DMSO
CLM
- + - +
α-FUS (pSer57)
Merge
α-FUS (pThr71)
Merge
α-FUS (pSer96)
Merge
α-FUS
α-tubulin
B
FUS knockdown following CLM treatment
Knockdown Efficency (Percent)
n.s.
α-FUS
α-FUS (pSer57)
α-FUS (pThr71)
α-FUS (pSer96)
C
Vehicle
α-FUS
α-FUS (pSer57)
DAPI
α-FUS (pThr71)
α-FUS (pSer96)
scramble siRNA
FUS siRNA
50 nM CLM
D
Normalized fluorescence signal
**
Scrambled siRNA
FUS siRNA

Fig 18. Phospho-specific antibodies recognize non-PIKK sites within FUS's prion-like domain

(A) H4 cells with FUS knockdown by siRNA treated with DMSO or 50 nM calicheamicin (CLM) were analyzed by Western Blots probed with commercially available FUS and custom phospho-FUS antibodies. (B) Quantification of percent reduction in Western blot band intensity of both FUS and phospho-FUS blots in figure A (n=3). Raw data in S1A. (C, D) H4 neuroglioma cells treated with 50 nM CLM after FUS knockdown were fixed and probed with commercially available FUS and custom phospho-specific antibodies; nuclear fluorescence signal was quantified and normalized to total fluorescence for each experiment; Figure data analyzed using a student t-test (n=3).

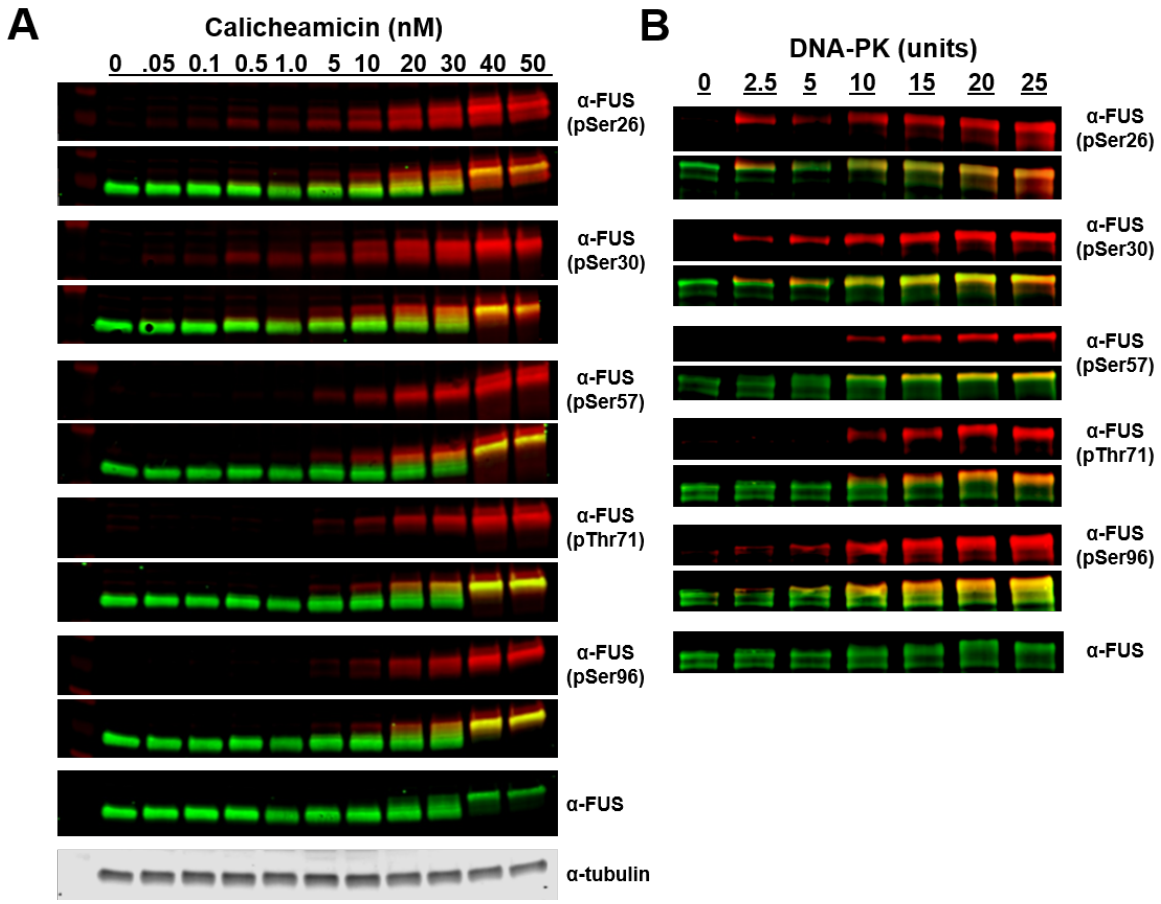

Fig 19. DNA damage induces multi-phosphorylation of FUS's prion-like domain at PIKK and non-PIKK sites

(A) H4 cells treated with a dose series of calicheamicin were analyzed by Western blot probed with anti-phospho-FUS(pSer26, pSer30, pSer57, pThr71, and pSer96) and anti-FUS antibodies. (B) Recombinant DNA-PK was used to phosphorylate MBP-FUS *in vitro.* Reaction was analyzed by Western blot and probed with commercial FUS and phospho-specific antibodies.

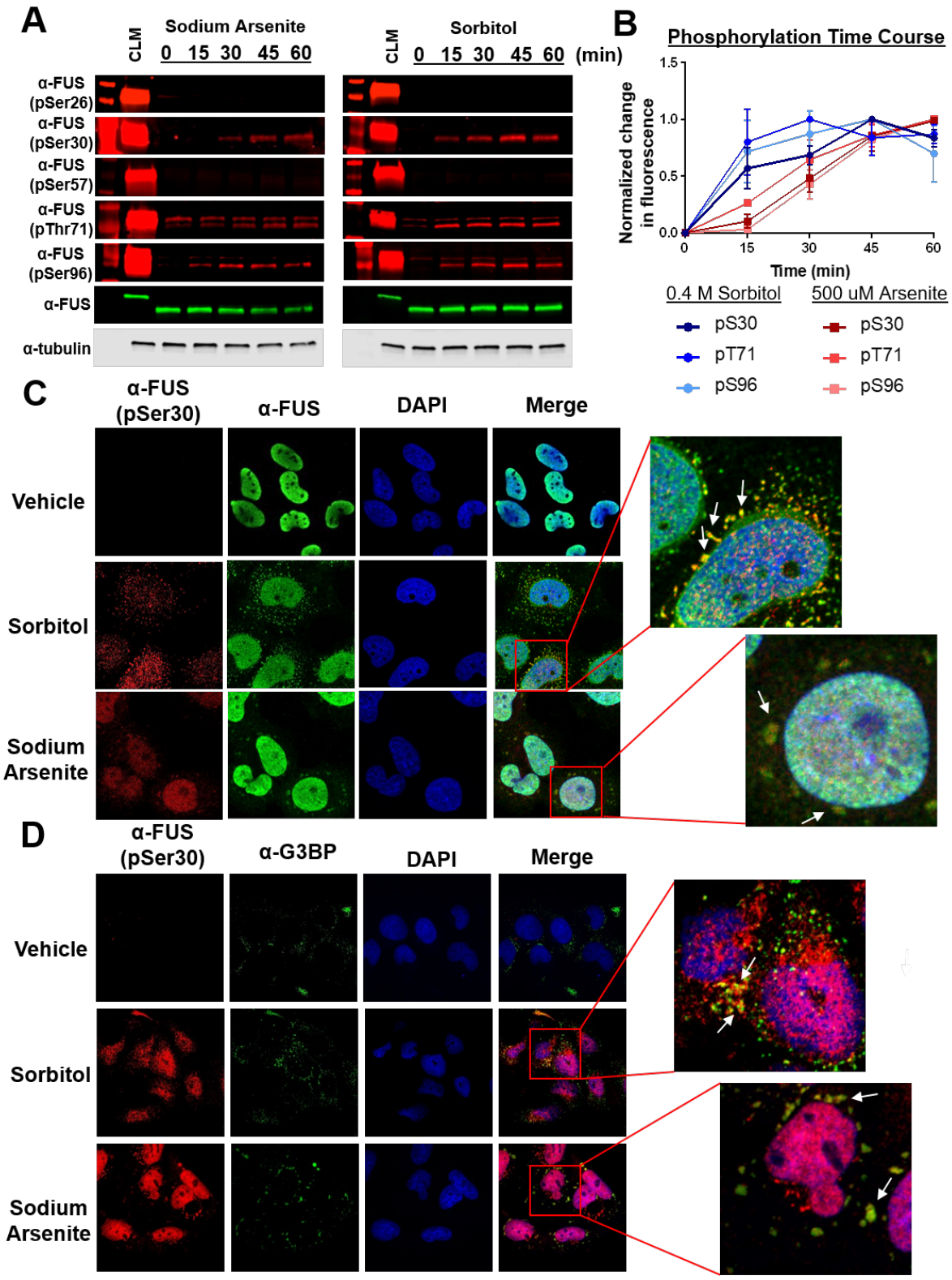
A
CLM
Sodium Arsenite
0 15 30 45 60
CLM
Sorbitol
0 15 30 45 60 (min)
α-FUS (pSer26)
α-FUS (pSer30)
α-FUS (pSer57)
α-FUS (pThr71)
α-FUS (pSer96)
α-FUS
α-tubulin
B
Phosphorylation Time Course
Normalized change in fluorescence
1.5
1.0
0.5
0.0
0
15
30
45
60
Time (min)
0.4 M Sorbitol
pS30
pT71
pS96
500 uM Arsenite
pS30
pT71
pS96
C
α-FUS (pSer30)
α-FUS
DAPI
Merge
Vehicle
Sorbitol
Sodium Arsenite
D
α-FUS (pSer30)
α-G3BP
DAPI
Merge
Vehicle
Sorbitol
Sodium Arsenite

Fig 20. FUS is phosphorylated at both PIKK and non-PIKK sites following non-DNA damaging stress

(A) H4 cells treated with 500 μM sodium arsenite or 0.4 M sorbitol at various time points were analyzed by Western Blot using anti-phospho-FUS(pSer26, pSer30, pSer57, pThr71, and pSer96) and anti-FUS antibodies. The time courses show only three of the five sites analyzed are phosphorylated by non-DNA-damaging stress. (B) The normalized band signal intensities from figure A; 95% CI error bars (n=3). (C) H4 cells treated with either sodium arsenite or sorbitol for one hour were analyzed using confocal microscopy. Both FUS and phospho-FUS (pSer30 – representative images) are found in cytoplasmic granules. (D) H4 cells treated with either sodium arsenite or sorbitol one hour were analyzed using confocal microscopy. Phospho-FUS (pSer30 - representative images) colocalizes with stress granule marker G3BP.

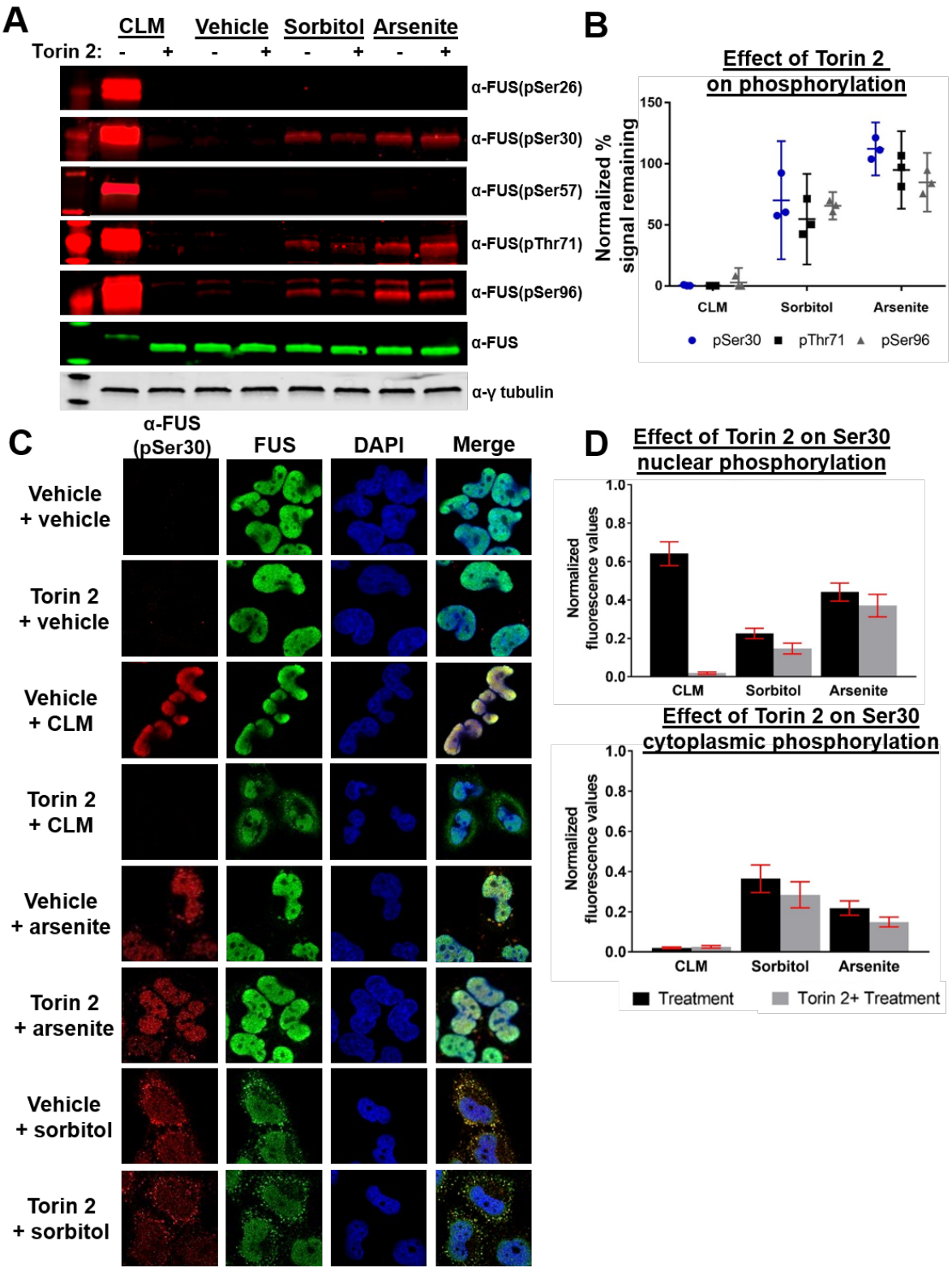
A
CLM
Vehicle
Sorbitol
Arsenite
Torin 2: - + - + - + - +
α-FUS(pSer26)
α-FUS(pSer30)
α-FUS(pSer57)
α-FUS(pThr71)
α-FUS(pSer96)
α-FUS
α-γ tubulin
B
Effect of Torin 2 on phosphorylation
Normalized % signal remaining
150
100
50
0
CLM
Sorbitol
Arsenite
pSer30
pThr71
pSer96
C
α-FUS (pSer30)
FUS
DAPI
Merge
Vehicle + vehicle
Torin 2 + vehicle
Vehicle + CLM
Torin 2 + CLM
Vehicle + arsenite
Torin 2 + arsenite
Vehicle + sorbitol
Torin 2 + sorbitol
D
Effect of Torin 2 on Ser30 nuclear phosphorylation
Normalized fluorescence values
1.0
0.8
0.6
0.4
0.2
0.0
CLM
Sorbitol
Arsenite
Effect of Torin 2 on Ser30 cytoplasmic phosphorylation
Normalized fluorescence values
1.0
0.8
0.6
0.4
0.2
0.0
CLM
Sorbitol
Arsenite
Treatment
Torin 2+ Treatment

Fig 21. Inhibition of PIKK-family kinases does not prevent phosphorylation of the FUS prion-like domain following osmotic and oxidative stress

(A) Phosphorylation status of FUS from H4 cells treated with or without Torin 2 under varying stress conditions were analyzed by Western blot. (B) Quantification of band fluorescence normalized to total FUS; error bars represent 95% CI (n=3). (C) Phosphorylation of FUS in H4 cells treated with or without Torin 2 under varying stress conditions. Fixed cells imaged using confocal microscopy. Cells were probed with FUS and phospho- FUS(pS30) antibodies. (D) Quantification of nuclear and cytoplasmic phospho-FUS(pS30); fluorescence error bars represent 95% CI (n=3).

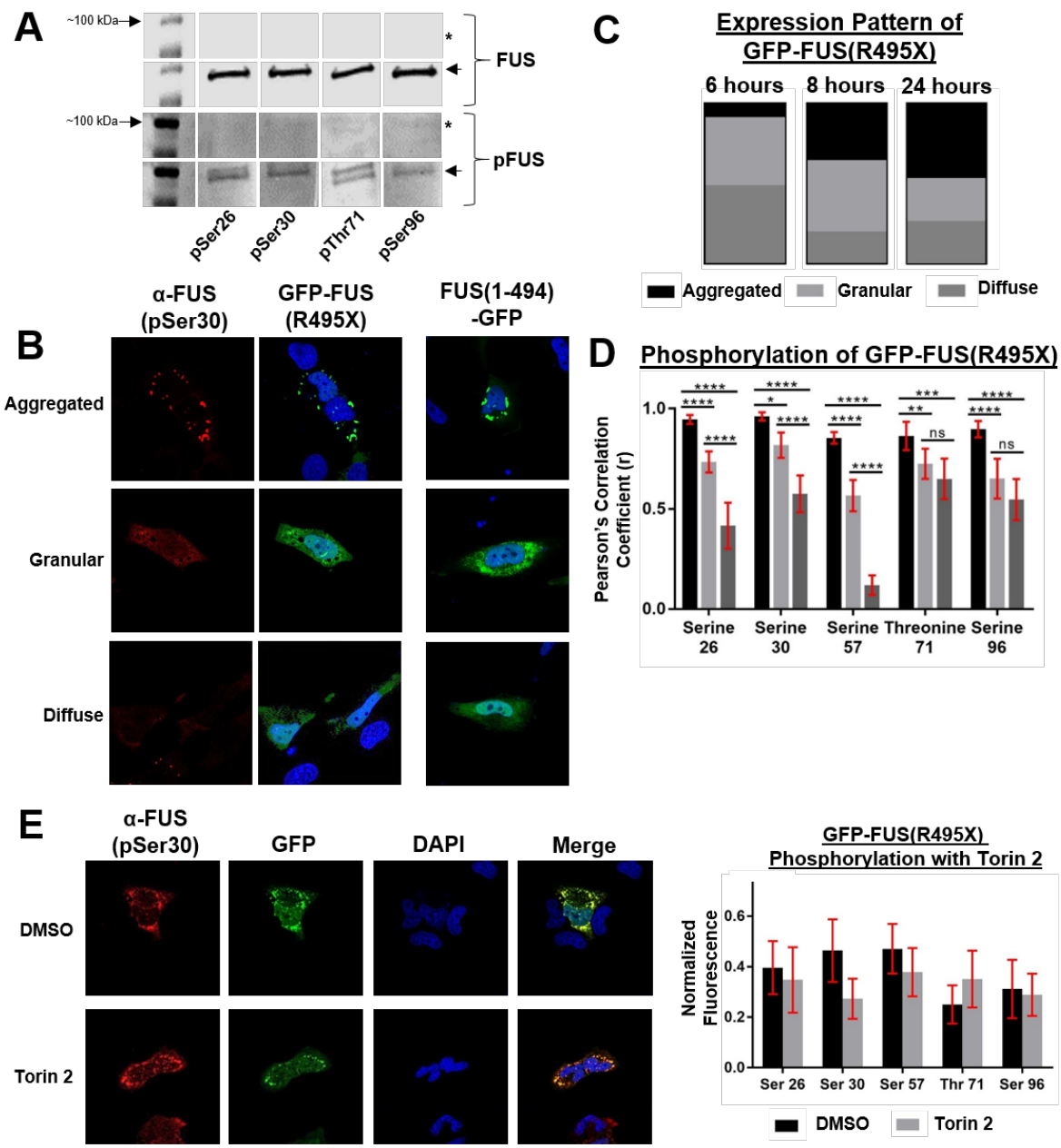
A
~100 kDa
FUS
~100 kDa
pFUS
pSer26
pSer30
pThr71
pSer96
B
α-FUS (pSer30)
GFP-FUS (R495X)
FUS(1-494) -GFP
Aggregated
Granular
Diffuse
C
Expression Pattern of GFP-FUS(R495X)
6 hours
8 hours
24 hours
Aggregated
Granular
Diffuse
D
Phosphorylation of GFP-FUS(R495X)
Pearson's Correlation Coefficient (r)
1.0
0.5
0.0
Serine 26
Serine 30
Serine 57
Threonine 71
Serine 96
ns
E
α-FUS (pSer30)
GFP
DAPI
Merge
DMSO
Torin 2
GFP-FUS(R495X) Phosphorylation with Torin 2
Normalized Fluorescence
0.6
0.4
0.2
0.0
Ser 26
Ser 30
Ser 57
Thr 71
Ser 96
DMSO
Torin 2

Fig 22. Phosphorylated ALS-mutant FUS is present in cytoplasmic granules

(A) H4 cell transfected with GFP-FUS(R495X) for 24 hours or untransfected control(*). GFP-FUS(R495X) was pulled down from cell lysates using GFP immunoprecipitation (IP). IP products were analyzed by Western blot and probed with anti-FUS (Santa Cruz) and phospho-FUS (pSer26, pSer30, pThr71, and pSer96). GFP-FUS(495X) is denoted with an arrow at roughly 100 kDa. (B) Ectopic expression of mutant FUS(R495X) in H4 cells with N- or C-terminal GFP. Anti-phospho-FUS (pSer30) antibody was used to probe for phosphorylated FUS. (C) Quantification of number of cells expressing diffuse, granular, or aggregated FUS(R495X) at 6, 8, or 24 hours post transfection (n=3). (D) Quantification using Pearson's correlation coefficient of phospho-FUS (pSer26, pSer30, pSer57, pThr71, and pSer96) to the GFP-FUS(R495X) signal; error bars represent 95% CI; (n=30). (E) H4 cells transfected with GFP-FUS(495X) treated with torin 2 6 hours post transfection. Cells were analyzed 8 hours post transfection and probed with phospho-FUS antibodies. Error bars represent 95% CI; (n=30).

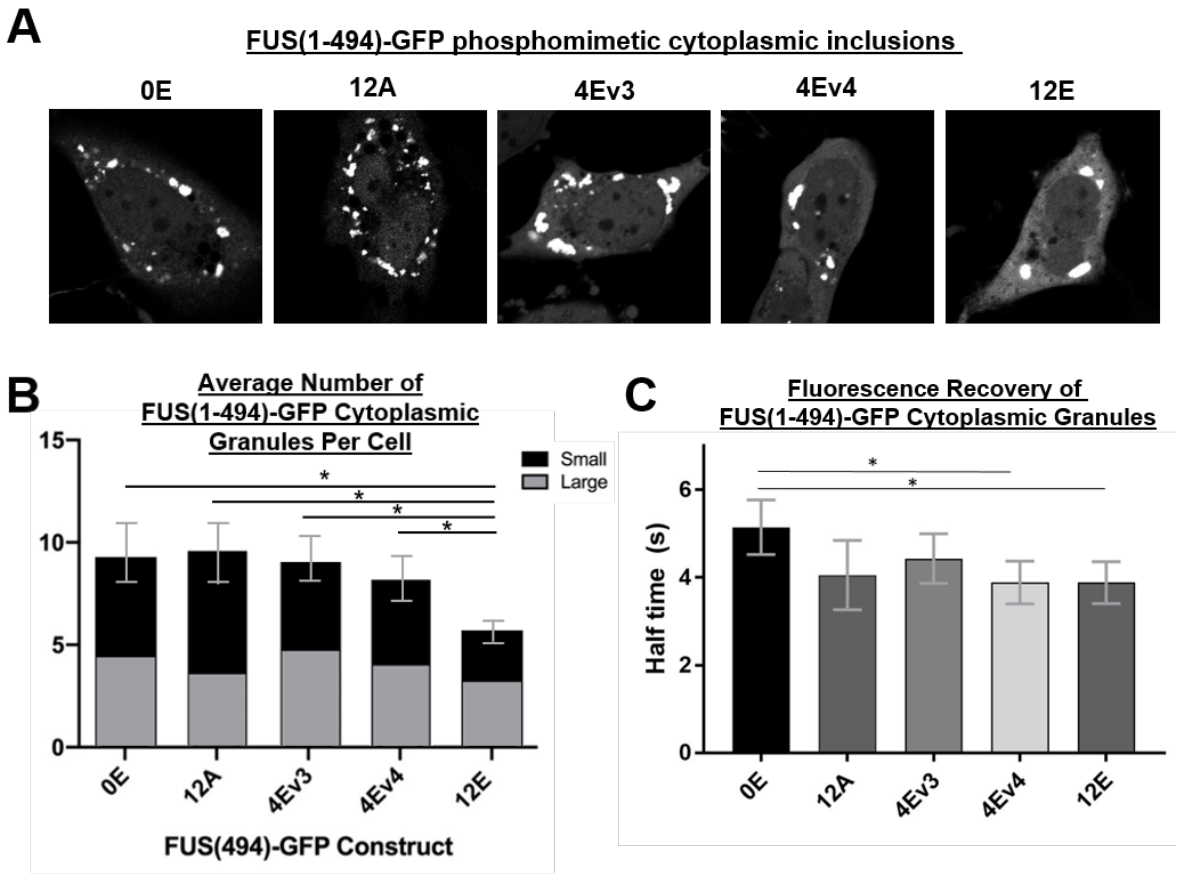

Fig 23. ALS-mutant FUS forms cytoplasmic droplets – phosphomimetic substitutions in the prion-like domain do not alter droplet dynamics

(A) Representative images of FUS(494)-GFP phosphomimetic constructs 24 hours post-transfection. (B) Average number of large (>1 micron^2) or small (<1 micron^2) FUS(494)-GFP cytoplasmic granules per cell 24 hours post-transfection; error bars represent SEM; (n=17). (C) FRAP half times of FUS(494)-GFP 24 hours post-transfection; error bars represent 95% CI; (n=30). Student t test was used for statistical analysis.

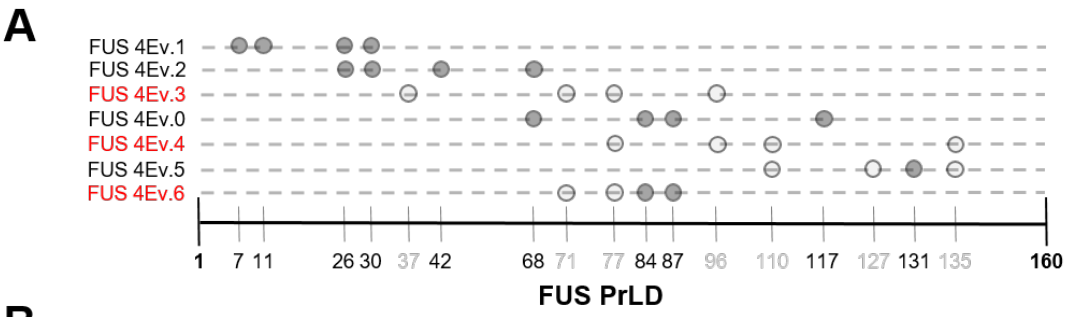
A
FUS 4Ev.1
FUS 4Ev.2
FUS 4Ev.3
FUS 4Ev.0
FUS 4Ev.4
FUS 4Ev.5
FUS 4Ev.6
1 7 11 26 30 37 42 68 71 77 84 87 96 110 117 127 131 135 160
FUS PrLD

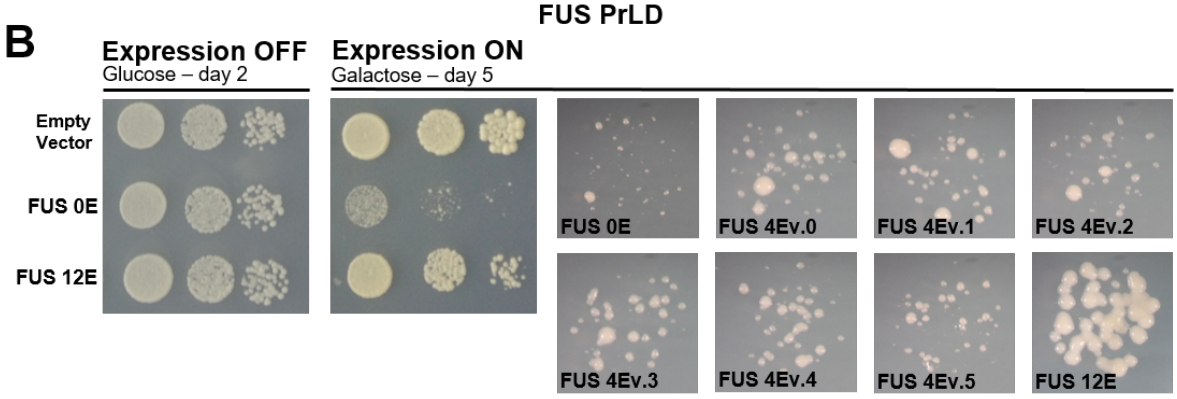
B
Expression OFF
Glucose – day 2
Expression ON
Galactose – day 5
Empty Vector
FUS 0E
FUS 12E
FUS 0E
FUS 4Ev.0
FUS 4Ev.1
FUS 4Ev.2
FUS 4Ev.3
FUS 4Ev.4
FUS 4Ev.5
FUS 12E

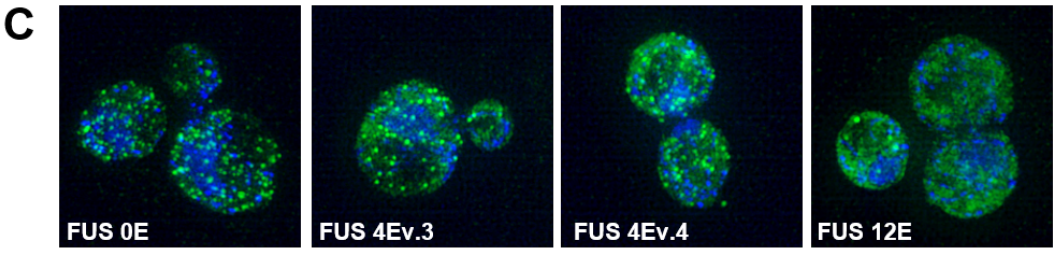
C
FUS 0E
FUS 4Ev.3
FUS 4Ev.4
FUS 12E

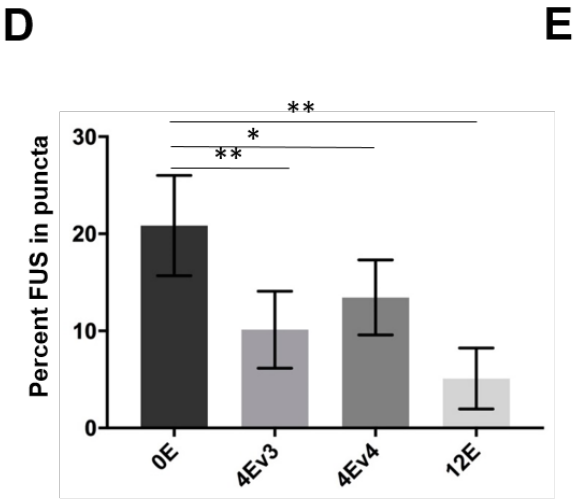
D
Percent FUS in puncta
30
20
10
0
**
*
**
0E
4Ev3
4Ev4
12E

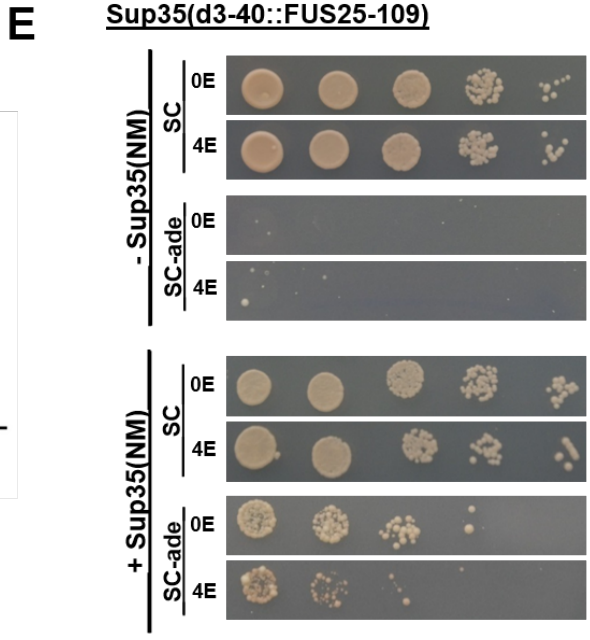
E
Sup35(d3-40::FUS25-109)
- Sup35(NM)
SC
0E
4E
SC-ade
0E
4E
+ Sup35(NM)
SC
0E
4E
SC-ade
0E
4E

Fig 24. Non-PIKK phosphomimetic substitution decreases FUS toxicity and prion-like aggregation in yeast.

(A) Schematic of the various phosphomimetic constructs used in the lab. Solid gray circles indicate PIKK consensus sites and light gray indicate non-PIKK sites. The constructs are in red font to indicate their use in subsequent experiments. The black-highlighted axis indicates the FUS fragment inserted into Sup35 and used in Panel E. (B) Phosphomimetic substitution in the prion-like domain rescues FUS toxicity in yeast. (C) Ectopic expression of FUS 4Ev3 and 4Ev4 analyzed by structured illumination microscopy. Cells were probed with anti-FUS. (D) Quantification of FUS signal in punctate structures compared to total FUS expression; error bars represent 95% CI. Figure data analyzed using a student t-test (n=9). (E) Sup35-FUS or Sup35-FUS 4E were expressed in yeast on SC or SC-ade media. Sup35NM was added to promote prion-formation under both conditions.

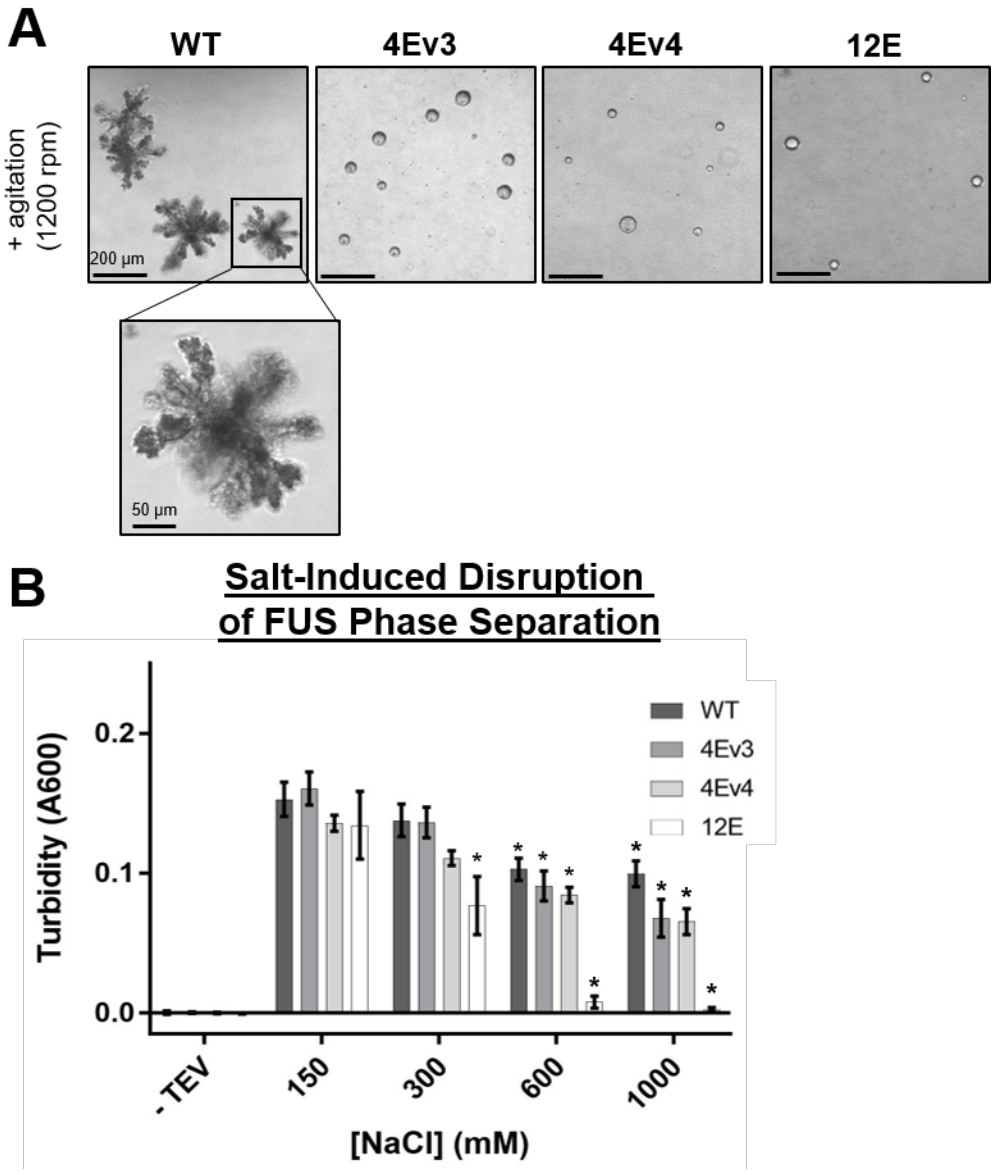

Fig 25. Phosphomimetic substitution reduces FUS solid-phase aggregation *in vitro*

(A) Differential interference microscopy of full-length and phosphomimetic variants of FUS (4Ev3, 4Ev4, or 12E). Maltose binding protein (MBP)-tagged FUS proteins were agitated for 1 day at 25 C after the addition of TEV protease. (B) Turbidity assay of full-length FUS in the presence of varying salt concentrations. Turbidity was assessed 45 minutes following TEV addition (n=10). Two-way ANOVA was used for statistical analysis (*indicates significance relative to 150 mM NaCl.)

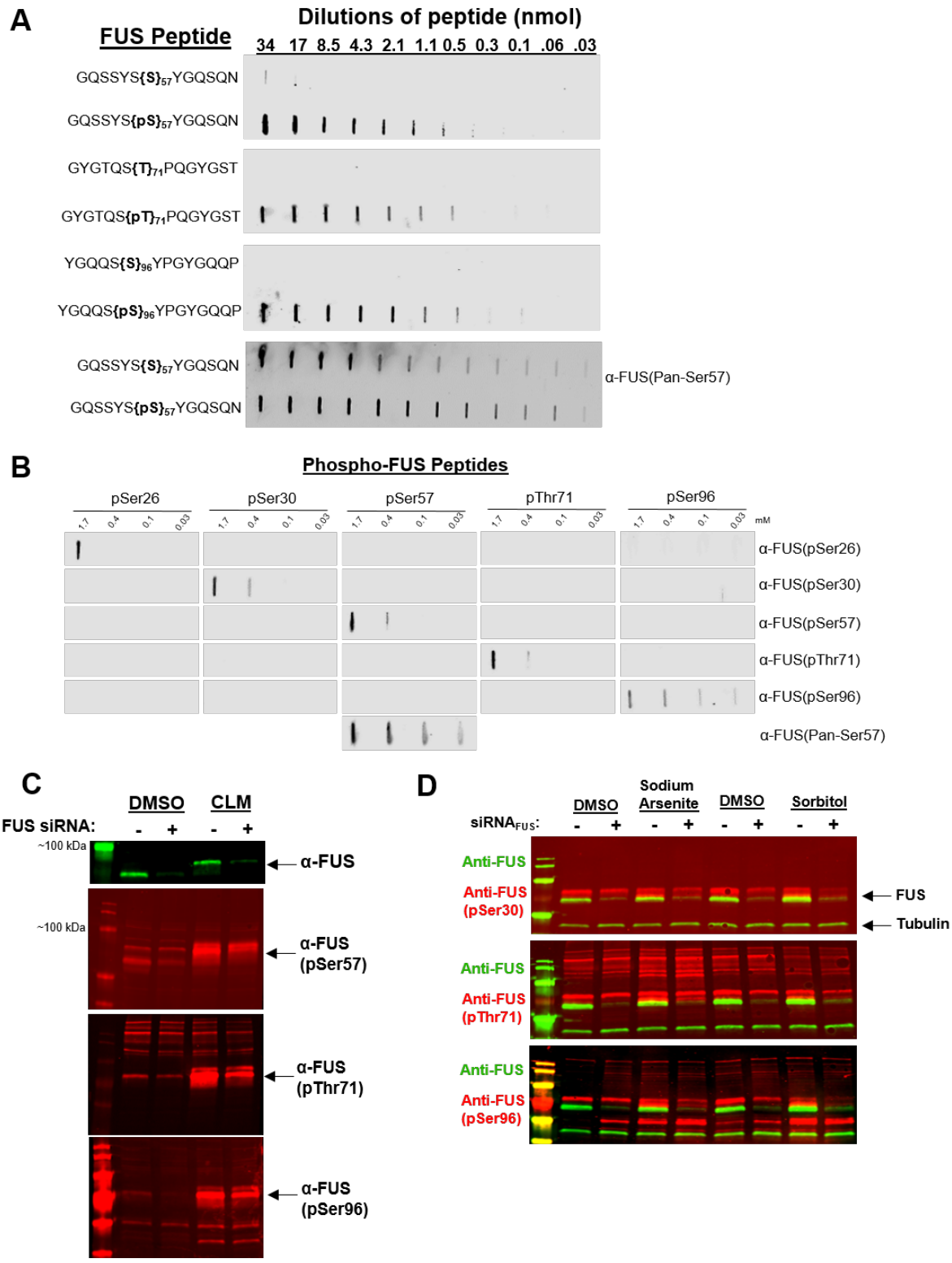
A
FUS Peptide
Dilutions of peptide (nmol)
34 17 8.5 4.3 2.1 1.1 0.5 0.3 0.1 .06 .03
GQSSYS{S}57YGQSQN
GQSSYS{pS}57YGQSQN
GYGTQS{T}71PQGYGST
GYGTQS{pT}71PQGYGST
YGQQS{S}96YPGYGQQP
YGQQS{pS}96YPGYGQQP
GQSSYS{S}57YGQSQN
GQSSYS{pS}57YGQSQN
α-FUS(Pan-Ser57)
B
Phospho-FUS Peptides
pSer26
pSer30
pSer57
pThr71
pSer96
1.7 0.4 0.1 0.03
mM
α-FUS(pSer26)
α-FUS(pSer30)
α-FUS(pSer57)
α-FUS(pThr71)
α-FUS(pSer96)
α-FUS(Pan-Ser57)
C
DMSO
CLM
FUS siRNA: - + - +
~100 kDa
α-FUS
~100 kDa
α-FUS (pSer57)
α-FUS (pThr71)
α-FUS (pSer96)
D
DMSO
Sodium Arsenite
DMSO
Sorbitol
siRNAFUS: - + - + - + - +
Anti-FUS
Anti-FUS (pSer30)
FUS
Tubulin
Anti-FUS
Anti-FUS (pThr71)
Anti-FUS
Anti-FUS (pSer96)

Fig 26. Phospho-specific antibodies show non-specific bands by Western Blot.

(A) Phospho-specific antibodies against Serine 57, Threonine 71, and Serine 96 within the FUS prion-like domain recognize the phosphorylated and not the unmodified peptide as shown by dot blot. Serine 57 peptide dilution was probed with a non-phosphospecific antibody (Pan-Ser57) to confirm proper peptide loading. (B) Western Blots of serial diluted phospho-FUS peptides. Each peptide dilution was probed with each of the phospho-specific antibodies (pSer26, pSer30, pSer57, pThr71, or pSer96). Serine 57 blot probed with Pan-Ser57 was used as a peptide loading control. (C, D) Full Western Blots from H4 cells with or without FUS knockdown treated with DMSO or 50 nM Calicheamicin (C) or sodium arsenite or sorbitol (D). Blots were probed with anti-FUS (pSer30, pSer57, pThr71, or pSer96(red) and commercial FUS (SC373698) (green)).

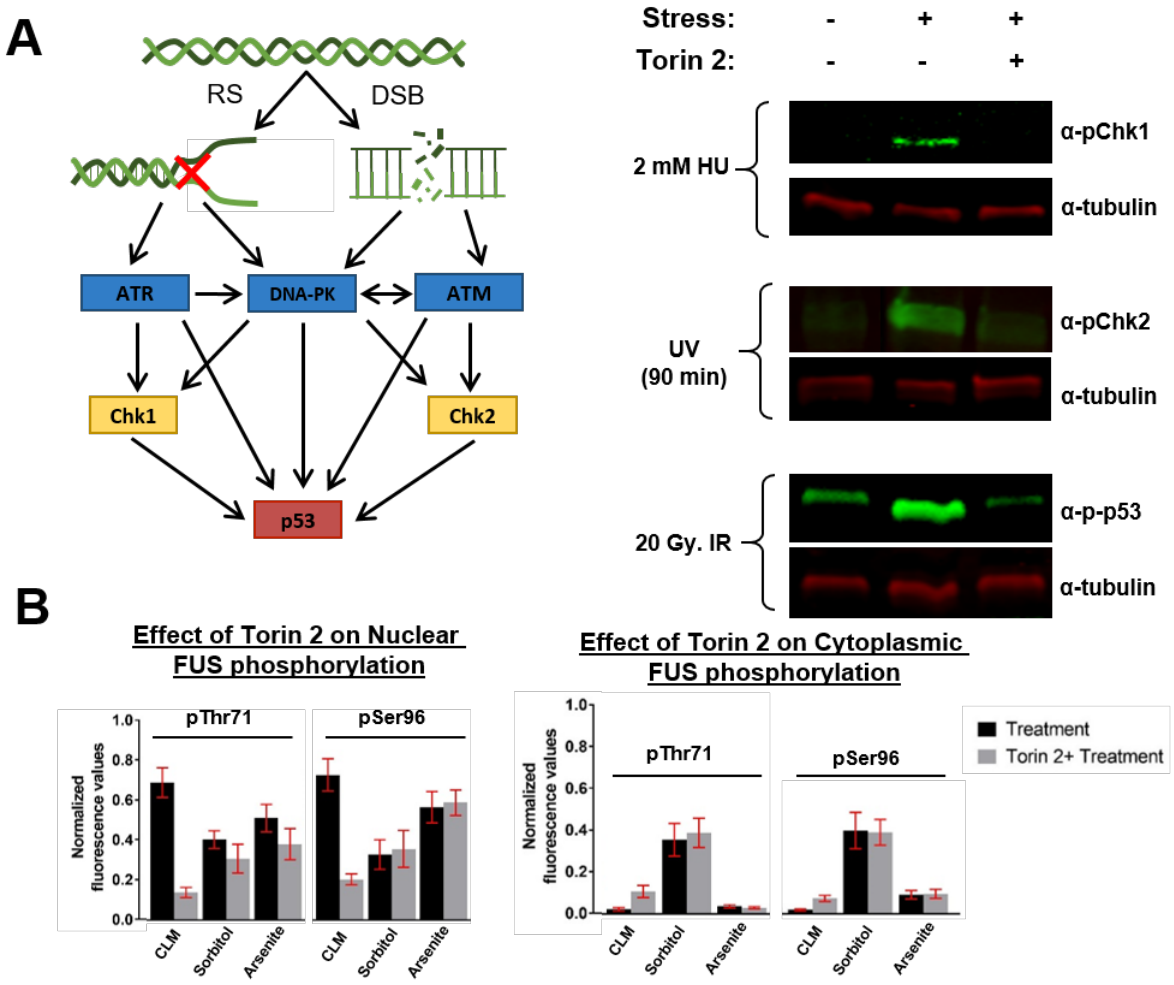

Fig 27. Torin 2 inhibits the PIKK family kinases.

(A) Schematic of known targets of the PIKK family kinases. Replication stress (RS) or double stranded breaks (DSB) cause activation of the PIKK family kinases. (Schematic adapted from (Ashley and Kemp, 2018)). Western blot (right panels) of H4 cells placed under various stressors to activate the PIKK family kinases**.** Cells were pretreated with torin 2 (200 uM) for 1 hour followed by treatment with 2 mM hyroxyurea for 1 hour to activate ATR, UV radiation for 90 minutes to activate ATM, or irradiated with ~20 Gy to activate DNA-PK. (B) Quantification (lower panels) of nuclear and cytoplasmic FUS(pT71) and FUS(pS96) fluorescence following cellular stress with or without torin 2.

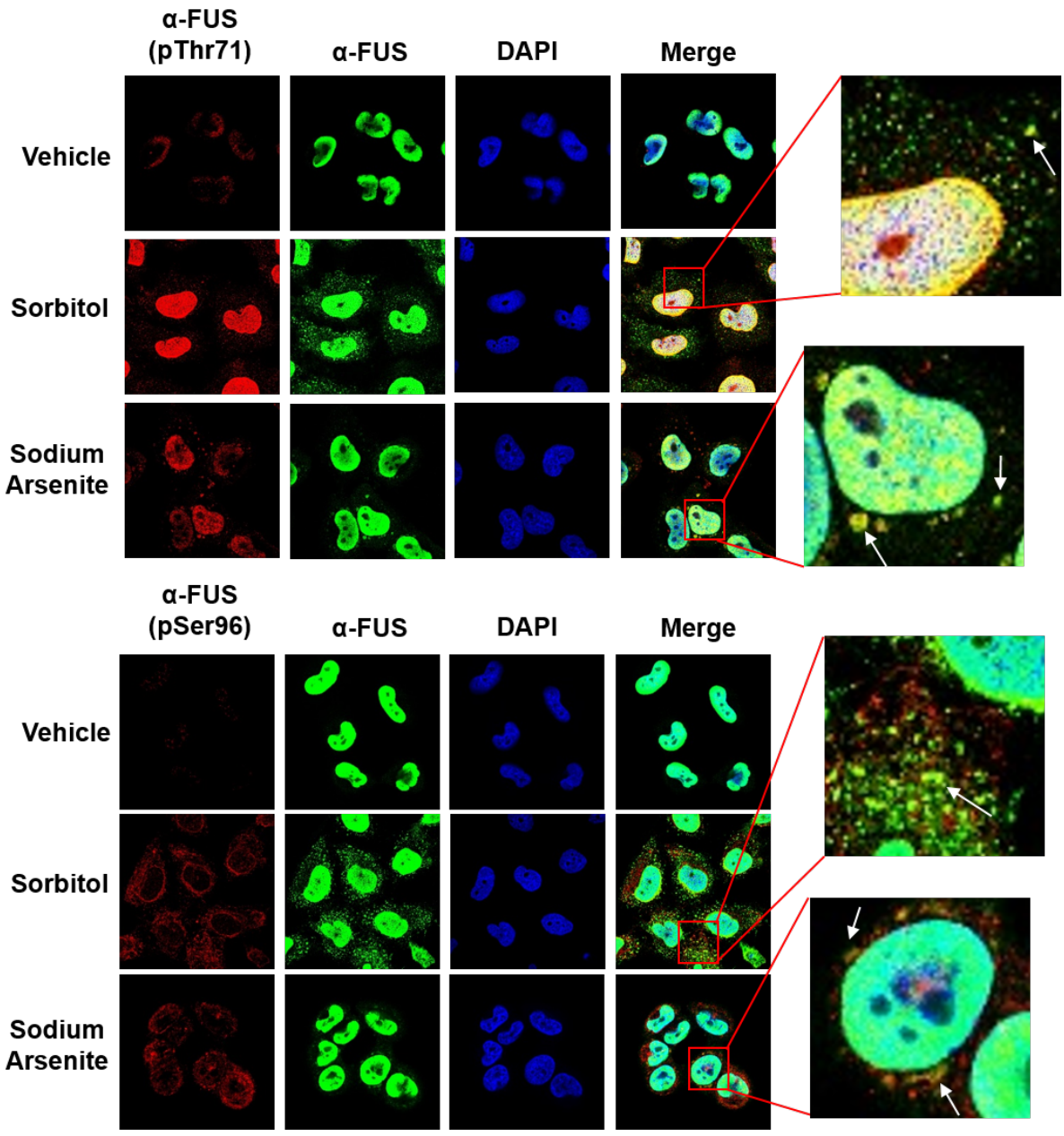

Fig 28. FUS phosphorylated at non-PIKK consensus sites localizes to cytoplasmic granules.

H4 cells treated with either Sodium Arsenite or Sorbitol for one hour were analyzed using confocal microscopy. Both FUS and pFUS (pThr71 and pSer96) are found in cytoplasmic granules.

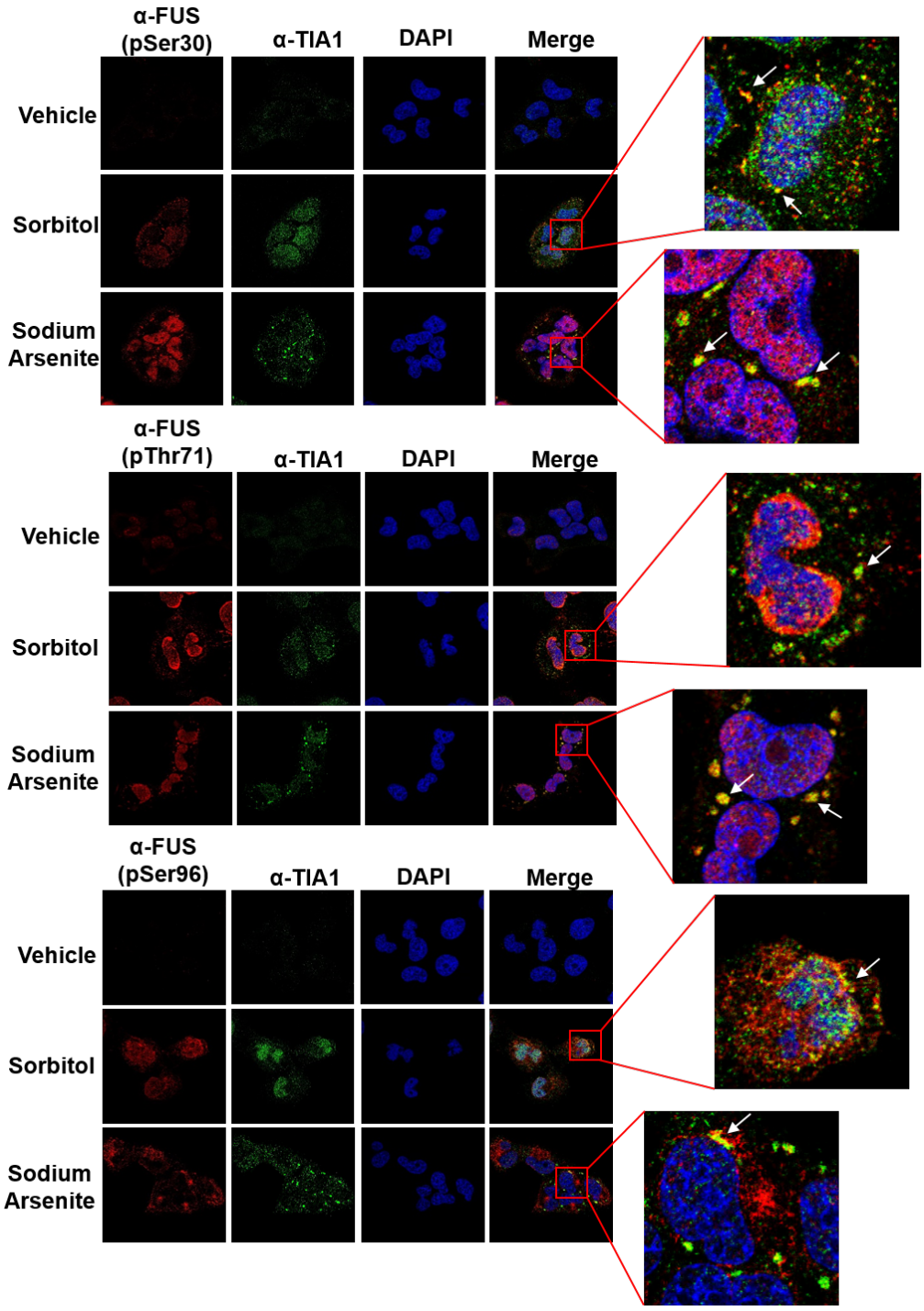

Fig 29. Phosphorylated FUS localizes to TIA1+ cytoplasmic stress granules.

H4 cells were treated for 1 hour with sorbitol or sodium arsenite and probed for TIA1 and phospho-FUS (pSer30, pThr71, or pSer96). Cells were analyzed by confocal microcopy.

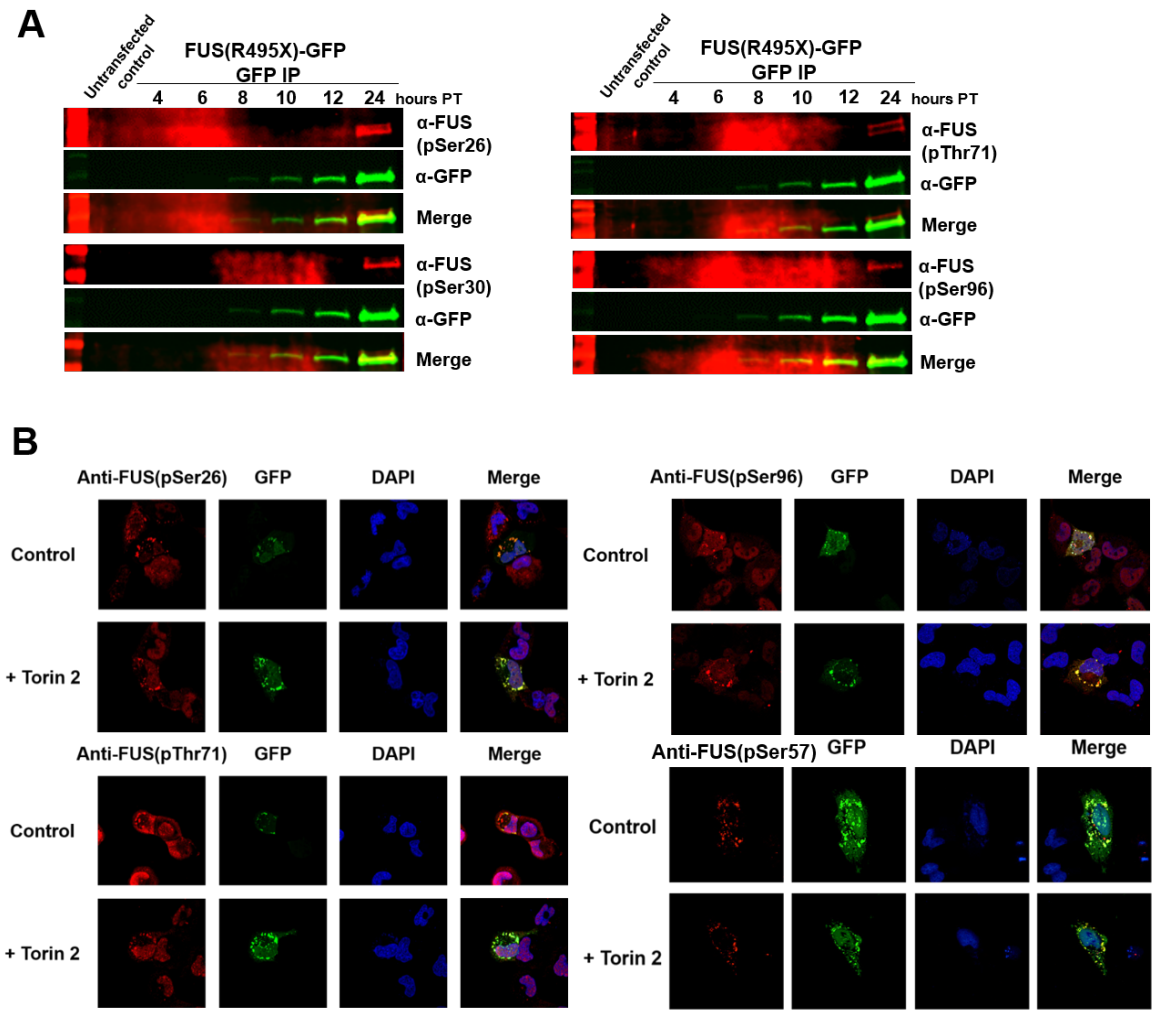

Fig 30. Cytoplasmic mutant FUS is phosphorylated at multiple sites regardless of PIKK kinase inhibition.

(A) H4 cells were transfected with GFP-FUS(495X) and immunoprecipitated (IP) using anti-GFP antibodies and dynabeads at various time points post transfection (PT). Western blots of IP products were probed with phospho-FUS (pSer26, pSer30, pThr71, and pSer96) and anti-GFP antibodies. (B) H4 cells were transfected with FUS(494)-GFP. 6-hours post-transfection cells were treated with torin2. At 8 hours post-transfection cells were fixed and imaged using confocal microscopy.

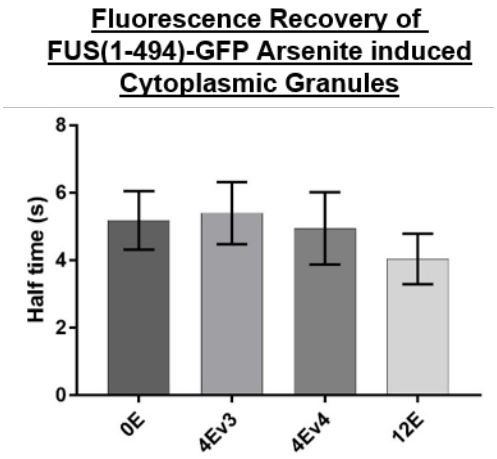

Fig 31. FUS phosphomimetic substitution do not alter liquid like dynamics of arsenite induced stress granules.

FRAP half times of arsenite-induced stress granules containing FUS(494)-GFP phosphomimetic constructs 24 hours post-transfection; error bars represent 95% CI; (n=30).

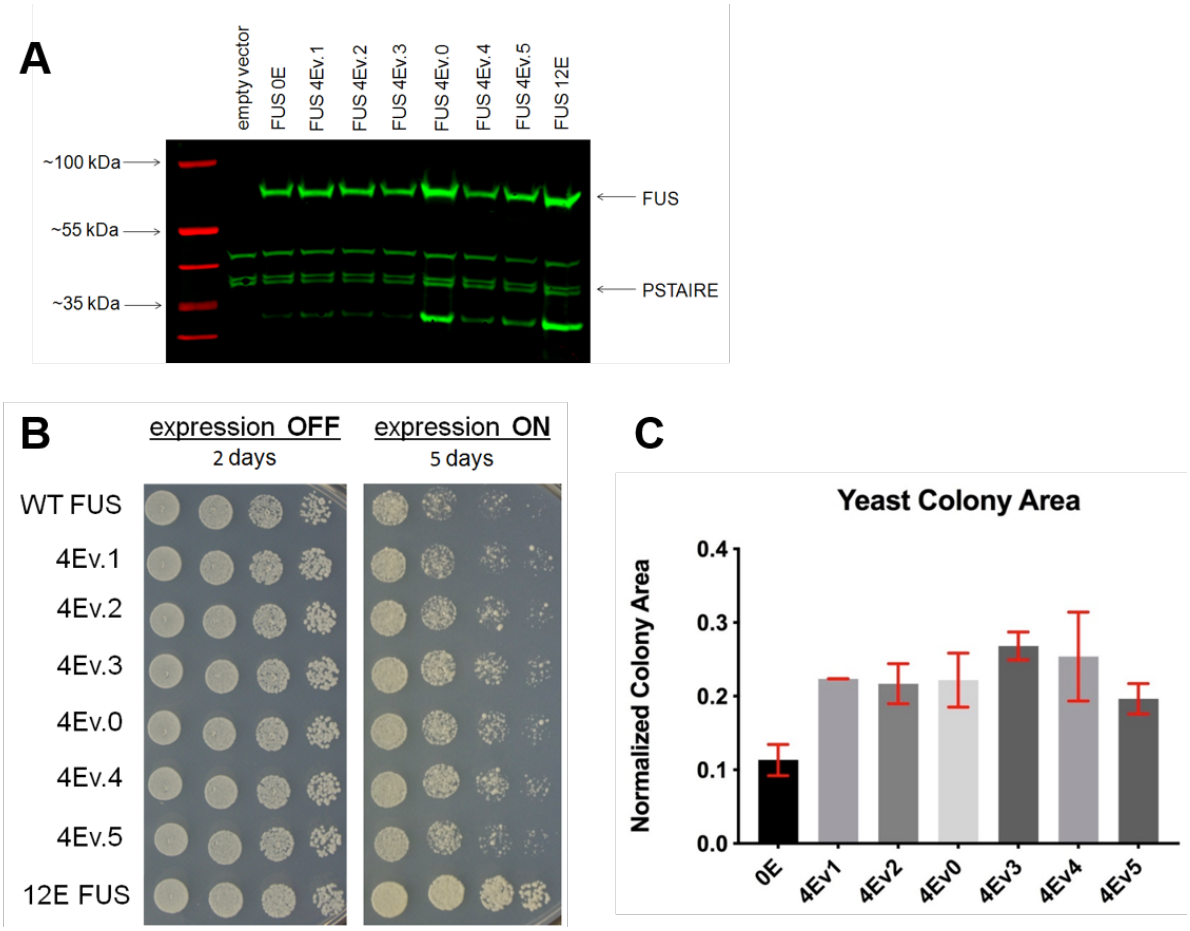

Fig 32. FUS Phosphomimetic construct expression in yeast.

(A) Western blot from yeast lysate showing expression of all phosphomimetic constructs used. Blots were probed with anti-FUS and anti-PSTAIRE (loading control) antibodies. (B) All variants with phosphomimetic substitutions in the prion-like domain rescue FUS toxicity in yeast. (C) Colony areas from experiments shown in Figure 25B were quantified using ImageJ and normalized to 12E area (n=12). Student t test was used for statistical analysis (All P values < 0.0001).

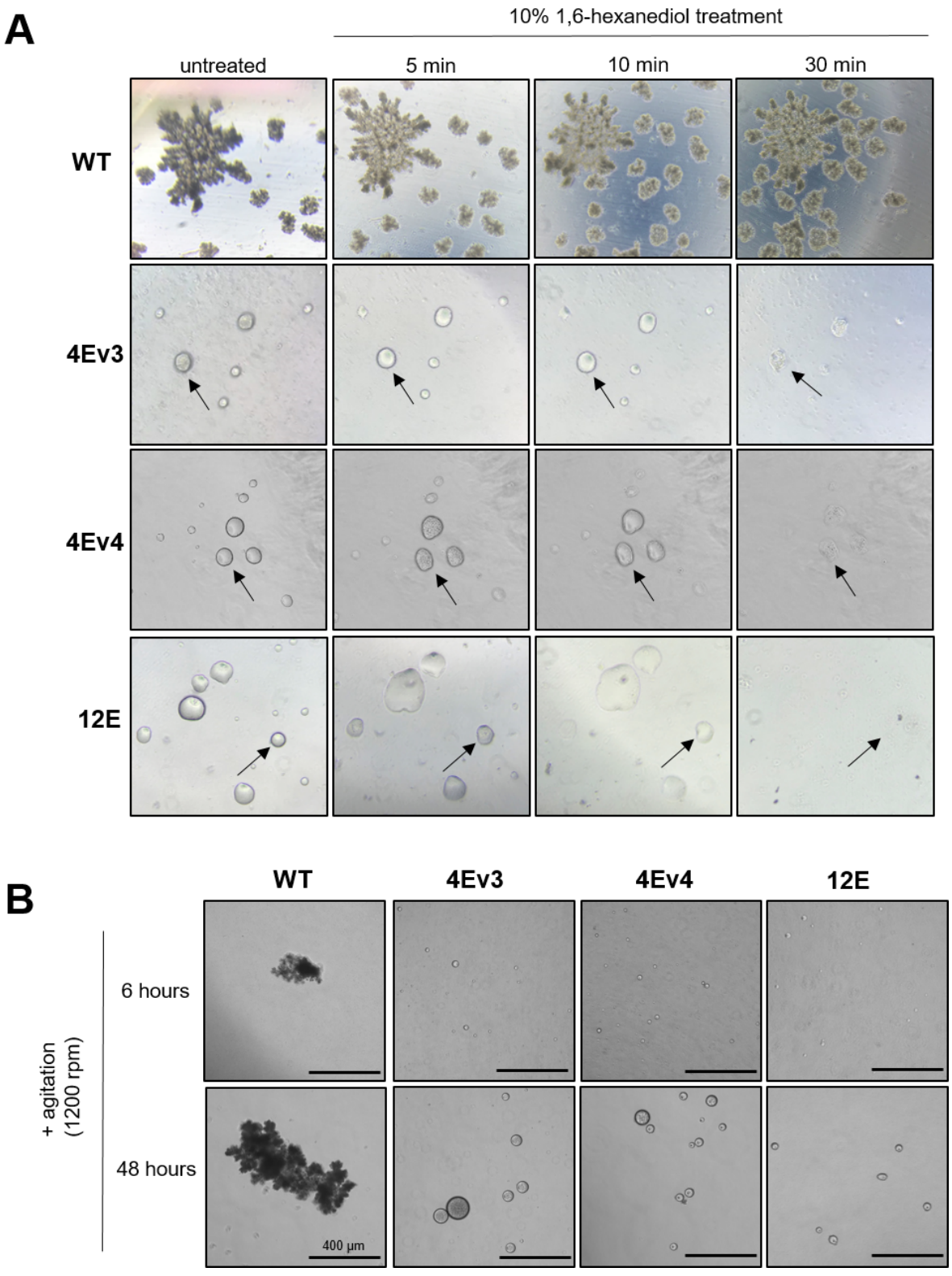
A
10% 1,6-hexanediol treatment
untreated
5 min
10 min
30 min
WT
4Ev3
4Ev4
12E
B
WT
4Ev3
4Ev4
12E
6 hours
48 hours
+ agitation (1200 rpm)
400 µm

Fig 33. Phosphomimetic FUS variants form spherical droplets with liquid-like characteristics that persist over 48 hours.

(A) Phosphomimetic FUS droplets, but not wild-type FUS aggregates, dissolve following treatment with10% 1,6-hexanediol. (B) Wild-type FUS amorphous aggregates form with 6 hours of agitation, while the phosphomimetic variants form small spherical droplets. By 48 hours, FUS has formed large aggregates and the phosphomimetic variants remain in droplets.

CHAPTER 4: Conclusions and Implications for Future Work

FUS phase transition is a driver of pathology in both cancer and neurodegeneration. Here, we show novel and aberrant LLPS of the oncogenic transcription factor FUS-CHOP. We hypothesize this phase separation capacity could be driving oncogenic transcriptional reprogramming. To assess a mechanism, we confirmed FUS-CHOP puncta localize with known super-enhancer condensates. We also show phase transition of FUS-CHOP is dependent on the PrLD of FUS, making the PrLD a therapeutic target. Our previous work showed phase separation of FUS can be modulated by post-translational modification of the PrLD. Using an established ALS-FUS model, we discovered phosphorylation of FUS PrLD at both PIKK and non-PIKK consensus sites occurs following cellular stress, and that phosphorylation of FUS is not dependent solely on the PIKKs. We found that phosphomimetic substitution at both PIKK and non-PIKK consensus sites modulates FUS phase transition, reducing the propensity of the protein to form solid aggregates and cause cytotoxicity. Together, our work shows novel FUS-driven phase separation in cancer and provides a potential mechanism for modulation of phase transition in both neurodegeneration and cancer.

FUS-CHOP PHASE SEPARATION AS A NOVEL MECHANISM OF ONCOGENESIS

FUS-CHOP undergoes nuclear liquid-liquid phase separation

The PrLD of FUS drives LLPS of full length FUS and mutant FUS, but phase separation of FUS-CHOP had not been evaluated. In myxoid liposarcoma, the N-terminus of FUS gives CHOP an unknown oncogenic capacity (Perez-Losada et al., 2000). We hypothesized that the FUS fusion results in a LLPS gain of function for

CHOP, allowing for new binding partners and downstream activation of oncogenes. Previous work confirmed homologous protein, EWS, can drive EWS-FLI phase separation *in vitro* (Zuo et al., 2021). Here, we confirm phase separation of FUS-CHOP *in vitro* and in NIH 3T3 cells (Figure 6, 7, 8). An important finding of our work is that CHOP cannot phase separate *in vitro* without the fusion of the FUS IDR (Figure 6, 7). We evaluated the two most common types of FUS-CHOP fusions from patient samples, type I and type II, harboring the first 266 and 175 amino acids of FUS fused to full length CHOP, respectively. Both types of FUS-CHOP condensates are spherical in shape, fuse upon touching, and undergo internal rearrangement and external exchange on the timescale of seconds when evaluated by FRAP, satisfying the known hallmarks of liquid-phase separated condensates in cells (Figure 7, 8) (Hyman et al., 2014). Similarly, endogenous FUS-CHOP (type I or type VIII) in three different myxoid liposarcoma cell lines is localized to small nuclear puncta, similar to the nuclear hubs formed by EWS-FLI1 in Ewing's sarcoma cell lines (Figure 11) (Chong et al., 2018). FUS-CHOP can undergo liquid-phase separation in cells, which could be a potential mechanism of FUS-CHOP induced oncogenesis in MLS.

Phase separation of the FET family of proteins has been characterized (Maharana et al., 2018; Wang et al., 2018), but research is lacking on the involvement of phase separation of the FET oncogene fusions. Numerous studies have shown a role of phase separation in transcriptional activation (Boehning et al., 2018; Chong et al., 2018; Cho et al., 2018; Gurumurthy et al., 2019; Klein et al., 2020; Lu et al., 2019; Lu et al., 2020; Sabari et al., 2015; Wei et al., 2020) and others have alluded to the role of fusion oncoprotein in a phase separation induced transcriptional activation (Boija et al., 2018;

Davis et al., 2021; Taniue and Akimitsu, 2021; Jiang et al., 2020; Zuo et al., 2021), but no definitive mechanisms have been shown. Our data lays the groundwork for future studies on oncogenic phase separation. We have confirmed FUS-CHOP can undergo a liquid phase transition in cells, but more research is necessary to evaluate the contribution of phase separation to oncogenesis.

FUS-CHOP phase separation is dependent on the length of the prion-like domain of FUS

To determine if there is a specific region of the PrLD necessary for FUS-CHOP phase separation, we serially truncated the N-terminus of the protein and ectopically expressed the constructs in NIH 3T3 cells. Previous work showed large truncations of the N-terminus of FUS reduced the punctate nature of the fusion protein (Goransson et al., 2002). We truncated the first 25, 50, 75 and 125 amino acids of FUS PrLD and assessed punctate formation in cells. We observed removal of 75 amino acids (Δ 75) was sufficient to disrupt condensate formation (Figure 8, 16). In addition, we assessed how the dynamics of these puncta changed when shorter PrLD sequences were present. The half time of recovery decreased as a result of the decrease in length of the protein. We show the smaller truncated proteins can partition in and out of the condensate more rapidly than the full-length protein (Figure 8).

A core region of the PrLD was shown to be important for FUS fibril formation (amino acids 39-95) (Murray et al., 2017). Since the interactions driving liquid phase separation are dynamic and not rigid, we hypothesized that the length, not the region, of the intrinsically disordered PrLD was necessary for phase separation. To this end, we truncated 25, 50, and 75 amino acids within the PrLD of FUS-CHOP type I and II

constructs (Figure 9, 17). We found that deletion of 75 amino acids within the PrLD yielded the same results as removal from the N-terminus. These data show FUS-CHOP phase separation is dependent on the PrLD of FUS, in cells and *in vitro*, and the multivalency of a longer domain is necessary to form the interactions that drive phase separation. The PrLD consists disproportionately of only a few amino acids (i.e. low-complexity), thus the length, but not any particular segment appears to drive phase separation. Understanding the necessary PrLD-PrLD interactions that are driving this atypical phase separation is important for development of targeted therapies for MLS.

FUS-CHOP can phase separate with BRD4 and this interaction is governed by DNA binding

To start to answer the questions surrounding mechanisms of FUS-CHOP phase separation and transcriptional activation, we assessed FUS-CHOP localization with a known phase separating super enhancer protein, BRD4. BRD4 binds acetylated histones and is known for its ability to form super enhancers upstream of oncogenes in several types of cancer (Donati et al., 2018). Previous work showed FUS-CHOP and BRD4 are cooperating at super enhancer sites to induce oncogenic transcriptional reprogramming in myxoid liposarcoma (Chen et al., 2019b). BRD4 has a C-terminal IDR that is necessary for function and drives phase separation at super enhancer sites (Wang et al., 2018). In myxoid liposarcoma cell lines, we observed modest colocalization of BRD4 and FUS-CHOP puncta. Interestingly, when we ectopically expressed FUS-CHOP in NIH 3T3 cells, we saw BRD4 recruitment to larger FUS-CHOP condensates (Figure 12), suggesting a cause and effect relationship. These data, along with previous work,

suggests FUS-CHOP and BRD4 could be phase separating together at novel FUS-CHOP-positive super enhancers and inducing oncogenic transcriptional reprogramming.

To determine if DNA-binding is essential for FUS-CHOP phase separation, we mutated the DNA-binding domain (ΔDBD), or the basic region, of CHOP in both type I and II constructs (Ubeda et al., 1996). We ectopically expressed both ΔDBD constructs in NIH 3T3 cells and saw no change in puncta formation when the DNA-binding domain is mutated; confirming FUS IDR is the underlying modulator of phase separation (Figure 10, 17). Further, we wanted to understand how DNA-binding is contributing to BRD4 interaction at super enhancers. We probed our cells expressing the ΔDBD FUS-CHOP constructs for BRD4 and saw a significant decrease in colocalization of puncta when assessed by Pearson's correlation coefficient. From this, we conclude that DNA-binding plays an important role in recruitment of BRD4, but FUS IDR governs phase transition of FUS-CHOP at super enhancer condensates.

In vitro studies (published concurrently with our work) of the fusion FUS-GAL4 and EWS-FLI1 showed disruption of condensate formation along DNA strands reduced transcriptional output (Zuo et al., 2021). These data strengthen our hypothesis, but in-cell studies to corroborate these findings has yet to be conducted. Other mechanisms of FUS-CHOP induced oncogenesis have been proposed, most of which involve FUS-CHOP actively recruiting chromatin-remodeling complex proteins (Davis et al., 2021; Linden et al.). Our data and these published works are not mutually exclusive, as phase separation was recently proposed as a recruitment mechanism for the mSWI/SNF complex proteins (Davis et al., 2021). We show recruitment of BRD4, a super enhancer protein, could be a

concurrent mechanism occurring while chromatin-remodeling complexes unwind heterochromatin, allowing for oncogenic super-enhancer formation.

To better understand the contribution of phase separation to transcriptional regulation and tumorigenesis, future studies are needed. RNA-sequencing and oncogenic growth assays between cells expressing wild type and a phase separation incompetent (Δ 75) FUS-CHOP would provide evidence for an essential role of phase separation in MLS oncogenesis.

Overall, these data show a novel characteristic of a fusion oncogene. FUS-CHOP undergoes a liquid-phase transition that is dependent on the PrLD of FUS. Our data show FUS-CHOP could be utilizing super-enhancer proteins and condensates to reprogram oncogenic transcriptional changes. Disrupting phase separation of FUS-CHOP using targeted therapies and in turn reducing oncogenic transcription is a novel therapeutic approach for MLS.

PHOSPHORYLATION OF THE PRION-LIKE DOMAIN DISRUPTS FUS PHASE TRANSITION

FUS is phosphorylated by multiple kinases

The PrLD of FUS is highly post-translationally modified. In the PrLD alone, 32 putative phosphorylation sites have been identified, 12 of which are PIKK consensus sites (Rhoads et al., 2018b). Our previous work showed that incubating recombinant FUS IDR with DNA-PK or mutating the known PIKK consensus sites to glutamic acid (phosphomimetic substitution) disrupted both the liquid and solid-phase transition *in vitro*. Our lab confirmed FUS is phosphorylated by PIKKs in the nucleus following DNA

damage (Rhoads et al., 2018a). Here, we use phospho-specific antibodies and confirmed FUS is phosphorylated at non-PIKK consensus sites by DNA-PK *in vitro* and following DNA damage in cells (Figure 18, 19). We also show that FUS is differentially phosphorylated depending on the type of cellular stress (Figure 19). Osmotic and oxidative stress cause cytoplasmic FUS to phase separate into stress granules (Andersson et al., 2008; Sama et al., 2013). Here, we observe phosphorylated FUS is also recruited to cytoplasmic granules (Figure 19). To determine if the PIKKs were responsible for cytoplasmic phosphorylation, we inhibited the PIKKs using Torin 2 (Figure 27). DNA-damage-induced phosphorylation of FUS is dependent on the PIKKs, but osmotic and oxidative stress activate, unknown, potentially cytoplasmic, kinases that phosphorylate FUS at both PIKK and non-PIKK consensus sites (Figure 21).

Future research needs to be completed to determine the unidentified kinases acting on the PrLD of FUS. We utilized a kinase prediction algorithm (NetPhos) and determined the most likely kinases for the non-PIKK sites examined here. Our initial data using pharmacological inhibitors against the top NetPhos kinases were inconclusive, leaving an avenue for further research on kinase identification. Another viable option is to assess phosphatase activity. Recent work has identified links between stress granule misprocessing and RNA-binding protein pathological aggregation (Baradaran-Heravi et al., 2020; Zhang et al., 2020). Phosphorylation of FUS is occurring in cells during a stress response and negative charges have an inhibitory effect on solid-phase transition. Inhibition of phosphatase activity could result in persistent phosphorylation of FUS, deterring the interactions necessary for solid aggregation.

Mutant cytoplasmic FUS is undergoing LLPS and can be phosphorylated in cells

We observed full-length phosphorylated FUS can phase separate into stress granules in the cytoplasm (Figure 20). To better understand phosphorylation in our ALS model, we ectopically expressed ALS mutant FUS, FUS(R495X), in H4 human neuroglioma cells. Interestingly, FUS(R495X) was phosphorylated at all PIKK and non-PIKK sites examined here (Figure 22). The phosphorylation of FUS(R495X) increased over time and as the protein became more aggregated in the cytoplasm. Because the mutant FUS aggregates are cytoplasmic, we asked if this phosphorylation was dependent on the nuclear PIKKs. Inhibition of the PIKKs revealed phosphorylation of mutant FUS is not dependent on the PIKKs and other unknown kinases are phosphorylating FUS(R495X) PrLD (Figure 22).

To determine how phosphorylation affected the localization and dynamics of FUS(R495X) aggregates, we created phosphomimetic variants with glutamic acid substitutions at 4 non-PIKK sites (4E) or 12 PIKK site (12E) within the PrLD (Figure 23). We also created a non-phosphorylatable construct, 12A, in which the 12 PIKK sites are substituted with alanine residues. We observed the majority of the protein in puncta for the unmodified and 12A constructs (Figure 23). The constructs with phosphomimetic substitutions showed an increase in background fluorescence when compared to controls, suggesting less sequestration of mutant FUS into the granules (Figure 23). Previous work shows mutant FUS can undergo LLPS *in vitro* (Patel et al., 2015). Here, we subjected the cytoplasmic puncta to FRAP and determined that mutant FUS has liquid-like characteristics after 24 hours of ectopic expression. Our data verify mutant FUS can be phosphorylated in cells and phosphomimetic substitution can alter the recruitment of FUS

into granules, confirming PrLD phosphorylation as a viable target for therapeutic intervention.

Further evaluation of these cellular puncta is necessary to determine the long-term effects of phosphorylation. Our previous *in vitro* work showed an abrogation of solid aggregate formation when 12 phosphomimetic substitutions are implemented (Monahan et al., 2017). Here, using an in-cell model we see phosphorylated FUS and our 12E construct in cytoplasmic puncta. The question remains as to whether the negative charges introduced by the phosphoryl groups impedes the pathogenic liquid-to-solid phase transition. Evaluation of these cytoplasmic puncta over time, similar to what we have shown *in vitro*, would be invaluable to the field.

Phosphomimetic substitution at Non-PIKK sites reduces FUS cellular toxicity and aggregation propensity

Yeast, specifically *Saccharomyces cerevisiae*, has been a powerful system for studying protein aggregation (Krobitsch and Lindquist, 2000). Several mammalian disease-associated and aggregate prone proteins have been studied using this simple eukaryotic model (Bagriantsev et al., 2006; Johnson et al., 2008; Outeiro and Lindquist, 2003; Tank et al., 2007). There is no homolog of FUS in *Saccharomyces cerevisiae* and previous work shows ectopic expression of FUS in yeast results in cytoplasmic aggregation that causes cytotoxicity (Fushimi et al., 2011). FUS forms insoluble toxic aggregates in the cytoplasm, similar to what is seen in ALS patient neurons (Kryndushkin et al., 2011). Our previous work showed 12, 6, or 4 phosphomimetic substitutions at PIKK consensus sites in the PrLD reduced FUS toxicity in yeast (Monahan et al., 2017). Here, we examined if 4 phosphomimetic substitutions (4E) at both PIKK and non-PIKK

sites reduced cellular toxicity. We ectopically expressed 6 different FUS 4E phosphomimetic constructs using a galactose-driven promoter system. When plated on galactose plates, we saw yeast expressing full-length FUS had very little colony formation, while 4E FUS had a moderate rescue of toxicity when compared to wild type (Figure 24). In addition, we examined a more diffuse pattern of localization of the FUS 4E constructs in the cytoplasm of yeast cells when compared to wild type FUS (Figure 24). These data suggest phosphorylation anywhere within FUS's PrLD could favor a reduction in both aggregation and toxicity.

Subsequently, because ALS-FUS aggregates have a prion-like pattern of spreading along neuroanatomical pathways, we were interested in how phosphomimetic substitution changes the prion-like nature of FUS. To this end, we modified a known yeast prion protein: SUP35 (Kim et al., 2013; Wickner et al., 1995). Similar to the SUP35 prion aggregates, *in vitro* work shows FUS PrLD can form aggregates with in-register parallel cross-β structure (Murray et al., 2017; Shewmaker et al., 2006). To form this confirmation, monomers align closely via hydrogen bonds, and disruption of these interactions will deter fibril formation. Here, we removed a portion of the SUP35 prion domain and replaced it with a fragment of FUS or 4E FUS PrLD, creating SUP35-FUS constructs. Our data showed 4 phosphomimetic substitutions reduced the aggregation propensity of SUP35-FUS, leaving a more soluble, functional protein when compared to unmodified SUP35-FUS. These data suggest phosphorylation could reduce the prion-like activity of the FUS PrLD and are a strong indication of how promising phosphorylation could be as a therapeutic approach against amyloid-like aggregation. Future work needs

to be completed to understand cell-to-cell spreading of FUS aggregates and how phosphorylation or phosphomimetic substitution alters propagation.

To examine *in vitro* aggregation propensity of recombinant FUS, we purified wild-type FUS, two 4E non-PIKK constructs, and 12E FUS. We agitated the protein for 24 hours and observed wild type FUS forms large aggregates (Figure 25). Under the same conditions, we observed 4E and 12E FUS formed liquid condensates and did not form solid aggregates after 24 or 48 hours of agitation (Figure 25, 33). These data provide evidence that phosphorylation at both PIKK and non-PIKK sites in the PrLD can impede the pathogenic phase transition that occurs in ALS patients. Determining kinases and phosphatases that act on FUS PrLD and can be modulated in patients is the next necessary step of this work.

Our findings surrounding ALS-FUS phosphorylation are not limited to neurodegeneration, and can be applied to our FUS-CHOP research. Previously, we used our phospho-specific antibodies in MLS cancer lines and saw FUS-CHOP is not endogenously phosphorylated, but can be phosphorylated following cellular stress (data not shown). These data suggest kinases do act on the oncogenic fusion protein and phosphorylation could be a potential therapeutic for disruption of ALS-FUS solid aggregates and oncogenic FUS-CHOP condensates. Because of our previous work showing incubation with DNA-PK or phosphomimetic substitution at the PIKK consensus sites disrupted FUS IDR phase transition (Monahan et al., 2017), it is important to determine how several phosphorylation events could affect FUS-CHOP phase separation. We and others hypothesize that phase separation is necessary for oncogenesis, therefore activating kinases or inhibiting phosphatases that act on the PrLD

could be a potential target for disrupting oncogenic condensate formation as well as modulating aggregate formation in neurodegeneration.

In conclusion, research surrounding LLPS and liquid-to-solid phase transitions is still in its infancy. In the past 10 years, novel proteins, functions, and disease pathways have been attributed to LLPS (Lyon et al., 2021). Our work contributes to the field by showing novel FUS-PrLD driven phase separation in cancer and by providing a mechanism in which phase transition of FUS can be modulated. Our work has just scratched the surface for future research surrounding FUS self-association in both cancer and neurodegeneration.

REFERENCES

Aguzzi, A., and M. Altmeyer. 2016. Phase Separation: Linking Cellular Compartmentalization to Disease. *Trends Cell Biol*. 26:547-558.

Alberti, S., A. Gladfelter, and T. Mittag. 2019. Considerations and Challenges in Studying Liquid-Liquid Phase Separation and Biomolecular Condensates. *Cell*. 176:419-434.

Alberti, S., and A.A. Hyman. 2021. Biomolecular condensates at the nexus of cellular stress, protein aggregation disease and ageing. *Nat Rev Mol Cell Biol*.

Amado, D.A., and B.L. Davidson. 2021. Gene therapy for ALS: A review. *Mol Ther*.

Aman, P., D. Ron, N. Mandahl, T. Fioretos, S. Heim, K. Arheden, H. Willen, A. Rydholm, and F. Mitelman. 1992. Rearrangement of the transcription factor gene CHOP in myxoid liposarcomas with t(12;16)(q13;p11). *Genes Chromosomes Cancer*. 5:278-285.

Andersson, M.K., A. Stahlberg, Y. Arvidsson, A. Olofsson, H. Semb, G. Stenman, O. Nilsson, and P. Aman. 2008. The multifunctional FUS, EWS and TAF15 proto-oncoproteins show cell type-specific expression patterns and involvement in cell spreading and stress response. *BMC Cell Biol*. 9:37.

Araki, K., N. Yagi, K. Aoyama, C.J. Choong, H. Hayakawa, H. Fujimura, Y. Nagai, Y. Goto, and H. Mochizuki. 2019. Parkinson's disease is a type of amyloidosis featuring accumulation of amyloid fibrils of alpha-synuclein. *Proc Natl Acad Sci U S A*. 116:17963-17969.

Armstrong, R.A. 2017. Neuronal cytoplasmic inclusions in tau, TDP-43, and FUS molecular subtypes of frontotemporal lobar degeneration share similar spatial patterns. *Folia Neuropathol*. 55:185-192

Bagriantsev, S.N., V.V. Kushnirov, and S.W. Liebman. 2006. Analysis of amyloid aggregates using agarose gel electrophoresis. *Methods Enzymol*. 412:33-48.

Bah, A., and J.D. Forman-Kay. 2016. Modulation of Intrinsically Disordered Protein Function by Post-translational Modifications. *J Biol Chem*. 291:6696-6705.

Balamuth, N.J., and R.B. Womer. 2010. Ewing's sarcoma. *Lancet Oncol*. 11:184-192.

Banani, S.F., H.O. Lee, A.A. Hyman, and M.K. Rosen. 2017. Biomolecular condensates: organizers of cellular biochemistry. *Nat Rev Mol Cell Biol*. 18:285-298.

Baradaran-Heravi, Y., C. Van Broeckhoven, and J. van der Zee. 2020. Stress granule mediated protein aggregation and underlying gene defects in the FTD-ALS spectrum. *Neurobiol Dis*. 134:104639.

Benatar, M., J. Wuu, P.M. Andersen, N. Atassi, W. David, M. Cudkowicz, and D. Schoenfeld. 2018. Randomized, double-blind, placebo-controlled trial of arimoclomol in rapidly progressive SOD1 ALS. *Neurology*. 90:e565-e574.

Berry, J., S.C. Weber, N. Vaidya, M. Haataja, and C.P. Brangwynne. 2015. RNA transcription modulates phase transition-driven nuclear body assembly. *Proc Natl Acad Sci U S A*. 112:E5237-5245.

Blackford, A.N., and S.P. Jackson. 2017. ATM, ATR, and DNA-PK: The Trinity at the Heart of the DNA Damage Response. *Mol Cell*. 66:801-817.

Blokhuis, A.M., E.J. Groen, M. Koppers, L.H. van den Berg, and R.J. Pasterkamp. 2013. Protein aggregation in amyotrophic lateral sclerosis. *Acta Neuropathol*. 125:777-794.

Bock, S., D.G. Hoffmann, Y. Jiang, H. Chen, and D. Il'yasova. 2020. Increasing Incidence of Liposarcoma: A Population-Based Study of National Surveillance Databases, 2001-2016. *Int J Environ Res Public Health*. 17.

Bode-Lesniewska, B., S. Frigerio, U. Exner, M.T. Abdou, H. Moch, and D.R. Zimmermann. 2007. Relevance of translocation type in myxoid liposarcoma and identification of a novel EWSR1-DDIT3 fusion. *Genes Chromosomes Cancer*. 46:961-971.

Boehning, M., C. Dugast-Darzacq, M. Rankovic, A.S. Hansen, T. Yu, H. Marie-Nelly, D.T. McSwiggen, G. Kokic, G.M. Dailey, P. Cramer, X. Darzacq, and M. Zweckstetter. 2018. RNA polymerase II clustering through carboxy-terminal domain phase separation. *Nat Struct Mol Biol*. 25:833-840.

Boija, A., I.A. Klein, B.R. Sabari, A. Dall'Agnese, E.L. Coffey, A.V. Zamudio, C.H. Li, K. Shrinivas, J.C. Manteiga, N.M. Hannett, B.J. Abraham, L.K. Afeyan, Y.E. Guo, J.K. Rimel, C.B. Fant, J. Schuijers, T.I. Lee, D.J. Taatjes, and R.A. Young. 2018. Transcription Factors Activate Genes through the Phase-Separation Capacity of Their Activation Domains. *Cell*. 175:1842-1855 e1816.

Boija, A., I.A. Klein, and R.A. Young. 2021. Biomolecular Condensates and Cancer. *Cancer Cell*. 39:174-192.

Bouchard, J.J., J.H. Otero, D.C. Scott, E. Szulc, E.W. Martin, N. Sabri, D. Granata, M.R. Marzahn, K. Lindorff-Larsen, X. Salvatella, B.A. Schulman, and T. Mittag. 2018. Cancer Mutations of the Tumor Suppressor SPOP Disrupt the Formation of Active, Phase-Separated Compartments. *Mol Cell*. 72:19-36 e18.

Boulay, G., G.J. Sandoval, N. Riggi, S. Iyer, R. Buisson, B. Naigles, M.E. Awad, S. Rengarajan, A. Volorio, M.J. McBride, L.C. Broye, L. Zou, I. Stamenkovic, C. Kadoch, and M.N. Rivera. 2017. Cancer-Specific Retargeting of BAF Complexes by a Prion-like Domain. *Cell*. 171:163-178 e119.

Boylan, K. 2015. Familial Amyotrophic Lateral Sclerosis. *Neurol Clin*. 33:807-830.

Bradner, J.E., D. Hnisz, and R.A. Young. 2017. Transcriptional Addiction in Cancer. *Cell*. 168:629-643.

Brangwynne, C.P., C.R. Eckmann, D.S. Courson, A. Rybarska, C. Hoege, J. Gharakhani, F. Julicher, and A.A. Hyman. 2009. Germline P granules are liquid droplets that localize by controlled dissolution/condensation. *Science*. 324:1729-1732.

Bravo-Hernandez, M., T. Tadokoro, M.R. Navarro, O. Platoshyn, Y. Kobayashi, S. Marsala, A. Miyanohara, S. Juhas, J. Juhasova, H. Skalnikova, Z. Tomori, I. Vanicky, H. Studenovska, V. Proks, P. Chen, N. Govea-Perez, D. Ditsworth, J.D.

Ciacci, S. Gao, W. Zhu, E.T. Ahrens, S.P. Driscoll, T.D. Glenn, M. McAlonis-Downes, S. Da Cruz, S.L. Pfaff, B.K. Kaspar, D.W. Cleveland, and M. Marsala. 2020. Spinal subpial delivery of AAV9 enables widespread gene silencing and blocks motoneuron degeneration in ALS. *Nat Med*. 26:118-130.

Burke, K.A., A.M. Janke, C.L. Rhine, and N.L. Fawzi. 2015. Residue-by-Residue View of In Vitro FUS Granules that Bind the C-Terminal Domain of RNA Polymerase II. *Mol Cell*. 60:231-241.

Chen, C., X. Ding, N. Akram, S. Xue, and S.Z. Luo. 2019a. Fused in Sarcoma: Properties, Self-Assembly and Correlation with Neurodegenerative Diseases. *Molecules*. 24.

Chen, Y., L. Xu, A. Mayakonda, M.L. Huang, D. Kanojia, T.Z. Tan, P. Dakle, R.Y. Lin, X.Y. Ke, J.W. Said, J. Chen, S. Gery, L.W. Ding, Y.Y. Jiang, A. Pang, M.E. Puhaindran, B.C. Goh, and H.P. Koeffler. 2019b. Bromodomain and extraterminal proteins foster the core transcriptional regulatory programs and confer vulnerability in liposarcoma. *Nat Commun*. 10:1353.

Chia, R., A. Chio, and B.J. Traynor. 2018. Novel genes associated with amyotrophic lateral sclerosis: diagnostic and clinical implications. *Lancet Neurol*. 17:94-102.

Cho, W.K., J.H. Spille, M. Hecht, C. Lee, C. Li, V. Grube, and Cisse, II. 2018. Mediator and RNA polymerase II clusters associate in transcription-dependent condensates. *Science*. 361:412-415.

Chong, S., C. Dugast-Darzacq, Z. Liu, P. Dong, G.M. Dailey, C. Cattoglio, A. Heckert, S. Banala, L. Lavis, X. Darzacq, and R. Tjian. 2018. Imaging dynamic and selective low-complexity domain interactions that control gene transcription. *Science*. 361.

Courchaine, E.M., A. Lu, and K.M. Neugebauer. 2016. Droplet organelles? *EMBO J*. 35:1603-1612.

Creytens, D. 2019. A contemporary review of myxoid adipocytic tumors. *Semin Diagn Pathol*. 36:129-141.

Crozat, A., P. Aman, N. Mandahl, and D. Ron. 1993. Fusion of CHOP to a novel RNA-binding protein in human myxoid liposarcoma. *Nature*. 363:640-644.

Crump, N.T., E. Ballabio, L. Godfrey, R. Thorne, E. Repapi, J. Kerry, M. Tapia, P. Hua, C. Lagerholm, P. Filippakopoulos, J.O.J. Davies, and T.A. Milne. 2021. BET inhibition disrupts transcription but retains enhancer-promoter contact. *Nat Commun*. 12:223.

Daigle, J.G., N.A. Lanson, Jr., R.B. Smith, I. Casci, A. Maltare, J. Monaghan, C.D. Nichols, D. Kryndushkin, F. Shewmaker, and U.B. Pandey. 2013. RNA-binding ability of FUS regulates neurodegeneration, cytoplasmic mislocalization and incorporation into stress granules associated with FUS carrying ALS-linked mutations. *Hum Mol Genet*. 22:1193-1205.

Davis, R.B., T. Kaur, M.M. Moosa, and P.R. Banerjee. 2021. FUS oncofusion protein condensates recruit mSWI/SNF chromatin remodeler via heterotypic interactions between prion-like domains. *Protein Sci*. 30:1454-1466.

de Graaff, M.A., J.S. Yu, H.C. Beird, D.R. Ingram, T. Nguyen, J. Juehui Liu, S. Bolshakov, K. Szuhai, P. Aman, K.E. Torres, D. Lev, T.O. Nielsen, J.V. Bovee, A.J. Lazar, and N. Somaiah. 2016. Establishment and characterization of a new human myxoid liposarcoma cell line (DL-221) with the FUS-DDIT3 translocation. *Lab Invest*. 96:885-894.

Deng, Q., C.J. Holler, G. Taylor, K.F. Hudson, W. Watkins, M. Gearing, D. Ito, M.E. Murray, D.W. Dickson, N.T. Seyfried, and T. Kukar. 2014. FUS is phosphorylated by DNA-PK and accumulates in the cytoplasm after DNA damage. *J Neurosci*. 34:7802-7813.

Devoy, A., B. Kalmar, M. Stewart, H. Park, B. Burke, S.J. Noy, Y. Redhead, J. Humphrey, K. Lo, J. Jaeger, A. Mejia Maza, P. Sivakumar, C. Bertolin, G. Soraru, V. Plagnol, L. Greensmith, A. Acevedo Arozena, A.M. Isaacs, B. Davies, P. Fratta, and E.M.C. Fisher. 2017. Humanized mutant FUS drives progressive motor neuron degeneration without aggregation in 'FUSDelta14' knockin mice. *Brain*. 140:2797-2805.

Donati, B., E. Lorenzini, and A. Ciarrocchi. 2018. BRD4 and Cancer: going beyond transcriptional regulation. *Mol Cancer*. 17:164.

Dormann, D., R. Rodde, D. Edbauer, E. Bentmann, I. Fischer, A. Hruscha, M.E. Than, I.R. Mackenzie, A. Capell, B. Schmid, M. Neumann, and C. Haass. 2010. ALS-associated fused in sarcoma (FUS) mutations disrupt Transportin-mediated nuclear import. *EMBO J*. 29:2841-2857.

Du, M., and Z.J. Chen. 2018. DNA-induced liquid phase condensation of cGAS activates innate immune signaling. *Science*. 361:704-709.

Feric, M., N. Vaidya, T.S. Harmon, D.M. Mitrea, L. Zhu, T.M. Richardson, R.W. Kriwacki, R.V. Pappu, and C.P. Brangwynne. 2016. Coexisting Liquid Phases Underlie Nucleolar Subcompartments. *Cell*. 165:1686-1697.

Ferrari, R., D. Kapogiannis, E.D. Huey, and P. Momeni. 2011. FTD and ALS: a tale of two diseases. *Curr Alzheimer Res*. 8:273-294.

Flores, B.N., M.E. Dulchavsky, A. Krans, M.R. Sawaya, H.L. Paulson, P.K. Todd, S.J. Barmada, and M.I. Ivanova. 2016. Distinct C9orf72-Associated Dipeptide Repeat Structures Correlate with Neuronal Toxicity. *PLoS One*. 11:e0165084.

Franzmann, T.M., and S. Alberti. 2019. Prion-like low-complexity sequences: Key regulators of protein solubility and phase behavior. *J Biol Chem*. 294:7128-7136.

Fujioka, Y., J.M. Alam, D. Noshiro, K. Mouri, T. Ando, Y. Okada, A.I. May, R.L. Knorr, K. Suzuki, Y. Ohsumi, and N.N. Noda. 2020. Phase separation organizes the site of autophagosome formation. *Nature*. 578:301-305.

Fushimi, K., C. Long, N. Jayaram, X. Chen, L. Li, and J.Y. Wu. 2011. Expression of human FUS/TLS in yeast leads to protein aggregation and cytotoxicity, recapitulating key features of FUS proteinopathy. *Protein Cell*. 2:141-149.

Gal, J., J. Zhang, D.M. Kwinter, J. Zhai, H. Jia, J. Jia, and H. Zhu. 2011. Nuclear localization sequence of FUS and induction of stress granules by ALS mutants. *Neurobiol Aging*. 32:2323 e2327-2340.

Gardiner, M., R. Toth, F. Vandermoere, N.A. Morrice, and J. Rouse. 2008. Identification and characterization of FUS/TLS as a new target of ATM. *Biochem J*. 415:297-307.

Gitler, A.D., and J. Shorter. 2011. RNA-binding proteins with prion-like domains in ALS and FTLD-U. *Prion*. 5:179-187.

Gollavilli, P.N., A. Pawar, K. Wilder-Romans, R. Natesan, C.G. Engelke, V.L. Dommeti, P.M. Krishnamurthy, A. Nallasivam, I.J. Apel, T. Xu, Z.S. Qin, F.Y. Feng, and I.A. Asangani. 2018. EWS/ETS-Driven Ewing Sarcoma Requires BET Bromodomain Proteins. *Cancer Res*. 78:4760-4773.

Goransson, M., M. Wedin, and P. Aman. 2002. Temperature-dependent localization of TLS-CHOP to splicing factor compartments. *Exp Cell Res*. 278:125-132.

Gotor, N.L., A. Armaos, G. Calloni, M. Torrent Burgas, R.M. Vabulas, N.S. De Groot, and G.G. Tartaglia. 2020. RNA-binding and prion domains: the Yin and Yang of phase separation. *Nucleic Acids Res*. 48:9491-9504.

Guo, Y.E., J.C. Manteiga, J.E. Henninger, B.R. Sabari, A. Dall'Agnese, N.M. Hannett, J.H. Spille, L.K. Afeyan, A.V. Zamudio, K. Shrinivas, B.J. Abraham, A. Boija, T.M. Decker, J.K. Rimel, C.B. Fant, T.I. Lee, Cisse, II, P.A. Sharp, D.J. Taatjes, and R.A. Young. 2019. Pol II phosphorylation regulates a switch between transcriptional and splicing condensates. *Nature*. 572:543-548.

Gurumurthy, A., Y. Shen, E.M. Gunn, and J. Bungert. 2019. Phase Separation and Transcription Regulation: Are Super-Enhancers and Locus Control Regions Primary Sites of Transcription Complex Assembly? *Bioessays*. 41:e1800164.

Hardiman, O., A. Al-Chalabi, A. Chio, E.M. Corr, G. Logroscino, W. Robberecht, P.J. Shaw, Z. Simmons, and L.H. van den Berg. 2017. Amyotrophic lateral sclerosis. *Nat Rev Dis Primers*. 3:17071.

Hergesheimer, R.C., A.A. Chami, D.R. de Assis, P. Vourc'h, C.R. Andres, P. Corcia, D. Lanznaster, and H. Blasco. 2019. The debated toxic role of aggregated TDP-43 in amyotrophic lateral sclerosis: a resolution in sight? *Brain*. 142:1176-1194.

Hnisz, D., K. Shrinivas, R.A. Young, A.K. Chakraborty, and P.A. Sharp. 2017. A Phase Separation Model for Transcriptional Control. *Cell*. 169:13-23.

Hoell, J.I., E. Larsson, S. Runge, J.D. Nusbaum, S. Duggimpudi, T.A. Farazi, M. Hafner, A. Borkhardt, C. Sander, and T. Tuschl. 2011. RNA targets of wild-type and mutant FET family proteins. *Nat Struct Mol Biol*. 18:1428-1431.

Hu, H., M. Tian, C. Ding, and S. Yu. 2018. The C/EBP Homologous Protein (CHOP) Transcription Factor Functions in Endoplasmic Reticulum Stress-Induced Apoptosis and Microbial Infection. *Front Immunol*. 9:3083.

Huang, W.Y.C., S. Alvarez, Y. Kondo, Y.K. Lee, J.K. Chung, H.Y.M. Lam, K.H. Biswas, J. Kuriyan, and J.T. Groves. 2019. A molecular assembly phase transition and kinetic proofreading modulate Ras activation by SOS. *Science*. 363:1098-1103.

Hyman, A.A., C.A. Weber, and F. Julicher. 2014. Liquid-liquid phase separation in biology. *Annu Rev Cell Dev Biol*. 30:39-58.

Iglesias, V., L. Paladin, T. Juan-Blanco, I. Pallares, P. Aloy, S.C.E. Tosatto, and S. Ventura. 2019. In silico Characterization of Human Prion-Like Proteins: Beyond Neurological Diseases. *Front Physiol*. 10:314.

Irwin, D.J., N.J. Cairns, M. Grossman, C.T. McMillan, E.B. Lee, V.M. Van Deerlin, V.M. Lee, and J.Q. Trojanowski. 2015. Frontotemporal lobar degeneration: defining phenotypic diversity through personalized medicine. *Acta Neuropathol*. 129:469-491.

Ishigaki, S., and G. Sobue. 2018. Importance of Functional Loss of FUS in FTLD/ALS. *Front Mol Biosci*. 5:44.

Jiang, S., J.B. Fagman, C. Chen, S. Alberti, and B. Liu. 2020. Protein phase separation and its role in tumorigenesis. *Elife*. 9.

Johnson, B.S., J.M. McCaffery, S. Lindquist, and A.D. Gitler. 2008. A yeast TDP-43 proteinopathy model: Exploring the molecular determinants of TDP-43 aggregation and cellular toxicity. *Proc Natl Acad Sci U S A*. 105:6439-6444.

Joseph, C.G., H. Hwang, Y. Jiao, L.D. Wood, I. Kinde, J. Wu, N. Mandahl, J. Luo, R.H. Hruban, L.A. Diaz, Jr., T.C. He, B. Vogelstein, K.W. Kinzler, F. Mertens, and N. Papadopoulos. 2014. Exomic analysis of myxoid liposarcomas, synovial sarcomas, and osteosarcomas. *Genes Chromosomes Cancer*. 53:15-24.

Kamagata, K., S. Kanbayashi, M. Honda, Y. Itoh, H. Takahashi, T. Kameda, F. Nagatsugi, and S. Takahashi. 2020. Liquid-like droplet formation by tumor suppressor p53 induced by multivalent electrostatic interactions between two disordered domains. *Sci Rep*. 10:580.

Karch, C.M., N. Wen, C.C. Fan, J.S. Yokoyama, N. Kouri, O.A. Ross, G. Hoglinger, U. Muller, R. Ferrari, J. Hardy, G.D. Schellenberg, P.M. Sleiman, P. Momeni, C.P. Hess, B.L. Miller, M. Sharma, V. Van Deerlin, O.B. Smeland, O.A. Andreassen, A.M. Dale, R.S. Desikan, I.C.f.F.D.P.S.P.G.C. International Frontotemporal Dementia -Genomics Consortium, and C. International Parkinson's Disease Genomics. 2018. Selective Genetic Overlap Between Amyotrophic Lateral Sclerosis and Diseases of the Frontotemporal Dementia Spectrum. *JAMA Neurol*. 75:860-875.

Kato, M., T.W. Han, S. Xie, K. Shi, X. Du, L.C. Wu, H. Mirzaei, E.J. Goldsmith, J. Longgood, J. Pei, N.V. Grishin, D.E. Frantz, J.W. Schneider, S. Chen, L. Li, M.R. Sawaya, D. Eisenberg, R. Tycko, and S.L. McKnight. 2012. Cell-free formation of RNA granules: low complexity sequence domains form dynamic fibers within hydrogels. *Cell*. 149:753-767.

Kedersha, N., and P. Anderson. 2007. Mammalian stress granules and processing bodies. *Methods Enzymol*. 431:61-81.

Kilic, S., A. Lezaja, M. Gatti, E. Bianco, J. Michelena, R. Imhof, and M. Altmeyer. 2019. Phase separation of 53BP1 determines liquid-like behavior of DNA repair compartments. *EMBO J*. 38:e101379.

Kim, H.J., N.C. Kim, Y.D. Wang, E.A. Scarborough, J. Moore, Z. Diaz, K.S. MacLea, B. Freibaum, S. Li, A. Molliex, A.P. Kanagaraj, R. Carter, K.B. Boylan, A.M. Wojtas, R. Rademakers, J.L. Pinkus, S.A. Greenberg, J.Q. Trojanowski, B.J. Traynor, B.N. Smith, S. Topp, A.S. Gkazi, J. Miller, C.E. Shaw, M. Kottlors, J. Kirschner, A. Pestronk, Y.R. Li, A.F. Ford, A.D. Gitler, M. Benatar, O.D. King, V.E. Kimonis, E.D. Ross, C.C. Weihl, J. Shorter, and J.P. Taylor. 2013. Mutations in prion-like domains in hnRNPA2B1 and hnRNPA1 cause multisystem proteinopathy and ALS. *Nature*. 495:467-473.

Kirsanov, K.I., E.A. Lesovaya, T.I. Fetisov, B.Y. Bokhyan, G.A. Belitsky, and M.G. Yakubovskaya. 2020. Current Approaches for Personalized Therapy of Soft Tissue Sarcomas. *Sarcoma*. 2020:6716742.

Klein, I.A., A. Boija, L.K. Afeyan, S.W. Hawken, M. Fan, A. Dall'Agnese, O. Oksuz, J.E. Henninger, K. Shrinivas, B.R. Sabari, I. Sagi, V.E. Clark, J.M. Platt, M. Kar, P.M. McCall, A.V. Zamudio, J.C. Manteiga, E.L. Coffey, C.H. Li, N.M. Hannett, Y.E. Guo, T.M. Decker, T.I. Lee, T. Zhang, J.K. Weng, D.J. Taatjes, A. Chakraborty, P.A. Sharp, Y.T. Chang, A.A. Hyman, N.S. Gray, and R.A. Young. 2020. Partitioning of cancer therapeutics in nuclear condensates. *Science*. 368:1386-1392.

Knight, J.C., P.J. Renwick, P. Dal Cin, H. Van den Berghe, and C.D. Fletcher. 1995. Translocation t(12;16)(q13;p11) in myxoid liposarcoma and round cell liposarcoma: molecular and cytogenetic analysis. *Cancer Res*. 55:24-27.

Kovar, H. 2011. Dr. Jekyll and Mr. Hyde: The Two Faces of the FUS/EWS/TAF15 Protein Family. *Sarcoma*. 2011:837474.

Krobitsch, S., and S. Lindquist. 2000. Aggregation of huntingtin in yeast varies with the length of the polyglutamine expansion and the expression of chaperone proteins. *Proc Natl Acad Sci U S A*. 97:1589-1594.

Kryndushkin, D., R.B. Wickner, and F. Shewmaker. 2011. FUS/TLS forms cytoplasmic aggregates, inhibits cell growth and interacts with TDP-43 in a yeast model of amyotrophic lateral sclerosis. *Protein Cell*. 2:223-236.

Kwiatkowski, T.J., Jr., D.A. Bosco, A.L. Leclerc, E. Tamrazian, C.R. Vanderburg, C. Russ, A. Davis, J. Gilchrist, E.J. Kasarskis, T. Munsat, P. Valdmanis, G.A. Rouleau, B.A. Hosler, P. Cortelli, P.J. de Jong, Y. Yoshinaga, J.L. Haines, M.A. Pericak-Vance, J. Yan, N. Ticozzi, T. Siddique, D. McKenna-Yasek, P.C. Sapp, H.R. Horvitz, J.E. Landers, and R.H. Brown, Jr. 2009. Mutations in the FUS/TLS gene on chromosome 16 cause familial amyotrophic lateral sclerosis. *Science*. 323:1205-1208.

Laflamme, G., and K. Mekhail. 2020. Biomolecular condensates as arbiters of biochemical reactions inside the nucleus. *Commun Biol*. 3:773.

Lallemand-Breitenbach, V., and H. de The. 2018. PML nuclear bodies: from architecture to function. *Curr Opin Cell Biol*. 52:154-161.

Larson, A.G., D. Elnatan, M.M. Keenen, M.J. Trnka, J.B. Johnston, A.L. Burlingame, D.A. Agard, S. Redding, and G.J. Narlikar. 2017. Liquid droplet formation by HP1alpha suggests a role for phase separation in heterochromatin. *Nature*. 547:236-240.

Levone, B.R., S.C. Lenzken, M. Antonaci, A. Maiser, A. Rapp, F. Conte, S. Reber, J. Mechtersheimer, A.E. Ronchi, O. Muhlemann, H. Leonhardt, M.C. Cardoso, M.D. Ruepp, and S.M.L. Barabino. 2021. FUS-dependent liquid-liquid phase separation is important for DNA repair initiation. *J Cell Biol*. 220.

Li, C.H., E.L. Coffey, A. Dall'Agnese, N.M. Hannett, X. Tang, J.E. Henninger, J.M. Platt, O. Oksuz, A.V. Zamudio, L.K. Afeyan, J. Schuijers, X.S. Liu, S. Markoulaki, T. Lungjangwa, G. LeRoy, D.S. Svoboda, E. Wogram, T.I. Lee, R. Jaenisch, and R.A. Young. 2020. MeCP2 links heterochromatin condensates and neurodevelopmental disease. *Nature*. 586:440-444.

Li, H.Y., P.A. Yeh, H.C. Chiu, C.Y. Tang, and B.P. Tu. 2011. Hyperphosphorylation as a defense mechanism to reduce TDP-43 aggregation. *PLoS One*. 6:e23075.

Lin, Y., S.L. Currie, and M.K. Rosen. 2017. Intrinsically disordered sequences enable modulation of protein phase separation through distributed tyrosine motifs. *J Biol Chem*. 292:19110-19120.

Linden, M., C. Thomsen, P. Grundevik, E. Jonasson, D. Andersson, R. Runnberg, S. Dolatabadi, C. Vannas, M. Luna Santamariotaa, H. Fagman, A. Stahlberg, and P. Aman. 2019. FET family fusion oncoproteins target the SWI/SNF chromatin remodeling complex. *EMBO Rep*. 20.

Loven, J., H.A. Hoke, C.Y. Lin, A. Lau, D.A. Orlando, C.R. Vakoc, J.E. Bradner, T.I. Lee, and R.A. Young. 2013. Selective inhibition of tumor oncogenes by disruption of super-enhancers. *Cell*. 153:320-334.

Lu, H., R. Liu, and Q. Zhou. 2019. Balanced between order and disorder: a new phase in transcription elongation control and beyond. *Transcription*. 10:157-163.

Lu, Y., T. Wu, O. Gutman, H. Lu, Q. Zhou, Y.I. Henis, and K. Luo. 2020. Phase separation of TAZ compartmentalizes the transcription machinery to promote gene expression. *Nat Cell Biol*. 22:453-464.

Lyon, A.S., W.B. Peeples, and M.K. Rosen. 2021. A framework for understanding the functions of biomolecular condensates across scales. *Nat Rev Mol Cell Biol*. 22:215-235.

Maharana, S., J. Wang, D.K. Papadopoulos, D. Richter, A. Pozniakovsky, I. Poser, M. Bickle, S. Rizk, J. Guillen-Boixet, T.M. Franzmann, M. Jahnel, L. Marrone, Y.T. Chang, J. Sterneckert, P. Tomancak, A.A. Hyman, and S. Alberti. 2018. RNA buffers the phase separation behavior of prion-like RNA binding proteins. *Science*. 360:918-921.

Maher, P. 2019. The Potential of Flavonoids for the Treatment of Neurodegenerative Diseases. *Int J Mol Sci*. 20.

Maier, M., T. Welt, F. Wirth, F. Montrasio, D. Preisig, J. McAfoose, F.G. Vieira, L. Kulic, C. Spani, T. Stehle, S. Perrin, M. Weber, C. Hock, R.M. Nitsch, and J. Grimm. 2018. A human-derived antibody targets misfolded SOD1 and ameliorates motor symptoms in mouse models of amyotrophic lateral sclerosis. *Sci Transl Med*. 10.

Majumdar, A., P. Dogra, S. Maity, and S. Mukhopadhyay. 2019. Liquid-Liquid Phase Separation Is Driven by Large-Scale Conformational Unwinding and Fluctuations of Intrinsically Disordered Protein Molecules. *J Phys Chem Lett*. 10:3929-3936.

Malik, R., and M. Wiedau. 2020. Therapeutic Approaches Targeting Protein Aggregation in Amyotrophic Lateral Sclerosis. *Front Mol Neurosci*. 13:98.

Manasanch, E.E., and R.Z. Orlowski. 2017. Proteasome inhibitors in cancer therapy. *Nat Rev Clin Oncol*. 14:417-433.

Mandrioli, J., V. Crippa, C. Cereda, V. Bonetto, E. Zucchi, A. Gessani, M. Ceroni, A. Chio, R. D'Amico, M.R. Monsurro, N. Riva, M. Sabatelli, V. Silani, I.L. Simone, G. Soraru, A. Provenzani, V.G. D'Agostino, S. Carra, and A. Poletti. 2019. Proteostasis and ALS: protocol for a phase II, randomised, double-blind, placebo-controlled, multicentre clinical trial for colchicine in ALS (Co-ALS). *BMJ Open*. 9:e028486.

March, Z.M., O.D. King, and J. Shorter. 2016. Prion-like domains as epigenetic regulators, scaffolds for subcellular organization, and drivers of neurodegenerative disease. *Brain Res*. 1647:9-18.

Martin, E.W., and T. Mittag. 2018. Relationship of Sequence and Phase Separation in Protein Low-Complexity Regions. *Biochemistry*. 57:2478-2487.

Mastrocola, A.S., S.H. Kim, A.T. Trinh, L.A. Rodenkirch, and R.S. Tibbetts. 2013. The RNA-binding protein fused in sarcoma (FUS) functions downstream of poly(ADP-ribose) polymerase (PARP) in response to DNA damage. *J Biol Chem*. 288:24731-24741.

McCluggage, F., and A.H. Fox. 2021. Paraspeckle nuclear condensates: Global sensors of cell stress? *Bioessays*. 43:e2000245.

McGlinchey, R.P., D. Kryndushkin, and R.B. Wickner. 2011. Suicidal [PSI+] is a lethal yeast prion. *Proc Natl Acad Sci U S A*. 108:5337-5341.

McSwiggen, D.T., M. Mir, X. Darzacq, and R. Tjian. 2019. Evaluating phase separation in live cells: diagnosis, caveats, and functional consequences. *Genes Dev*. 33:1619-1634.

Meissner, M., S. Lopato, J. Gotzmann, G. Sauermann, and A. Barta. 2003. Proto-oncoprotein TLS/FUS is associated to the nuclear matrix and complexed with splicing factors PTB, SRm160, and SR proteins. *Exp Cell Res*. 283:184-195.

Mejzini, R., L.L. Flynn, I.L. Pitout, S. Fletcher, S.D. Wilton, and P.A. Akkari. 2019. ALS Genetics, Mechanisms, and Therapeutics: Where Are We Now? *Front Neurosci*. 13:1310.

Molliex, A., J. Temirov, J. Lee, M. Coughlin, A.P. Kanagaraj, H.J. Kim, T. Mittag, and J.P. Taylor. 2015. Phase separation by low complexity domains promotes stress granule assembly and drives pathological fibrillization. *Cell*. 163:123-133.

Monahan, Z., V.H. Ryan, A.M. Janke, K.A. Burke, S.N. Rhoads, G.H. Zerze, R. O'Meally, G.L. Dignon, A.E. Conicella, W. Zheng, R.B. Best, R.N. Cole, J. Mittal, F. Shewmaker, and N.L. Fawzi. 2017. Phosphorylation of the FUS low-complexity domain disrupts phase separation, aggregation, and toxicity. *EMBO J*. 36:2951-2967.

Monahan, Z.T., S.N. Rhoads, D.S. Yee, and F.P. Shewmaker. 2018. Yeast Models of Prion-Like Proteins That Cause Amyotrophic Lateral Sclerosis Reveal Pathogenic Mechanisms. *Front Mol Neurosci*. 11:453.

Mulcahy Levy, J.M., and A. Thorburn. 2020. Autophagy in cancer: moving from understanding mechanism to improving therapy responses in patients. *Cell Death Differ*. 27:843-857.

Murakami, T., S. Qamar, J.Q. Lin, G.S. Schierle, E. Rees, A. Miyashita, A.R. Costa, R.B. Dodd, F.T. Chan, C.H. Michel, D. Kronenberg-Versteeg, Y. Li, S.P. Yang, Y. Wakutani, W. Meadows, R.R. Ferry, L. Dong, G.G. Tartaglia, G. Favrin, W.L. Lin, D.W. Dickson, M. Zhen, D. Ron, G. Schmitt-Ulms, P.E. Fraser, N.A. Shneider, C. Holt, M. Vendruscolo, C.F. Kaminski, and P. St George-Hyslop. 2015. ALS/FTD Mutation-Induced Phase Transition of FUS Liquid Droplets and Reversible Hydrogels into Irreversible Hydrogels Impairs RNP Granule Function. *Neuron*. 88:678-690.

Murray, D.T., M. Kato, Y. Lin, K.R. Thurber, I. Hung, S.L. McKnight, and R. Tycko. 2017. Structure of FUS Protein Fibrils and Its Relevance to Self-Assembly and Phase Separation of Low-Complexity Domains. *Cell*. 171:615-627 e616.

Murthy, A.C., G.L. Dignon, Y. Kan, G.H. Zerze, S.H. Parekh, J. Mittal, and N.L. Fawzi. 2019. Molecular interactions underlying liquid-liquid phase separation of the FUS low-complexity domain. *Nat Struct Mol Biol*. 26:637-648.

Nair, S.J., L. Yang, D. Meluzzi, S. Oh, F. Yang, M.J. Friedman, S. Wang, T. Suter, I. Alshareedah, A. Gamliel, Q. Ma, J. Zhang, Y. Hu, Y. Tan, K.A. Ohgi, R.S. Jayani, P.R. Banerjee, A.K. Aggarwal, and M.G. Rosenfeld. 2019. Phase separation of ligand-activated enhancers licenses cooperative chromosomal enhancer assembly. *Nat Struct Mol Biol*. 26:193-203.

Nedelsky, N.B., and J.P. Taylor. 2019. Bridging biophysics and neurology: aberrant phase transitions in neurodegenerative disease. *Nat Rev Neurol*. 15:272-286.

Neugebauer, K.M. 2017. Special focus on the Cajal Body. *RNA Biol*. 14:669-670.

Niaki, A.G., J. Sarkar, X. Cai, K. Rhine, V. Vidaurre, B. Guy, M. Hurst, J.C. Lee, H.R. Koh, L. Guo, C.M. Fare, J. Shorter, and S. Myong. 2020. Loss of Dynamic RNA Interaction and Aberrant Phase Separation Induced by Two Distinct Types of ALS/FTD-Linked FUS Mutations. *Mol Cell*. 77:82-94 e84.

Nomura, T., S. Watanabe, K. Kaneko, K. Yamanaka, N. Nukina, and Y. Furukawa. 2014. Intranuclear aggregation of mutant FUS/TLS as a molecular pathomechanism of amyotrophic lateral sclerosis. *J Biol Chem*. 289:1192-1202.

Oakley, S.S., M.B. Maina, K.E. Marshall, Y.K. Al-Hilaly, C.R. Harrington, C.M. Wischik, and L.C. Serpell. 2020. Tau Filament Self-Assembly and Structure: Tau as a Therapeutic Target. *Front Neurol*. 11:590754.

Ohoka, N., T. Hattori, M. Kitagawa, K. Onozaki, and H. Hayashi. 2007. Critical and functional regulation of CHOP (C/EBP homologous protein) through the N-terminal portion. *J Biol Chem*. 282:35687-35694.

Oikawa, K., M. Tanaka, S. Itoh, M. Takanashi, T. Ozaki, Y. Muragaki, and M. Kuroda. 2012. A novel oncogenic pathway by TLS-CHOP involving repression of MDA-7/IL-24 expression. *Br J Cancer*. 106:1976-1979.

Orszulak, M., K. Mizia-Stec, A. Siennicka, K. Goscinska-Bis, K. Waga, M. Wojcik, R. Blaszczyk, B. Michalski, F.M. Szymanski, K. Ptaszynska-Kopczynska, G. Kopec, P. Nadrowski, A. Hrynkiewicz-Szymanska, L. Krzych, and E.A. Jankowska. 2016. Differences of psychological features in patients with heart failure with regard to gender and aetiology - Results of a CAPS-LOCK-HF (Complex Assessment of Psychological Status Located in Heart Failure) study. *Int J Cardiol*. 219:380-386.

Outeiro, T.F., and S. Lindquist. 2003. Yeast cells provide insight into alpha-synuclein biology and pathobiology. *Science*. 302:1772-1775.

Owen, I., S. Rhoads, D. Yee, H. Wyne, K. Gery, I. Hannula, M. Sundrum, and F. Shewmaker. 2020. The prion-like domain of Fused in Sarcoma is phosphorylated by multiple kinases affecting liquid- and solid-phase transitions. *Mol Biol Cell*. 31:2522-2536.

Owen, I., and F. Shewmaker. 2019. The Role of Post-Translational Modifications in the Phase Transitions of Intrinsically Disordered Proteins. *Int J Mol Sci*. 20.

Pakravan, D., G. Orlando, V. Bercier, and L. Van Den Bosch. 2021. Role and therapeutic potential of liquid-liquid phase separation in amyotrophic lateral sclerosis. *J Mol Cell Biol*. 13:15-28.

Parker, M.W., M. Bell, M. Mir, J.A. Kao, X. Darzacq, M.R. Botchan, and J.M. Berger. 2019. A new class of disordered elements controls DNA replication through initiator self-assembly. *Elife*. 8.

Patel, A., H.O. Lee, L. Jawerth, S. Maharana, M. Jahnel, M.Y. Hein, S. Stoynov, J. Mahamid, S. Saha, T.M. Franzmann, A. Pozniakovski, I. Poser, N. Maghelli, L.A. Royer, M. Weigert, E.W. Myers, S. Grill, D. Drechsel, A.A. Hyman, and S. Alberti. 2015. A Liquid-to-Solid Phase Transition of the ALS Protein FUS Accelerated by Disease Mutation. *Cell*. 162:1066-1077.

Peng, L., E.M. Li, and L.Y. Xu. 2020. From start to end: Phase separation and transcriptional regulation. *Biochim Biophys Acta Gene Regul Mech*. 1863:194641.

Perez-Losada, J., M. Sanchez-Martin, M.A. Rodriguez-Garcia, P.A. Perez-Mancera, B. Pintado, T. Flores, E. Battaner, and I. Sanchez-Garcia. 2000. Liposarcoma initiated by FUS/TLS-CHOP: the FUS/TLS domain plays a critical role in the pathogenesis of liposarcoma. *Oncogene*. 19:6015-6022.

Perez-Mancera, P.A., and I. Sanchez-Garcia. 2005. Understanding mesenchymal cancer: the liposarcoma-associated FUS-DDIT3 fusion gene as a model. *Semin Cancer Biol*. 15:206-214.

Peskett, T.R., F. Rau, J. O'Driscoll, R. Patani, A.R. Lowe, and H.R. Saibil. 2018. A Liquid to Solid Phase Transition Underlying Pathological Huntingtin Exon1 Aggregation. *Mol Cell*. 70:588-601 e586.

Powers, M.P., W.L. Wang, V.S. Hernandez, K.S. Patel, D.C. Lev, A.J. Lazar, and D.H. Lopez-Terrada. 2010. Detection of myxoid liposarcoma-associated FUS-DDIT3 rearrangement variants including a newly identified breakpoint using an optimized RT-PCR assay. *Mod Pathol*. 23:1307-1315.

Pozzi, S., S.S. Thammisetty, P. Codron, R. Rahimian, K.V. Plourde, G. Soucy, C. Bareil, D. Phaneuf, J. Kriz, C. Gravel, and J.P. Julien. 2019. Virus-mediated delivery of antibody targeting TAR DNA-binding protein-43 mitigates associated neuropathology. *J Clin Invest*. 129:1581-1595.

Prusiner, S.B. 1982. Novel proteinaceous infectious particles cause scrapie. *Science*. 216:136-144.

Rai, A.K., J.X. Chen, M. Selbach, and L. Pelkmans. 2018. Kinase-controlled phase transition of membraneless organelles in mitosis. *Nature*. 559:211-216.

Rawat, P., M. Boehning, B. Hummel, F. Aprile-Garcia, A.S. Pandit, N. Eisenhardt, A. Khavaran, E. Niskanen, S.M. Vos, J.J. Palvimo, A. Pichler, P. Cramer, and R.

Sawarkar. 2021. Stress-induced nuclear condensation of NELF drives transcriptional downregulation. *Mol Cell*. 81:1013-1026 e1011.

Rhoads, S.N., Z.T. Monahan, D.S. Yee, A.Y. Leung, C.G. Newcombe, R.N. O'Meally, R.N. Cole, and F.P. Shewmaker. 2018a. The prionlike domain of FUS is multiphosphorylated following DNA damage without altering nuclear localization. *Mol Biol Cell*. 29:1786-1797.

Rhoads, S.N., Z.T. Monahan, D.S. Yee, and F.P. Shewmaker. 2018b. The Role of Post-Translational Modifications on Prion-Like Aggregation and Liquid-Phase Separation of FUS. *Int J Mol Sci*. 19.

Riggi, N., L. Cironi, M.L. Suva, and I. Stamenkovic. 2007. Sarcomas: genetics, signalling, and cellular origins. Part 1: The fellowship of TET. *J Pathol*. 213:4-20.

Ross, E.D., and J.A. Toombs. 2010. The effects of amino acid composition on yeast prion formation and prion domain interactions. *Prion*. 4:60-65.

Ryan, V.H., G.L. Dignon, G.H. Zerze, C.V. Chabata, R. Silva, A.E. Conicella, J. Amaya, K.A. Burke, J. Mittal, and N.L. Fawzi. 2018. Mechanistic View of hnRNPA2 Low-Complexity Domain Structure, Interactions, and Phase Separation Altered by Mutation and Arginine Methylation. *Mol Cell*. 69:465-479 e467.

Sabari, B.R., A. Dall'Agnese, A. Boija, I.A. Klein, E.L. Coffey, K. Shrinivas, B.J. Abraham, N.M. Hannett, A.V. Zamudio, J.C. Manteiga, C.H. Li, Y.E. Guo, D.S. Day, J. Schuijers, E. Vasile, S. Malik, D. Hnisz, T.I. Lee, Cisse, II, R.G. Roeder, P.A. Sharp, A.K. Chakraborty, and R.A. Young. 2018. Coactivator condensation at super-enhancers links phase separation and gene control. *Science*. 361.

Saberi, S., J.E. Stauffer, D.J. Schulte, and J. Ravits. 2015. Neuropathology of Amyotrophic Lateral Sclerosis and Its Variants. *Neurol Clin*. 33:855-876.

Sama, R.R., C.L. Ward, L.J. Kaushansky, N. Lemay, S. Ishigaki, F. Urano, and D.A. Bosco. 2013. FUS/TLS assembles into stress granules and is a prosurvival factor during hyperosmolar stress. *J Cell Physiol*. 228:2222-2231.

Sangwan, S., A. Zhao, K.L. Adams, C.K. Jayson, M.R. Sawaya, E.L. Guenther, A.C. Pan, J. Ngo, D.M. Moore, A.B. Soriaga, T.D. Do, L. Goldschmidt, R. Nelson, M.T. Bowers, C.M. Koehler, D.E. Shaw, B.G. Novitch, and D.S. Eisenberg. 2017. Atomic structure of a toxic, oligomeric segment of SOD1 linked to amyotrophic lateral sclerosis (ALS). *Proc Natl Acad Sci U S A*. 114:8770-8775.

Schindelin, J., I. Arganda-Carreras, E. Frise, V. Kaynig, M. Longair, T. Pietzsch, S. Preibisch, C. Rueden, S. Saalfeld, B. Schmid, J.Y. Tinevez, D.J. White, V. Hartenstein, K. Eliceiri, P. Tomancak, and A. Cardona. 2012. Fiji: an open-source platform for biological-image analysis. *Nat Methods*. 9:676-682.

Schneider, N., F.G. Wieland, D. Kong, A.A.M. Fischer, M. Horner, J. Timmer, H. Ye, and W. Weber. 2021. Liquid-liquid phase separation of light-inducible transcription factors increases transcription activation in mammalian cells and mice. *Sci Adv*. 7.

Schwartz, J.C., C.C. Ebmeier, E.R. Podell, J. Heimiller, D.J. Taatjes, and T.R. Cech. 2012. FUS binds the CTD of RNA polymerase II and regulates its phosphorylation at Ser2. *Genes Dev*. 26:2690-2695.

Shang, Y., and E.J. Huang. 2016. Mechanisms of FUS mutations in familial amyotrophic lateral sclerosis. *Brain Res*. 1647:65-78.

Sharma, A., A.K. Lyashchenko, L. Lu, S.E. Nasrabady, M. Elmaleh, M. Mendelsohn, A. Nemes, J.C. Tapia, G.Z. Mentis, and N.A. Shneider. 2016. ALS-associated mutant FUS induces selective motor neuron degeneration through toxic gain of function. *Nat Commun*. 7:10465.

Shelkovnikova, T.A., H.K. Robinson, C. Troakes, N. Ninkina, and V.L. Buchman. 2014. Compromised paraspeckle formation as a pathogenic factor in FUSopathies. *Hum Mol Genet*. 23:2298-2312.

Shewmaker, F., R.B. Wickner, and R. Tycko. 2006. Amyloid of the prion domain of Sup35p has an in-register parallel beta-sheet structure. *Proc Natl Acad Sci U S A*. 103:19754-19759.

Shin, Y., and C.P. Brangwynne. 2017. Liquid phase condensation in cell physiology and disease. *Science*. 357.

Siddique, T., and S. Ajroud-Driss. 2011. Familial amyotrophic lateral sclerosis, a historical perspective. *Acta Myol*. 30:117-120.

Siegel, R.L., K.D. Miller, and A. Jemal. 2015. Cancer statistics, 2015. *CA Cancer J Clin*. 65:5-29.

Singatulina, A.S., L. Hamon, M.V. Sukhanova, B. Desforges, V. Joshi, A. Bouhss, O.I. Lavrik, and D. Pastre. 2019. PARP-1 Activation Directs FUS to DNA Damage Sites to Form PARG-Reversible Compartments Enriched in Damaged DNA. *Cell Rep*. 27:1809-1821 e1805.

Snowden, J.S., Q. Hu, S. Rollinson, N. Halliwell, A. Robinson, Y.S. Davidson, P. Momeni, A. Baborie, T.D. Griffiths, E. Jaros, R.H. Perry, A. Richardson, S.M. Pickering-Brown, D. Neary, and D.M. Mann. 2011. The most common type of FTLD-FUS (aFTLD-U) is associated with a distinct clinical form of frontotemporal dementia but is not related to mutations in the FUS gene. *Acta Neuropathol*. 122:99-110.

Soding, J., D. Zwicker, S. Sohrabi-Jahromi, M. Boehning, and J. Kirschbaum. 2020. Mechanisms for Active Regulation of Biomolecular Condensates. *Trends Cell Biol*. 30:4-14.

Sonja Kroschwald, S.M., Simon Alberti. 2017. Hexanediol: a chemical probe to investigate the material properties of membrane-less compartments. *Science Matters*.

Stauffer, W., H. Sheng, and H.N. Lim. 2018. EzColocalization: An ImageJ plugin for visualizing and measuring colocalization in cells and organisms. *Sci Rep*. 8:15764.

Sun, S., S.C. Ling, J. Qiu, C.P. Albuquerque, Y. Zhou, S. Tokunaga, H. Li, H. Qiu, A. Bui, G.W. Yeo, E.J. Huang, K. Eggan, H. Zhou, X.D. Fu, C. Lagier-Tourenne, and D.W. Cleveland. 2015. ALS-causative mutations in FUS/TLS confer gain and loss of function by altered association with SMN and U1-snRNP. *Nat Commun*. 6:6171.

Suzuki, K., Y. Matsui, K. Endo, T. Kubo, T. Hasegawa, T. Kimura, O. Ohtani, and N. Yasui. 2010. Myxoid liposarcoma with EWS-CHOP type 1 fusion gene. *Anticancer Res*. 30:4679-4683.

Suzuki, K., Y. Matsui, N. Hashimoto, N. Naka, N. Araki, T. Kimura, H. Yoshikawa, and T. Ueda. 2012. Variation in myxoid liposarcoma: Clinicopathological examination of four cases with detectable TLS-CHOP or EWS-CHOP fusion transcripts whose histopathological diagnosis was other than myxoid liposarcoma. *Oncol Lett*. 3:293-296.

Tan, A.Y., T.R. Riley, T. Coady, H.J. Bussemaker, and J.L. Manley. 2012. TLS/FUS (translocated in liposarcoma/fused in sarcoma) regulates target gene transcription via single-stranded DNA response elements. *Proc Natl Acad Sci U S A*. 109:6030-6035.

Taniue, K., and N. Akimitsu. 2021. Aberrant phase separation and cancer. *FEBS J*.

Tank, E.M., D.A. Harris, A.A. Desai, and H.L. True. 2007. Prion protein repeat expansion results in increased aggregation and reveals phenotypic variability. *Mol Cell Biol*. 27:5445-5455.

Ter-Avanesyan, M.D., A.R. Dagkesamanskaya, V.V. Kushnirov, and V.N. Smirnov. 1994. The SUP35 omnipotent suppressor gene is involved in the maintenance of the non-Mendelian determinant [psi+] in the yeast Saccharomyces cerevisiae. *Genetics*. 137:671-676.

Thandapani, P. 2019. Super-enhancers in cancer. *Pharmacol Ther*. 199:129-138.

Thelin-Jarnum, S., M. Goransson, A.S. Burguete, A. Olofsson, and P. Aman. 2002. The myxoid liposarcoma specific TLS-CHOP fusion protein localizes to nuclear structures distinct from PML nuclear bodies. *Int J Cancer*. 97:446-450.

Thelin-Jarnum, S., C. Lassen, I. Panagopoulos, N. Mandahl, and P. Aman. 1999. Identification of genes differentially expressed in TLS-CHOP carrying myxoid liposarcomas. *Int J Cancer*. 83:30-33.

Thompson, V.F., R.A. Victor, A.A. Morera, M. Moinpour, M.N. Liu, C.C. Kisiel, K. Pickrel, C.E. Springhower, and J.C. Schwartz. 2018. Transcription-Dependent Formation of Nuclear Granules Containing FUS and RNA Pol II. *Biochemistry*. 57:7021-7032.

Toombs, J.A., B.R. McCarty, and E.D. Ross. 2010. Compositional determinants of prion formation in yeast. *Mol Cell Biol*. 30:319-332.

Tuite, M.F., G.L. Staniforth, and B.S. Cox. 2015. [PSI(+)] turns 50. *Prion*. 9:318-332.

Ubeda, M., X.Z. Wang, H. Zinszner, I. Wu, J.F. Habener, and D. Ron. 1996. Stress-induced binding of the transcriptional factor CHOP to a novel DNA control element. *Mol Cell Biol*. 16:1479-1489.

Udan, M., and R.H. Baloh. 2011. Implications of the prion-related Q/N domains in TDP-43 and FUS. *Prion*. 5:1-5.

Udayakumar, D., R.K. Pandita, N. Horikoshi, Y. Liu, Q. Liu, K.K. Wong, C.R. Hunt, N.S. Gray, J.D. Minna, T.K. Pandita, and K.D. Westover. 2016. Torin2 Suppresses Ionizing Radiation-Induced DNA Damage Repair. *Radiat Res*. 185:527-538.

Vance, C., B. Rogelj, T. Hortobagyi, K.J. De Vos, A.L. Nishimura, J. Sreedharan, X. Hu, B. Smith, D. Ruddy, P. Wright, J. Ganesalingam, K.L. Williams, V. Tripathi, S. Al-Saraj, A. Al-Chalabi, P.N. Leigh, I.P. Blair, G. Nicholson, J. de Belleroche, J.M. Gallo, C.C. Miller, and C.E. Shaw. 2009. Mutations in FUS, an RNA processing protein, cause familial amyotrophic lateral sclerosis type 6. *Science*. 323:1208-1211.

Vance, C., E.L. Scotter, A.L. Nishimura, C. Troakes, J.C. Mitchell, C. Kathe, H. Urwin, C. Manser, C.C. Miller, T. Hortobagyi, M. Dragunow, B. Rogelj, and C.E. Shaw. 2013. ALS mutant FUS disrupts nuclear localization and sequesters wild-type FUS within cytoplasmic stress granules. *Hum Mol Genet*. 22:2676-2688.

Wang, C., E. Zhang, F. Wu, Y. Sun, Y. Wu, B. Tao, Y. Ming, Y. Xu, R. Mao, and Y. Fan. 2019. The C-terminal low-complexity domain involved in liquid-liquid phase separation is required for BRD4 function in vivo. *J Mol Cell Biol*. 11:807-809.

Wang, J., J.M. Choi, A.S. Holehouse, H.O. Lee, X. Zhang, M. Jahnel, S. Maharana, R. Lemaitre, A. Pozniakovsky, D. Drechsel, I. Poser, R.V. Pappu, S. Alberti, and A.A. Hyman. 2018. A Molecular Grammar Governing the Driving Forces for Phase Separation of Prion-like RNA Binding Proteins. *Cell*. 174:688-699 e616.

Wang, W.Y., L. Pan, S.C. Su, E.J. Quinn, M. Sasaki, J.C. Jimenez, I.R. Mackenzie, E.J. Huang, and L.H. Tsai. 2013. Interaction of FUS and HDAC1 regulates DNA damage response and repair in neurons. *Nat Neurosci*. 16:1383-1391.

Wei, M.T., Y.C. Chang, S.F. Shimobayashi, Y. Shin, A.R. Strom, and C.P. Brangwynne. 2020. Nucleated transcriptional condensates amplify gene expression. *Nat Cell Biol*. 22:1187-1196.

Wheeler, J.R., T. Matheny, S. Jain, R. Abrisch, and R. Parker. 2016. Distinct stages in stress granule assembly and disassembly. *Elife*. 5.

Wheeler, R.J. 2020. Therapeutics-how to treat phase separation-associated diseases. *Emerg Top Life Sci*. 4:307-318.

Wickner, R.B. 1994. [URE3] as an altered URE2 protein: evidence for a prion analog in Saccharomyces cerevisiae. *Science*. 264:566-569.

Wickner, R.B., H.K. Edskes, D. Bateman, A.C. Kelly, and A. Gorkovskiy. 2011. The yeast prions [PSI+] and [URE3] are molecular degenerative diseases. *Prion*. 5:258-262.

Wickner, R.B., D.C. Masison, and H.K. Edskes. 1995. [PSI] and [URE3] as yeast prions. *Yeast*. 11:1671-1685.

Wolozin, B., and P. Ivanov. 2019. Stress granules and neurodegeneration. *Nat Rev Neurosci*. 20:649-666.

Yang, L., L.J. Embree, S. Tsai, and D.D. Hickstein. 1998. Oncoprotein TLS interacts with serine-arginine proteins involved in RNA splicing. *J Biol Chem*. 273:27761-27764.

Yang, L., J. Gal, J. Chen, and H. Zhu. 2014. Self-assembled FUS binds active chromatin and regulates gene transcription. *Proc Natl Acad Sci U S A*. 111:17809-17814.

Yang, Y., L. Liu, I. Naik, Z. Braunstein, J. Zhong, and B. Ren. 2017. Transcription Factor C/EBP Homologous Protein in Health and Diseases. *Front Immunol*. 8:1612.

Yasuda, S., H. Tsuchiya, A. Kaiho, Q. Guo, K. Ikeuchi, A. Endo, N. Arai, F. Ohtake, S. Murata, T. Inada, W. Baumeister, R. Fernandez-Busnadiego, K. Tanaka, and Y. Saeki. 2020. Stress- and ubiquitylation-dependent phase separation of the proteasome. *Nature*. 578:296-300.

Yu, J.S.E., S. Colborne, C.S. Hughes, G.B. Morin, and T.O. Nielsen. 2019. The FUS-DDIT3 Interactome in Myxoid Liposarcoma. *Neoplasia*. 21:740-751.

Zhang, X., F. Wang, Y. Hu, R. Chen, D. Meng, L. Guo, H. Lv, J. Guan, and Y. Jia. 2020. In vivo stress granule misprocessing evidenced in a FUS knock-in ALS mouse model. *Brain*. 143:1350-1367.

Zhao, B., K. Marciniuk, E. Gibbs, M. Yousefi, S. Napper, and N.R. Cashman. 2019. Therapeutic vaccines for amyotrophic lateral sclerosis directed against disease specific epitopes of superoxide dismutase 1. *Vaccine*. 37:4920-4927.

Zinszner, H., J. Sok, D. Immanuel, Y. Yin, and D. Ron. 1997. TLS (FUS) binds RNA in vivo and engages in nucleo-cytoplasmic shuttling. *J Cell Sci*. 110 (Pt 15):1741-1750.

Zuo, L., G. Zhang, M. Massett, J. Cheng, Z. Guo, L. Wang, Y. Gao, R. Li, X. Huang, P. Li, and Z. Qi. 2021. Loci-specific phase separation of FET fusion oncoproteins promotes gene transcription. *Nat Commun*. 12:1491.